Intelligent Modal Analysis System: Autonomous Identification and Tracking of Aircraft Modal Parameters

Robin Volkmar

Deutsches Zentrum für Luft- und Raumfahrt
Institut für Aeroelastik
Göttingen

Deutsches Zentrum
DLR für Luft- und Raumfahrt

Forschungsbericht 2025-04

Intelligent Modal Analysis System: Autonomous Identification and Tracking of Aircraft Modal Parameters

Robin Volkmar

Deutsches Zentrum für Luft- und Raumfahrt
Institut für Aeroelastik
Göttingen

138 Seiten
 77 Bilder
  8 Tabellen
108 Literaturstellen

Deutsches Zentrum
DLR für Luft- und Raumfahrt

DLR

Robin VOLKMAR
DLR, Institut für Aeroelastik, Göttingen

Intelligentes Modalanalysesystem: Autonome Identifikation und Verfolgung modaler Parameter von Flugzeugen
Technische Universität Carolo-Wilhelmina zu Braunschweig

Effizientes Flugzeugdesign erfordert Leichtbaukonstruktionen. Leichtbau führt jedoch zu aeroelastischen Herausforderungen in Bezug auf Lasten und Schwingungen. Ein Beispiel ist eine instabile, selbstangeregte Schwingung, die als Flattern bezeichnet wird und zu strukturellem Versagen führen kann. Flattern resultiert aus der Kopplung von einer oder mehrerer strukturdynamischer Eigenschwingungen (Moden) und der instationären Aerodynamik. Dieses aeroelastische Phänomen tritt bei bestimmten Flugbedingungen wie Flughöhen und Geschwindigkeiten auf. Die Dämpfung einer Mode wird bei der Flattergeschwindigkeit einer bestimmten Flughöhe negativ. Eine infinitesimal kleine Störung führt dann zu einer elastischen Deformation, die größer wird, bis die Struktur versagt. Um Flattern vorherzusagen und zu vermeiden, ist es notwendig, die modalen Parameter im Standschwingungsversuch (GVT) und zusätzlich im Flugschwingungsversuche (FVT) experimentell zu identifizieren.

Im GVT analysieren erfahrene Ingenieure die Messdaten in parallel, um schnelle Ergebnisse zu erzielen, da der Erstflug kurze Zeit später folgt. Unterschiedliche Ingenieure können jedoch zu leicht inkonsistenten Ergebnissen führen, insbesondere bei der identifizierten Dämpfung. Im FVT ermöglicht eine einfache Automatisierung eine Echtzeitschätzung und Überwachung der Eigenfrequenzen und Dämpfungswerte. Jedoch werden nicht alle Schwingungsformen (Moden) zuverlässig identifiziert und weisen generell eine hohe Streuung auf, sodass das Tracking der Moden aktuell noch nicht praktikabel ist. Bestehende Automatisierungen der Modalanalysen basieren auf Clustering-Techniken und betrachten häufig nur Eigenfrequenzen und Moden. Die Abhängigkeit vom Nutzer wird üblicherweise minimiert, indem die Zahl erforderlicher Hyperparameter, wie z.B. Schwellenwerte, reduziert wird. Die Reduktion führt jedoch oft zu Kompromissen zwischen der Diskriminierung falscher Moden aufgrund mathematischer Artefakte und der robusten Identifikation aller physikalischer Moden. Daher erreichen die automatisierten Methoden bisher nicht die Genauigkeit, die für die Identifikation der kritischen Flugzeugmoden erforderlich ist.

Diese Dissertation präsentiert eine neuartige Methode für autonome Modalanalyse (AMA). Durch die Kombination aktueller Modalanalysemethoden, eines robusten, mehrstufigen Clustering-Prozesses und adaptiver Hyperparameteroptimierung mittels Gaußscher Prozesse und Bayes'scher Optimierung erzielt AMA eine präzise Identifizierung aller modalen Parameter, während die Analysezeit und die Abhängigkeit vom Benutzer erheblich verringert werden. AMA ermöglicht die Echtzeitfusion von Modalanalysemethoden aus dem Zeit- und Frequenzbereich zur Erhöhung der Zuverlässigkeit und zur Reduktion der Unsicherheit. Zusätzlich wird ein Kalman Filter integriert, um die Identifikationsstreuung während des Trackings der modalen Parameter weiter zu verringern. AMA und die Datenfusionsmethoden wurden erfolgreich zu automatisierten Analyseketten für GVT und FVT erweitert. Die Funktionsweise des neuen Systems wurde mit Simulationsdaten und Daten realer GVTs und FVTs validiert.

In der GVT-Analyse erzielt das neuartige System eine drastische Reduktion der Analysezeit, während es alle Flugzeugmoden identifiziert, die Ingenieure mit erheblichem Aufwand identifiziert haben. Zudem erhöht AMA die Genauigkeit der identifizierten Dämpfungswerte signifikant. Für die FVT-Anwendung ist AMA für eine schnelle Analyse mit einer Laufzeit von unter zwei Sekunden optimiert, was eine Echtzeitüberwachung der modalen Parameter bei variierenden Flugbedingungen ermöglicht. Durch die Methoden der Datenfusion reduziert das System die Unsicherheit erheblich und gewährleistet ein zuverlässiges Tracking der Eigenfrequenzen und Dämpfungswerte, wodurch die identifizierten Flatterkurven während der Flugtests verbessert werden. Die validierte Fähigkeit, reproduzierbare AMA Ergebnisse mit hoher Genauigkeit zu erzielen, kann bei der Standardisierung in der strukturdynamischen und aeroelastischen Identifikation von Flugzeugen helfen. Die hier gezeigte Vorgehensweise kann auch auf andere

Strukturen wie Brücken, Gebäude oder Windkraftanlagen übertragen werden.

Robin VOLKMAR
German Aerospace Center (DLR), Institute of Aeroelasticity, Göttingen

Intelligent Modal Analysis System: Autonomous Identification and Tracking of Aircraft Modal Parameters

Technical University Carolo-Wilhelmina of Braunschweig

Efficient aircraft design necessitates lightweight constructions. However, this leads to aeroelastic challenges concerning loads and vibrations. One example is an unstable, self-excited vibration called flutter, which can result in structural failure. Flutter results from a coupling of one or more structural dynamic modes of the aircraft structure and the unsteady aerodynamics. This aeroelastic phenomenon happens at specific flight conditions, such as altitude and speed. The damping of one mode becomes negative at the flutter speed of a particular altitude. An infinitesimally small disturbance leads to elastic deformations of the aircraft, which increase until structural failure. It is essential to experimentally identify the modal parameters in a ground vibration test (GVT) and also in a flight vibration test (FVT) to predict and avoid flutter.

In GVT, multiple experienced engineers analyze measurement data in parallel to achieve rapid results, as the first flight follows shortly after the test. However, engineers with varying experience levels can lead to inconsistencies, particularly in the identified damping values. In FVT, simple automation allows for real-time estimation and monitoring of eigenfrequencies and damping values. Nevertheless, only a limited number of vibration modes are reliably identified under changing flight conditions, resulting in excessive scatter in mode tracking. Existing automation methods for modal analysis rely on clustering techniques and focus on eigenfrequencies and modes. User-dependency is typically minimized by reducing the number of required hyperparameters, e.g., threshold values. However, this reduction often compromises the discrimination of spurious modes and the robust identification of all physical modes. Consequently, these automated methods have not yet achieved the high accuracy required for identifying critical aircraft modes.

This dissertation presents a novel method for autonomous modal analysis (AMA). By combining state-of-the-art modal analysis methods (Stochastic Subspace Identification and Least-Squares Complex Frequency), a robust multi-tier clustering process, and adaptive hyperparameter optimization using Gaussian processes and Bayesian optimization, AMA achieves precise identification of all modal parameters while significantly reducing analysis time and user-dependency. AMA enables real-time fusion of identification methods from both time- and frequency-domain to enhance reliability and reduce uncertainty. Additionally, a Kalman filter is integrated to decrease the identification scatter further while tracking modal parameters. AMA and the data fusion methods have been successfully extended into automated analysis chains for GVT and FVT. The functionality of the new system has been validated using simulation data and during actual GVTs and FVTs.

In GVT analysis, the innovative system drastically reduces analysis time while identifying all aircraft modes that engineers have conventionally identified with significant effort. Furthermore, AMA enhances the accuracy of the identified damping values. For FVT applications, AMA is optimized for rapid analysis with a run time of under two seconds, enabling real-time monitoring of modal parameters under varying flight conditions. Through data fusion methods, the system significantly reduces uncertainty and ensures reliable tracking of eigenfrequencies and damping values, thereby improving the identification of flutter curves during flight tests. The validated capability to produce reproducible AMA results with high accuracy can help standardize structural dynamic and aeroelastic identification of aircraft. However, the learning process of AMA can also be transferred to other structures, such as bridges, buildings, or wind turbines.

Intelligent Modal Analysis System: Autonomous Identification and Tracking of Aircraft Modal Parameters

Von der Fakultät für Maschinenbau

der Technischen Universität Carolo-Wilhelmina zu Braunschweig

zur Erlangung der Würde

eines Doktor-Ingenieurs (Dr.-Ing.)

genehmigte Dissertation

von: Robin Volkmar, M.Sc.
geboren in: Göttingen

2025

"Do the best you can until you know better.
Then when you know better, do better."
Maya Angelou

Danksagung

An dieser Stelle möchte ich mich von Herzen bei all denjenigen bedanken, die mich auf meinem Weg zur Promotion unterstützt und begleitet haben.

Mein erster Dank gilt den Gutachtern Prof. Tichy, Prof. Baum und Prof. Römer. Ich schätze die Zeit und Mühe ungemein, die Sie in die Begutachtung meiner Arbeit investiert haben. Des Weiteren möchte ich Prof. Heimbs dafür danken, dass er den Vorsitz der Promotionskommission übernommen hat.

Ein großes Dankeschön geht an meinen Abteilungsleiter Dr. Marc Böswald sowie meine fachlichen Betreuer Dr. Yves Govers und Dr. Keith Soal. Ich konnte als wissenschaftlicher Mitarbeiter in der Abteilung unglaublich viel von euch über die Stukturdynamik, Systemidentifikation und praktische Messdatenverarbeitung lernen. Ohne die wissenschaftliche Exzellenz der Abteilung wäre die vorliegende Arbeit nicht möglich gewesen. Eure Unterstützung hat mir in vielen herausfordernden Momenten den Rücken gestärkt. Die fachliche Expertise und das Engagement der Betreuung haben nicht nur zur Entstehung dieser Arbeit beigetragen, sondern auch dazu, dass ich mich persönlich als Wissenschaftler weiterentwickeln konnte.

Ich möchte mich ebenso bei meinen weiteren Kolleginnen und Kollegen aus dem Institut für Aeroelastik bedanken, die mit ihren Ideen und Anregungen stets für spannende Diskussionen oder auch mal bei einem Kaffee für Abwechslung gesorgt haben. Ich danke hierfür dem gesamten Institut und möchte folgende Kollegen gerne hervorheben: Janto Gundlach, Julian Sinske, Ralf Buchbach, Tobias Meier, David Meier, Johannes Knebusch, Dr. Jan Schwochow, Martin Tang, Martin Gröhlich und Tobias Hecken. Euer Feedback und der kollegiale Austausch waren für mich von unschätzbarem Wert und haben mir geholfen, meine Gedanken zu schärfen und neue Perspektiven zu gewinnen.

Zu guter Letzt möchte ich meinen Eltern und meiner Frau Lena meinen tiefsten Dank aussprechen. Euer unermüdlicher Beistand, euer Verständnis und eure Geduld in den oft intensiven Phasen des Studiums und der Promotion haben mir den nötigen Rückhalt gegeben. Ihr habt mich motiviert, auch in schwierigen Zeiten nicht aufzugeben.
Euch widme ich diese Arbeit.

Göttingen, 2025

Robin Volkmar

Abstract

Efficient aircraft design necessitates lightweight constructions. However, this leads to aeroelastic challenges concerning loads and vibrations. One example is an unstable, self-excited vibration called flutter, which can result in structural failure. Flutter results from a coupling of one or more structural dynamic modes of the aircraft structure and the unsteady aerodynamics. This aeroelastic phenomenon happens at specific flight conditions, such as altitude and speed. The damping of one mode becomes negative at the flutter speed of a particular altitude. An infinitesimally small disturbance leads to elastic deformations of the aircraft, which increase until structural failure. It is essential to experimentally identify the modal parameters in a ground vibration test (GVT) and also in a flight vibration test (FVT) to predict and avoid flutter.

In GVT, multiple experienced engineers analyze measurement data in parallel to achieve rapid results, as the first flight follows shortly after the test. However, engineers with varying experience levels can lead to inconsistencies, particularly in the identified damping values. In FVT, simple automation allows for real-time estimation and monitoring of eigenfrequencies and damping values. Nevertheless, only a limited number of vibration modes are reliably identified under changing flight conditions, resulting in excessive scatter in mode tracking. Existing automation methods for modal analysis rely on clustering techniques and focus on eigenfrequencies and modes. User-dependency is typically minimized by reducing the number of required hyperparameters, e.g., threshold values. However, this reduction often compromises the discrimination of spurious modes and the robust identification of all physical modes. Consequently, these automated methods have not yet achieved the high accuracy required for identifying critical aircraft modes.

This dissertation presents a novel method for autonomous modal analysis (AMA). By combining state-of-the-art modal analysis methods (Stochastic Subspace Identification and Least-Squares Complex Frequency), a robust multi-tier clustering process, and adaptive hyperparameter optimization using Gaussian processes and Bayesian optimization, AMA achieves precise identification of all modal parameters while significantly reducing analysis time and user-dependency. AMA enables real-time fusion of identification methods from both time- and frequency-domain to enhance reliability and reduce uncertainty. Additionally, a Kalman filter is integrated to decrease the identification scatter further while tracking modal parameters. AMA and the data fusion methods have been successfully extended into automated analysis chains for GVT and FVT. The functionality of the new system has been validated using simulation data and during actual GVTs and FVTs.

In GVT analysis, the innovative system drastically reduces analysis time while identifying all aircraft modes that engineers have conventionally identified with significant effort. Furthermore, AMA enhances the accuracy of the identified damping values. For FVT applications, AMA is optimized for rapid analysis with a run time of under two seconds, enabling real-time monitoring of modal parameters under varying flight conditions. Through data fusion methods, the system significantly reduces uncertainty and ensures reliable tracking of eigenfrequencies and damping values, thereby improving the identification of flutter curves during flight tests. The validated capability to produce reproducible AMA results with high accuracy can help standardize structural dynamic

and aeroelastic identification of aircraft. However, the learning process of AMA can also be transferred to other structures, such as bridges, buildings, or wind turbines.

Zusammenfassung

Effizientes Flugzeugdesign erfordert Leichtbaukonstruktionen. Leichtbau führt jedoch zu aeroelastischen Herausforderungen in Bezug auf Lasten und Schwingungen. Ein Beispiel ist eine instabile, selbstangeregte Schwingung, die als Flattern bezeichnet wird und zu strukturellem Versagen führen kann. Flattern resultiert aus der Kopplung von einer oder mehrerer strukturdynamischer Eigenschwingungen (Moden) und der instationären Aerodynamik. Dieses aeroelastische Phänomen tritt bei bestimmten Flugbedingungen wie Flughöhen und Geschwindigkeiten auf. Die Dämpfung einer Mode wird bei der Flattergeschwindigkeit einer bestimmten Flughöhe negativ. Eine infinitesimal kleine Störung führt dann zu einer elastischen Deformation, die größer wird, bis die Struktur versagt. Um Flattern vorherzusagen und zu vermeiden, ist es notwendig, die modalen Parameter im Standschwingungsversuch (GVT) und zusätzlich im Flugschwingungsversuche (FVT) experimentell zu identifizieren.

Im GVT analysieren erfahrene Ingenieure die Messdaten in parallel, um schnelle Ergebnisse zu erzielen, da der Erstflug kurze Zeit später folgt. Unterschiedliche Ingenieure können jedoch zu leicht inkonsistenten Ergebnissen führen, insbesondere bei der identifizierten Dämpfung. Im FVT ermöglicht eine einfache Automatisierung eine Echtzeitschätzung und Überwachung der Eigenfrequenzen und Dämpfungswerte. Jedoch werden nicht alle Schwingungsformen (Moden) zuverlässig identifiziert und weisen generell eine hohe Streuung auf, sodass das Tracking der Moden aktuell noch nicht praktikabel ist. Bestehende Automatisierungen der Modalanalysen basieren auf Clustering-Techniken und betrachten häufig nur Eigenfrequenzen und Moden. Die Abhängigkeit vom Nutzer wird üblicherweise minimiert, indem die Zahl erforderlicher Hyperparameter, wie z.B. Schwellenwerte, reduziert wird. Die Reduktion führt jedoch oft zu Kompromissen zwischen der Diskriminierung falscher Moden aufgrund mathematischer Artefakte und der robusten Identifikation aller physikalischer Moden. Daher erreichen die automatisierten Methoden bisher nicht die Genauigkeit, die für die Identifikation der kritischen Flugzeugmoden erforderlich ist.

Diese Dissertation präsentiert eine neuartige Methode für autonome Modalanalyse (AMA). Durch die Kombination aktueller Modalanalysemethoden, eines robusten, mehrstufigen Clustering-Prozesses und adaptiver Hyperparameteroptimierung mittels Gaußscher Prozesse und Bayes'scher Optimierung erzielt AMA eine präzise Identifizierung aller modalen Parameter, während die Analysezeit und die Abhängigkeit vom Benutzer erheblich verringert werden. AMA ermöglicht die Echtzeitfusion von Modalanalysemethoden aus dem Zeit- und Frequenzbereich zur Erhöhung der Zuverlässigkeit und zur Reduktion der Unsicherheit. Zusätzlich wird ein Kalman Filter integriert, um die Identifikationsstreuung während des Trackings der modalen Parameter weiter zu verringern. AMA und die Datenfusionsmethoden wurden erfolgreich zu automatisierten Analyseketten für GVT und FVT erweitert. Die Funktionsweise des neuen Systems wurde mit Simulationsdaten und Daten realer GVTs und FVTs validiert.

In der GVT-Analyse erzielt das neuartige System eine drastische Reduktion der Analysezeit, während es alle Flugzeugmoden identifiziert, die Ingenieure mit erheblichem Aufwand identifiziert haben. Zudem erhöht AMA die Genauigkeit der identifizierten Dämpfungswerte signifikant. Für die FVT-Anwendung ist AMA für eine schnelle Analyse mit einer Laufzeit von unter zwei Sekunden optimiert, was eine Echtzeitüberwachung

der modalen Parameter bei variierenden Flugbedingungen ermöglicht. Durch die Methoden der Datenfusion reduziert das System die Unsicherheit erheblich und gewährleistet ein zuverlässiges Tracking der Eigenfrequenzen und Dämpfungswerte, wodurch die identifizierten Flatterkurven während der Flugtests verbessert werden. Die validierte Fähigkeit, reproduzierbare AMA Ergebnisse mit hoher Genauigkeit zu erzielen, kann bei der Standardisierung in der strukturdynamischen und aeroelastischen Identifikation von Flugzeugen helfen. Die hier gezeigte Vorgehensweise kann auch auf andere Strukturen wie Brücken, Gebäude oder Windkraftanlagen übertragen werden.

Contents

List of Figures

List of Tables

Acronyms

AI artificial intelligence. 42, 69

AMA autonomous modal analysis. x–xiii, xv, 2–4, 15, 20–22, 32, 34–37, 39–41, 44–47, 53, 56, 59, 60, 62, 64, 66–69, 73–77, 93, 97–103, 107–109

ANN artificial neural network. 103

APSDs auto-power spectral densities. 10

APU auxiliary power unit. 63, 78

BO Bayesian optimization. xi, xii, 34, 39, 42, 44–46, 75, 89, 100, 107, 108

CMIF complex MIF. 25, 26

CPSDs cross-power spectral densities. xii, 10, 30, 35, 41, 89

DBSCAN density-based clustering for applications with noise. 17, 18, 23, 26, 41, 42, 54

DLR German Aerospace Center (german: Deutsches Zentrum für Luft- und Raumfahrt). xi, xii, 2, 11–14, 21, 53, 54, 57, 66, 72, 76, 91

DoF degree of freedom. 15, 28, 39, 41, 47–49, 63, 89, 102

EASA European Aviation Safety Agency. 13

EI expected improvement. 44

EMA experimental modal analysis. 1, 2, 5, 8, 10, 12, 13, 21, 24, 26–28, 30, 39–42, 46, 53, 54, 57, 60, 65, 66, 99–101

FEM finite element method. 1, 5, 12, 102, 103

FIFO first-in first-out. 36, 82

FRF frequency response function. xi, 8–10, 12, 13, 28, 40, 47, 53, 57

FTI flight test instrumentation. 78, 102

FVT flight vibration test. x, xii, xiii, xv, 1–6, 11, 13, 14, 19–21, 30, 31, 33–35, 37, 38, 42, 45, 71–82, 84–92, 94, 96–102, 104, 107–109

GP Gaussian process. xi, 39, 42–44, 100, 107

GUI graphical user interface. xii, 54, 56, 59, 60, 62, 74

GVT ground vibration test. x–xii, xv, xix, 1–5, 11–13, 19–21, 30, 31, 44, 45, 53, 54, 56–59, 61, 62, 64, 66, 68, 69, 71, 74, 75, 77, 78, 89, 99–104, 108, 109

HDM hyperbolic distance metric. 74, 90

HO hyperparameter optimization. xii, 37, 42, 46, 60, 66, 75, 89, 97, 100, 101, 103, 104, 107, 108

HTP horizontal tail plane. xii, 63–65, 78

IMM-KF interacting multiple model KF. xi, 38, 94–97, 108

IPDA integrated probabilistic data association. 87, 97, 104

ISTAR in-flight systems and technology airborne research. xii, xv, 57–59, 76–81, 84, 87–90, 97, 107

IVM inverse-variance mean. xii, 21, 35, 36, 50–52, 77–80, 82, 83, 85–88, 97, 101, 108

KF Kalman filter. xii, xiii, 3, 4, 19, 21, 33, 36–38, 50–52, 77, 82–89, 91–98, 101, 104, 105, 107, 108

LCB lowest confidence bound. 43, 44

LOF local outlier factor. 54

LPV linear parameter-variant. 48

LSCF least-squares complex frequency. xii, xix, 8, 10–12, 16, 28, 29, 31, 32, 34, 35, 39–41, 47, 48, 50, 51, 60, 64, 69, 72–75, 77, 78, 82, 88, 89, 94, 95, 97, 99, 101

LSFD least-squares frequency domain. xi, 9, 28

LTI linear time-invariant. 2, 14, 35, 36, 47, 72, 89, 90

LTV linear time-variant. xii, 14, 72, 73, 75, 89, 90

MAC modal assurance criterion. xi, xii, 16, 17, 19, 23, 24, 41, 56, 60, 62–65, 74, 101, 102

MAC-XP expanded modal assurance criterion. xii, 19, 41, 45, 55, 56, 62, 63, 67, 68, 74, 82, 102

MEMs microelectromechanical systems. 91

MID modal identification method. xii, xv, 3, 4, 6, 8, 10, 18, 20, 21, 27, 31, 33–36, 39, 40, 44, 50, 52, 72–75, 77–80, 82, 83, 87, 89, 90, 93, 97–102, 108

MIF mode indicator function. xi, 15, 24–26, 41

MIF$_\psi$ mode indicator function according to Breitbach. 15, 16, 26, 27, 41, 45, 56, 65, 67, 74, 90

ML machine learning. 42

ML-MM maximum likelihood modal model. 28

MMIF multivariate MIF. 24, 25

MPC modal phase collinearity. 15, 16, 18, 27, 41, 45, 56, 67

MPD mean phase deviation. 15, 16, 26, 27, 41, 45, 67, 74, 90

MSD mean squared difference. xii, 83, 87

OMA operational modal analysis or output-only modal analysis. xix, 1–3, 5, 6, 10, 14, 19–21, 24, 26, 27, 30, 31, 33, 34, 39–42, 72, 74, 83, 89, 97, 99–101, 104, 107

OMAX OMA in presence of eXogenous inputs. 5, 6, 14, 98

pLSCF poly LSCF (also known as PolyMAX). xi, 12, 13, 23

PSO particle swarm optimization. xi, 21, 30, 31, 41, 46, 60, 64, 74, 109

RMIF real MIF. 25

RMS root mean squared. 51

SAGVT semi-autonomous GVT analysis. xii, 53, 56–59, 62–69, 100, 101, 103, 109

SSI stochastic subspace identification. 6, 10, 31, 32, 34, 35, 39, 41, 50, 51, 72, 73, 101

SSI-COV covariance-based SSI. xii, 6, 8, 10, 34, 35, 50, 51, 74, 75, 77, 78, 82, 83, 88, 89, 94, 95, 97

SSI-DAT data-driven SSI. xii, 6–8, 10, 34, 35, 50, 51, 74, 75, 77, 78, 82, 83, 88, 89, 94, 95, 97

SVD singular value decomposition. 7, 8

SVDP single virtual driving point. 12

TAS true air speed. xii, 77, 83, 90

TRL technology readiness level. 103

UAV unmanned aerial vehicle. xii, xiii, 53, 57, 66, 67, 69, 75, 91–95, 97, 98, 100, 101, 104, 107–109

VTOL vertical take-off and landing. 103

VTP vertical tail plane. 78

1 Introduction

1.1 Motivation and Objectives

Lightweight construction is a mandatory feature of aeronautic vehicles. However, lightweight structures are prone to vibration, which applies to aircraft. Aircraft can experience vibration excitation, for example, from aerodynamic turbulence, engine operation, or gusts. The vibration amplitude is limited and decays due to damping effects from the structure and aerodynamic forces. Indeed, the unsteady aerodynamics under varying flight conditions, like airspeed, altitude, and temperature, significantly impact the damping behavior. Therefore, the dynamic behavior of the aircraft structure and the aerodynamic-structure-interaction, i.e., aeroelastic behavior, must be identified precisely. The vibration behavior of the whole aircraft can be described by its modes or modal parameters: eigenfrequencies, damping ratios, mode shapes, and modal masses. Due to unsteady aerodynamics, eigenfrequencies can shift. If the eigenfrequencies of modes approach each other, modes can couple with each other, and the damping of one mode can become zero or negative. This phenomenon is known as aircraft flutter. The negative damping leads to an unstable self-excited vibration. Even a small disturbance can result in instabilities with rapidly increasing vibration amplitudes. Since flutter can result in catastrophic structural failure, the whole flight envelope must be proven to be flutter-free. This aeroelastic behavior is defined in the design process but must be validated experimentally on prototypes. The numerical structural dynamic model of a new aircraft prototype must be validated before the first flight. The ground vibration test (GVT) is performed to deliver an experimental structural dynamic model of the whole aircraft, called the modal model. The results consist of modes in the frequency range of interest. During the GVT, the aerodynamic effects are explicitly excluded in order to update the numerical structural model of the aircraft, e.g., the finite element method (FEM) model. The flutter calculations are based on the updated structural dynamic model and a coupled aerodynamic model. The flutter curves, describing the aeroelastic stability of the aircraft prototype, are validated for the whole flight envelope in a flight vibration test (FVT). Therefore, the test points (air speed/altitude combinations) are gradually extended until the entire flight envelope is covered up to the maximum airspeed, altitude and Mach number.

The identification of modal parameters is referred to as modal analysis. If (artificial) input forces, as well as responses (e.g., accelerations), can be measured, the task is referred to as experimental modal analysis (EMA). If the input forces cannot be measured (e.g., the aerodynamic forces in flight) and the identification must rely on the measured responses only, the task is referred to as operational modal analysis (OMA). Therefore, in all cases, the identification results of EMA are more certain than the results of OMA. In a GVT, the aircraft is artificially excited using, for example, electrodynamic shakers and modal parameters are extracted with high accuracy using EMA. In FVT, different approaches for artificial aircraft excitation exist, e.g., control surface excitation. However, those excitation approaches have strengths and weaknesses. Another approach is to use the unknown aerodynamic turbulence as the only excitation and to assume it is broadband. This assumption is not always fulfilled, but the identification can lead to reasonable results. In

such a case, the identification of modal parameters is based on the measured response signals; therefore, OMA is applied.

During a GVT performed by German Aerospace Center (DLR), engineers perform EMA right after the data acquisition. Two people often work in parallel, and multiple team shifts are involved in the test. This is necessary because the GVT is performed only a few weeks before the maiden flight, and therefore, the results must be delivered with high time pressure. Nevertheless, the accuracy of the modal parameters is safety-critical. Specifically trained engineers perform this challenging task. At DLR, engineers apply a combination of specifically defined quality criteria, an internal guideline, and engineering knowledge. However, the different experiences of the engineers lead to slightly different results. Even the same engineer may come to different results after gaining more insights into the structure under investigation (e.g. for nonlinear modes).

The main challenges of GVT data analysis sum up to time-criticality, the need for high identification accuracy, and a low user-dependency to ensure reproducible results.

In a FVT, optimized OMA methods can be applied close to real-time, accepting the inevitable increased uncertainty. This means the whole analysis is performed within two seconds and repeated two seconds later. In order to achieve this real-time processing, the analyzed time sequences are short and can compromise the accuracy of the results. However, the result is a potential online monitoring of the aeroelastic stability. Within this short time window, engineers cannot perform manual operations. Therefore, simple and fast automation of OMA has been developed. However, such monitoring of modal parameters in FVT is challenging, as Basseville et al. state:

> "In-flight vibration monitoring of aeronautical structures is a key objective of flight tests and a challenging task. Online delivery of the results is required, and critical parameters for flight domain exploration are the damping ratios, which are known to be difficult to estimate." [4]

Several reasons exist for high uncertainties in modal parameter identification in FVT. First, in modal analysis, the system under investigation is assumed to be linear time-invariant (LTI). Since the modes of an aircraft change with varying flight conditions, the system is parameter-variant. If the parameters change over time, the system under investigation varies over time, too. Second, the acceleration time data used for OMA should be as short as possible to achieve the real-time analysis and to reduce the effect of the time-varying system. But the shorter the acceleration time data for OMA is, the higher the scatter of the resulting modal parameters. Third, in addition to the high uncertainty for the reasons mentioned above, the signal-to-noise ratio of the measured responses is lower for turbulent excitation than, for example, for optimized excitation during a GVT. For FVT data analysis, the main challenges are the reliable identification of all modes of interest and monitoring these modes over changing flight conditions with acceptable uncertainties.

To address the mentioned challenges, this thesis aims to develop and test a new framework for autonomous modal analysis (AMA). This framework shall be applicable for structural dynamic system identification on the ground as well as aeroelastic system identification in aircraft flight. This means, in particular, that it produces mostly user-independent results in a very short time, which are as accurate as extensively produced manual results.
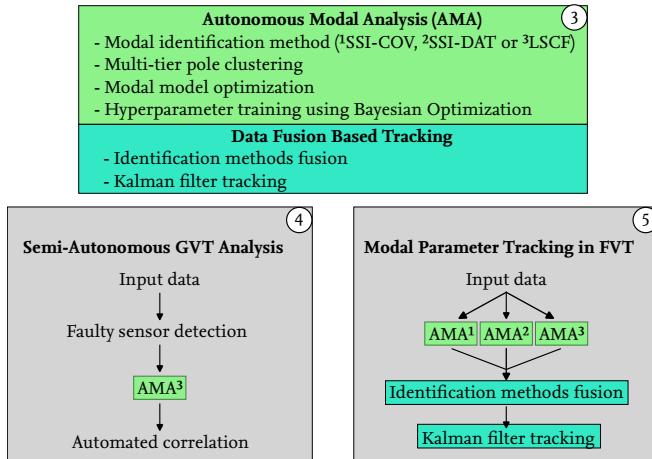
Figure 1.1: Organization of the method chapters

The methods shall be applied for the two main modal parameter identification tasks for aircraft: GVT and FVT.

1.2 Content and Organization of the Text

This thesis is divided into six chapters. In the second chapter, the relevant literature is reviewed concerning AMA of aircraft, and some theoretical background is explained. This includes autonomous modal parameter identification methodologies and the state-of-the-art analysis procedures for GVT and FVT. Figure 1.1 illustrates the method chapters of this thesis. The core method AMA and data fusion-based tracking are described in Chapter 3. This method builds upon a modal identification method (MID), performs multi-tier clustering, and optimizes the modal model. On top of that, the process can optimize the hyperparameters for the analysis in a supervised learning manner. Since the identification scatter is significantly higher for OMA in FVT, data fusion approaches are developed for uncertainty reduction. This core method is embedded into two analysis chains. The first chain analyses GVT data and is described in Chapter 4. AMA is enframed by an automated sensor anomaly detection and an automated mode correlation. The hyperparameter optimization of AMA is also expanded to be used for GVT analysis. Results from two GVTs are shown and discussed. In Chapter 5, the second analysis chain is described, which performs modal parameter identification and tracking in FVT. Since the uncertainties of MIDs for FVT are high, AMA is applied based on different MIDs in parallel. The unified processing of different MIDs via AMA allows fusion of their results, i.e., the modal models. To further reduce the uncertainties of identified model parameters in FVT, a Kalman filter (KF) is applied to track modal parameters smoothly. Results from FVTs of two aircraft with different FVT approaches are shown. The findings are concluded in Chapter 6, and an outlook of future research topics is given.

1.3 Research Contributions and Originalities

This thesis aims to develop an autonomous analysis system that identifies modal parameters of aircraft on the ground and in flight with high reliability and accuracy. The developed system is evaluated at GVTs and FVTs of two different aircraft. The following topics are novel developments:

- Optimization of hyperparameters for AMA: Training of all required hyperparameters for modal analysis based on Gaussian processes and results of an expert

- High automation of the GVT analysis process: From time data to correlated modal models using low engineers workload and low user-dependency

- Data fusion for modal parameter monitoring in FVT: Fusion of different MIDs and fusion of subsequently identified modal parameters using a KF to ensure reliable real-time identification of relevant modes and tracking with low uncertainties

2 Theoretical Background and Literature Review

2.1 Modal Parameter Identification

Validation of structural dynamic simulation models such as, for example, FEM models plays a crucial role, especially for safety-critical structures like aircraft. A common way for FEM model validation and model updating is using experimentally identified modal parameters [60, 28, 62]. For example, parameters of the FEM model of an aircraft are adjusted manually to meet the results of the GVT. Examples of gradient-based automation of FEM model updating of aircraft can be found in [32, 7, 35]. These examples use modal data identified in vibration tests. Figure 2.1 illustrates the basis of such a system identification. We simplify the structural dynamic system S of an aircraft by a simple mathematical
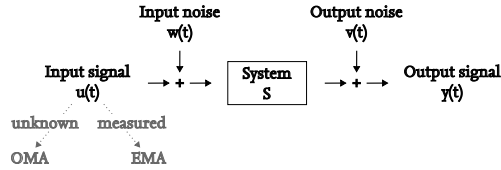
Figure 2.1: System identification with measured or unknown inputs

model, i.e., the modal model. The model can be identified based on the input signal $u(t)$, the output signal $y(t)$, the input noise $w(t)$ and the output noise $v(t)$. The characteristic equation of the dynamic system is

$$M\ddot{z}(t) + D\dot{z}(t) + Kz(t) = F(t) \ , \tag{2.1}$$

$$F(t) = bu(t) \ , \tag{2.2}$$

where M, D, and K are the mass, damping, and stiffness matrices of the system, and $z(t)$ is the displacement vector at time t. The input force $F(t)$ can be factorized into a matrix b and a vector $u(t)$.

The identification of the modal model is referred to as modal analysis. In the literature, three domains of modal analysis are distinguished concerning the input signal.

- experimental modal analysis (EMA): measured input

- operational modal analysis (OMA): unknown input

- OMA in presence of eXogenous inputs (OMAX): partially unknown and partially measured input

If the input cannot be measured, i.e., for OMA or partly for OMAX, it is assumed as random and stationary broadband excitation. During a GVT, the aircraft is excited artificially, and the input force is measured; therefore, EMA is applied. In a FVT, ambient excitation from aerodynamic turbulence is present. In addition, artificial excitation can be added to improve system identification, which is discussed in detail in 2.3. Since the turbulence

excitation of aircraft is often found to be sufficient in FVT [48], OMA is applied in this thesis. However, future extension of the developed methods for OMAX is possible.

2.1.1 Stochastic Subspace Identification

A well-known MID family for OMA is stochastic subspace identification (SSI). SSI is a time-domain method. Therefore, no spectra calculation has to be performed as preprocessing. However, the time data can be decimated if the sample rate is too high. The decimation can improve the results significantly. Several variants of SSI exist. A review of SSI for mechanical engineering is given in [21]. In this thesis, two methods are used: data-driven SSI (SSI-DAT) [97] and covariance-based SSI (SSI-COV) [66]. These methods have been chosen because they were applied successfully to in-flight modal parameter identification before [20, 78, 49]. For the sake of simplicity, only data-driven SSI (SSI-DAT) is presented in detail based on the descriptions from Brincker and Anderson [14] and Soal [86].

The basis for SSI is the state-space model of the dynamic system, in which the state matrix includes the system matrices. The state space is given as

$$x(t) = \begin{pmatrix} z(t) \\ \dot{z}(t) \end{pmatrix} \quad . \tag{2.3}$$

The differential Equation 2.1 becomes

$$\dot{x}(t) = Ax(t) + Bu(t) \quad , \tag{2.4}$$

with

$$A = \begin{pmatrix} 0 & I_n \\ -M^{-1}K & -M^{-1}D \end{pmatrix}, B = \begin{pmatrix} 0 \\ M^{-1}b \end{pmatrix} \quad , \tag{2.5}$$

where A is the state matrix and B is the input matrix. The measured output $y(t)$ is defined given the output matrix C and the direct transmission matrix E as

$$y(t) = Cx(t) + Eu(t) \quad . \tag{2.6}$$

The continuous time state-space model is reformulated into a discrete-time state-space model

$$x_{k+1} = Ax_k + w_k \quad , \tag{2.7}$$
$$y_k = Cx_k + v_k \quad , \tag{2.8}$$

with w_k is the process noise and v_k is the measurement noise. Since the input cannot be measured, it is assumed to be Gaussian white noise. The goal of SSI is to identify the state matrix A. The system response is represented in a data matrix Y

$$Y = [y_1 y_2 \ldots y_N] \quad , \tag{2.9}$$

with N is the number of samples. One defines $Y_{1:N-k}$ as the data matrix without the last k samples. The output measurements y are built into the block Hankel matrix Y_h as a combination of several shifted sub-matrices of Y

$$Y_h = \begin{bmatrix} Y_{1:N-2s} \\ Y_{2:N-2s+1} \\ \vdots \\ Y_{2s:N} \end{bmatrix} = \begin{bmatrix} Y_{hp} \\ Y_{hf} \end{bmatrix} \quad , \tag{2.10}$$

where Y_{hp} is referred to as the "past", Y_{hf} is called the "future", and $2s$ is the number of block rows (also referred to as Hankel size). In the next step, the so-called subspace matrix is built from the Hankel matrix, also called the projection of the future data space onto the past data space. For SSI-DAT, this can be done using a QR factorization of the Hankel matrix

$$\begin{bmatrix} Y_{hp} \\ Y_{hf} \end{bmatrix} = RQ^T \ , \tag{2.11}$$

where Q is an orthonormal matrix $(Q^T Q = QQ^T = I)$ and R is a lower triangular matrix.

$$\begin{bmatrix} Y_{hp} \\ Y_{hf} \end{bmatrix} = \begin{bmatrix} R_{1,1} & 0 \\ R_{2,1} & R_{2,2} \end{bmatrix} \begin{bmatrix} Q_1 \\ Q_2 \end{bmatrix} \rightarrow \mathcal{H} = R_{2,1} \ , \tag{2.12}$$

where $\mathcal{H}$ is the projection matrix. The projection matrix can also be factorized by

$$\mathcal{H} = O\hat{X} \ , \tag{2.13}$$

with O is the observability matrix and $\hat{X}$ is the state sequence

$$O = \begin{pmatrix} C \\ CA \\ CA^2 \\ \vdots \\ CA^{i-1} \end{pmatrix} \ , \hat{X} = (\hat{x}_i \quad \hat{x}_{i+1} \quad \dots \quad \hat{x}_{i+j-1}) \ . \tag{2.14}$$

The observability matrix and the state sequence are computed by a singular value decomposition (SVD)

$$\mathcal{H} \overset{\text{SVD}}{=} USV^T \ , \tag{2.15}$$

$$O = US^{\frac{1}{2}} \ , \hat{X} = O\mathcal{H} \ . \tag{2.16}$$

The system matrix A and output matrix C are found from the observability matrix O structure. The first row of O gives C, and A is calculated in a least-squares sense from the second row of O knowing C. The modal parameters are determined by an eigenvalue decomposition of the state matrix A

$$A = \Psi' \Lambda' \Psi'^{-1} \ , \tag{2.17}$$

where $\Lambda' = diag(\lambda_r'), r = 1, \dots, n$ contains the complex conjugate eigenvalues of the system and Ψ' contains the eigenvectors. The used state space is time-discrete; therefore, the eigenvalues need to be transformed into the continuous space

$$\lambda_r = \frac{ln\lambda_r'}{\Delta t} \ . \tag{2.18}$$

The angular eigenfrequency ω_r, eigenfrequency f_r and damping ratio ξ_r are given by

$$\omega_r = |\lambda_r| \ , f_r = \omega_r/2\pi \ , \xi_r = -\frac{\Re(\lambda_r)}{|\lambda_r|} \ . \tag{2.19}$$

The eigenvectors Ψ' of the state matrix do not necessarily have a physical meaning; therefore, they need to be transformed using the output matrix C

$$\Psi = C\Psi' \ . \tag{2.20}$$

The procedure for SSI-DAT can be summarized as

1. Decimation of output time data

2. Construction of the Hankel matrix

3. QR factorisation

4. SVD

5. Least-squares estimation of state matrix A

6. Extraction of modal parameters from A

A primary difference between SSI-DAT and SSI-COV is that in SSI-COV, a covariance estimation between all outputs and a set of references replaces the QR factorization. Therefore, SSI-COV has slightly shorter run-times but may be less accurate according to [86].

2.1.2 Least-Squares Complex Frequency

With respect to EMA a well-known MID is least-squares complex frequency (LSCF) [38, 99, 19]. LSCF is a frequency domain method with some variants. Since the differences in the variants are not in the scope of this thesis, interested readers are referred to [38, 99, 19, 69]. The method is also known as PolyMAX in the commercial software TestLab by Siemens. Based on the measured response and excitation time signals, frequency response functions (FRFs) are calculated. The FRF matrix $H(\omega)$ is reformulated to

$$[H(\omega)] = \sum_{r=1}^{R} \left(\frac{\psi_r \psi_r^T}{a_r(j\omega - \lambda_r)} + \frac{\psi_r^* \psi_r^H}{a_r^*(j\omega - \lambda_r*)} \right) \ , \tag{2.21}$$

with the modal parameters as eigenvalues λ_r, modal A's a_r and mode shape vectors $\{\psi\}_r$ and the excitation frequency ω. The frequency band is split into a smaller frequency band for the current identification to reduce the computational cost. A lower residual $[LR]$ and an upper residual $[UR]$ represent the residual information from outside of the current identification band.

$$[H(\omega)] = \frac{[LR]}{\omega^2} + \sum_{r=n}^{N} \left(\frac{\psi_r \psi_r^T}{a_r(j\omega - \lambda_r)} + \frac{\psi_r^* \psi_r^H}{a_r^*(j\omega - \lambda_r*)} \right) + [UR] \tag{2.22}$$

A rational fraction of complex polynomials can represent a single FRF in the frequency domain

$$H_{ij}(\omega) = \frac{B_{ij}(\omega)}{A(\omega)} = \frac{b_{ij,0} + b_{ij,1} \cdot j\omega + \cdots + b_{ij,M} \cdot (j\omega)^M}{a_0 + a_1 \cdot j\omega + \cdots + a_M \cdot (j\omega)^M} \ , \tag{2.23}$$

for the ith response and j^{th} excitation point. M is the order of the polynomial and is referred to as model order in the following. The choice of the model order is not trivial

since the number of modes is usually unknown a priori, and noise compromises the identification. While the numerator in Equation 2.23 depends on the response and excitation point, the denominator is unique for all FRFs. Therefore, it is referred to as the common denominator model. FRFs cannot be measured without noise. The measurement noise $\epsilon_{ij}(\omega_k)$ for the excitation frequency ω_k can be described by

$$\epsilon_{ij}(\omega_k) = B_{ij}(\omega_k) - A(\omega_k)H_{ij}(\omega_k) \ . \tag{2.24}$$

The global error summed over all FRFs can be minimized in a least-squares sense as

$$\epsilon(a_m, b_{ij,m}) = \sum_{i=1}^{I}\sum_{j=1}^{J}\sum_{k=1}^{K} |\epsilon_{ij}(\omega_k)|^2 \to min \ . \tag{2.25}$$

The least-squares minimization leads to the complex polynomial coefficients of the numerator polynomials and common denominator polynomials. The roots of the common denominator polynomial $A(\omega)$ lead to the poles of the system (i.e. the eigenvalues)

$$A(\omega) = a_0 + a_1 \cdot j\omega + \cdots + a_M \cdot (j\omega)^M = 0 \to \lambda_1, \lambda_2, \ldots, \lambda_M \ . \tag{2.26}$$

From all calculated poles $\lambda_1, \ldots, \lambda_M$, an engineer or an automated version selects the poles that describe the physical system λ_r. The eigenfrequencies and damping ratios are extracted from the eigenvalues as shown in Equation 2.19. The mode shapes and modal masses are identified in a consecutive step. A common method for this step is called least-squares frequency domain (LSFD)[96]. The mode shapes and modal A's are part of the residuals $R_{ij,r}$ in the current frequency identification band

$$H_{ij}(\omega_k) = \frac{LR_{ij}}{\omega^2} + \sum_{r=n}^{N} \left(\frac{R_{ij,r}}{j\omega - \lambda_r} + \frac{R_{ij,r}^*}{j\omega - \lambda_r*} \right) + UR_{ij} \ . \tag{2.27}$$

In order to solve Equation 2.27 for $R_{ij,r}$, LR_{ij} and UR_{ij} the equation can be formulated for the individual frequency point ω_k as the least-squares problem

$$\begin{Bmatrix} H_{ij}(\omega_1) \\ H_{ij}(\omega_2) \\ \vdots \\ H_{ij}(\omega_k) \end{Bmatrix} = \begin{bmatrix} \frac{1}{\omega_1^2} & \frac{1}{j\omega_1-\lambda_1} & \frac{1}{j\omega_1-\lambda_1^*} & \frac{1}{j\omega_1-\lambda_2} & \cdots & 1 \\ \frac{1}{\omega_2^2} & \frac{1}{j\omega_2-\lambda_1} & \frac{1}{j\omega_2-\lambda_1^*} & \frac{1}{j\omega_2-\lambda_2} & \cdots & 1 \\ \vdots & \vdots & \vdots & \vdots & \ddots & \vdots \\ \frac{1}{\omega_k^2} & \frac{1}{j\omega_k-\lambda_1} & \frac{1}{j\omega_k-\lambda_1^*} & \frac{1}{j\omega_k-\lambda_2} & \cdots & 1 \end{bmatrix} \begin{Bmatrix} LR_{ij} \\ R_{ij,1} \\ R_{ij,1}^* \\ R_{ij,2} \\ \vdots \\ UR_{ij} \end{Bmatrix} \ . \tag{2.28}$$

The mode shape and modal A can be extracted from

$$R_{ij,r} = \frac{\psi_{i,r}\psi_{j,r}}{a_r} \ . \tag{2.29}$$

The scaling constant modal A can be determined at the driving point $i = j$ as

$$R_{jj,r} = \frac{\psi_{j,r}\psi_{j,r}}{a_r} = \frac{1}{a_r} \ . \tag{2.30}$$

One component of the mode shape is set to one, and the other components can be derived. Usually, the highest component is set to 1 or the component of the driving point. The modal mass can be derived by

$$m_r = \frac{|a_r|}{2\omega_r\sqrt{1-\xi_r^2}} \ .$$

(2.31)

The procedure can be summarized as

1. Calculation of FRFs

2. Choice of identification bands

3. Identification of the eigenvalues

4. Identification of the mode shapes and modal masses.

Since in **OMA** the excitation is unknown, FRFs cannot be calculated. However, a variant of LSCF exists for output-only data. In this variant, cross-power spectral densities (CPSDs) are the basis for LSCF. The input is assumed to be a stationary broadband spectrum. Without going into detail, the main difference is that the modal mass cannot be calculated in this version. Further information about the output-only variant of LSCF can be found in [67].
The MIDs described for OMA have different assumptions and, therefore, different strengths and weaknesses. Since, in contrast to EMA, the uncertainties for OMA are significantly larger, the three methods (LSCF, SSI-DAT and SSI-COV) are applied in parallel, so that the strengths of the methods may complement each other.

2.1.3 Stabilization Diagram

One step of all aforementioned MIDs requires a model order as an input parameter. Since this parameter is usually unknown in advance, the so-called stabilization diagram (or stabilization chart) has become an essential tool to supervise the modal analysis [102, 95]. The measured data is processed multiple times for increasing model orders. Therefore, eigenvalues will be estimated for every model order. The resulting data pool consists of eigenfrequencies, damping ratios, and potential eigenvectors for several model orders. For SSI, the eigenvectors are identified directly for each mode as part of the state matrix. For LSCF, the eigenvalues of a potential modal model need to be selected to estimate the eigenvectors. A practical approach is to calculate the preliminary eigenvectors using all eigenvalues of one model order, taking each model order as a preliminary modal model. Figure 2.2 shows example stabilization diagrams. In the standard version, the model orders are plotted over the eigenfrequencies, see an example of a simulated simple beam-like system in Figure 2.2a (right ordinate). Often, this plot is enriched with channel-wise or summed spectra (blue line): FRFs, CPSDs, or auto-power spectral densities (APSDs) (left ordinate). Based on the selected modes (i.e., the current modal model), synthesized spectra are plotted (red line) next to the spectra of the measured data to check the coincidence. The modal parameters (e.g., the eigenfrequency, damping ratio, and eigenvectors), which do not change significantly with increasing model orders, are assumed to describe physical modes. Those identification results (poles) are called stable if the modal parameters

from one model order to the next vary less than a threshold. In [95], the authors suggest stability thresholds of 1% in frequency, 5% in damping ratio, and 2% in eigenvector. The stability of poles is indicated as frequency stable (symbol: +), damping stable (◇), unstable (o), or stable (□). Alternatively, the eigenvalues are plotted as damping ratios over eigenfrequencies [95], as can be seen for the simple simulated system in Figure 2.2b (right ordinate). The poles that identify a physical mode build a consolidated cluster in this format. Representative poles have to be selected from the stabilization diagram to build a modal

(a) Stabilization diagram of a simulated beam-like system

(b) Damping ratios over eigenfrequencies of a simulated beam-like system

(c) Stabilization diagram of aircraft flight test data

(d) Damping ratios over eigenfrequencies of aircraft flight test data
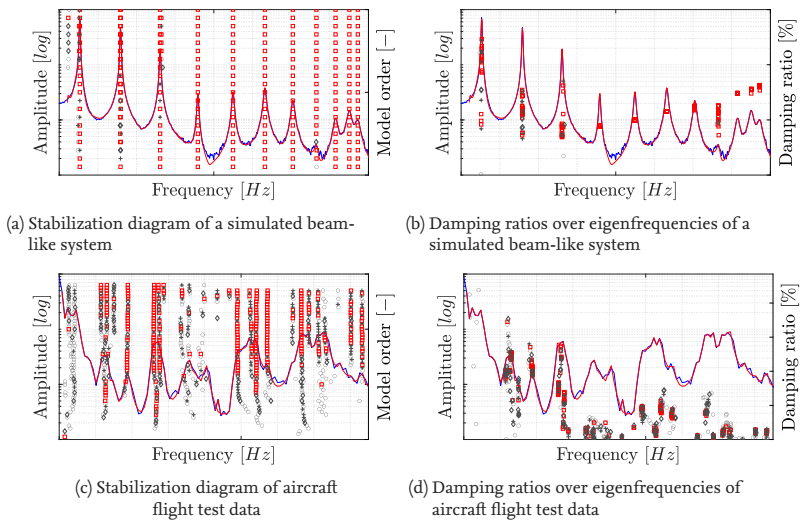
Figure 2.2: Examples of stabilization diagrams

model. All physical modes have to be part of the modal model to achieve a complete modal model. For LSCF, it might be required to include some spurious modes, which support the correct estimation of the eigenvectors of physical modes. Those spurious modes are usually removed from the final modal models after the modal analysis, e.g., at the GVT at the correlation station, without resynthesizing the modal parameters of the physical modes. The selection of poles is called the interpretation of the stabilization diagram and is one of the most challenging and user-dependent tasks when performing modal analysis. Figure 2.2c shows an example stabilization diagram of real aircraft data in flight, i.e., the DLR research aircraft HALO [84]. One can see that many spurious modes appear due to the required high model orders (high noise, turbulence excitation only, etc.). In addition, the high modal density leads to merging spectral peaks. A damping ratio plot of the real flight test data is shown in Figure 2.2d. Here, the damping ratios and eigenfrequencies also vary significantly for physical modes. The numerical values of the stabilization diagram data are removed due to confidentiality. However, quantitative results of real aircraft structures are shown in Sections 4 and 5 for GVT and FVT, respectively.

(a) Data flow at GVT   (b) DLR GVT data processing chain
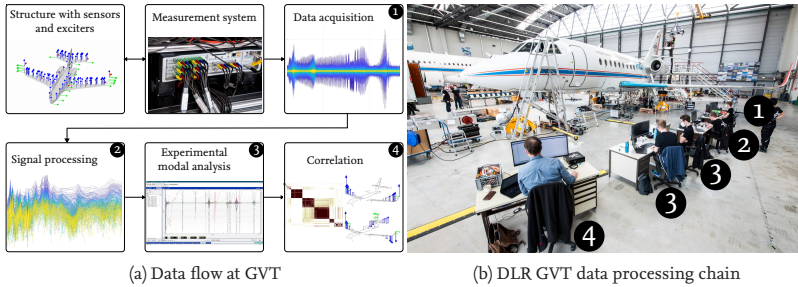
Figure 2.3: GVT onsite data analysis process at DLR

2.2 Ground Vibration Test

The GVT is part of the certification of a new aircraft prototype or significantly modified aircraft [26]. A GVT is performed to identify the complete structural dynamic system of an aircraft in terms of the modal model within the frequency range of interest. The test takes place shortly before the maiden flight of an aircraft prototype. Therefore, the test procedure, as well as the data analysis, is highly time-critical. The DLR vibration test team delivers preliminary modal models to the customer at the end of the measurement campaign of a GVT. This is possible only due to an efficient onsite data analysis chain with several trained engineers. The time pressure, however, must not affect the test accuracy since the final modal model is used for updating the FEM model and for performing the safety-critical flutter analysis. Since the FEM model describes the structural behavior only, the aerodynamic influences on the aircraft are explicitly excluded. For lightweight structures like aircraft, next to the eigenfrequencies, the mode shapes, the modal masses, and especially the damping ratios are essential. Since the correct identification of modal damping is highly complicated and associated with uncertainties, several factors must be considered: optimized excitation, appropriate response sensors (mainly acceleration), and a well-defined analysis process [89]. At DLR, the analysis process is split into four positions. These positions are shown in Figure 2.3. At the first station, the optimized excitation signals are controlled, and the force introduced into the structure, as well as the response signals, are measured in the time-domain (see number 1 in a black circle in Figure 2.3). These signals are checked for plausibility at the second station. The acceleration signal at the excitation point, i.e., at the driving point sensor, is checked to assess the excitation quality and each response signal is checked for loose cables or dropped sensors. The valid signals are transformed to the frequency-domain and FRFs are calculated. For symmetric structures, the single virtual driving point (SVDP) method leads to cleaner stabilization diagrams, simplifying EMA [29]. EMA is performed at the third station. Since the modal analysis station requires the most analysis time, two engineers work in parallel to catch up with the measurement runs. At a GVT performed by DLR, poly LSCF (also known as PolyMAX) (pLSCF) is used as the state-of-the-art EMA method [69]. The modes are selected with engineering knowledge combined with a DLR internal guideline to keep the user-dependency low and achieve the best possible results. The modal models of each measurement run are saved to a database and correlated into so-called mode

families. This is done at the last position of the analysis chain (station 4) with the DLR internally developed correlation tool [15]. All modes that describe the same physical behavior identified in different measurement runs are grouped into a mode family. This creates a complete modal model that includes modes from all excitation positions. In addition, the information from different excitation force levels can be used to quantify the nonlinearity of a mode, i.e., a change of eigenfrequency or damping ratio with increased excitation force. Further details about state-of-the-art methods for GVT of large aircraft are given in [33, 89, 36].

The main challenges remain the user-dependency of the modal analysis station and the increasing time pressure of the analysis. After time data acquisition, the complete analysis chain duration takes between 45 and 60 minutes, depending on the structure, frequency band of interest, and excitation. A typical measurement takes between 15-25 minutes. Sometimes, configuration or excitation changes between measurement runs delay the data acquisition. However, there are circumstances in which even two engineers performing EMA can not fully keep up with the newly performed measurements. In addition to the time challenge, the accurate estimation of damping ratios is challenging. The used EMA method pLSCF is known to be biased in the presence of noise [8, 6]. This bias is usually compensated by adjusting the analysis in order to fit the synthesized spectra of the chosen modal model to the FRFs of the measured data. These results, however, depend on the experience of the engineer.

2.3 Flight Vibration Test

The FVT is performed to demonstrate the absence of flutter (i.e., dynamic aeroelastic stability) in the full flight envelope. For certification of new aircraft prototypes or modified aircraft, the European Aviation Safety Agency (EASA) states, "these tests must demonstrate that the aeroplane has a proper margin of damping at all speeds up to VDF/MDF [demonstrated flight diving speed] and that there is no large and rapid reduction in damping as VDF/MDF is approached"[26]. The instrumentation for a FVT typically consists of acceleration sensors installed inside the wing, the fuselage, and the empennage, as well as a measurement system to record the acceleration signals together with operational and environmental parameters (e.g., flight speed and altitude). In conventional FVT, the structure can be excited artificially with control surface pulses or oscillating control surfaces. Additional possibilities for artificial excitation include the use of inertia shakers, thrusters, or oscillating vanes. Further general information about the FVT process is given in [52, 12, 71, 51]. Already in 1997, the uncertainties of eigenfrequency and damping identifications in flight are described as a critical research topic [12]. The authors describe the main challenges as poor excitation, inconsistent results from time, frequency, or wavelet analysis technologies, and difficult flutter prediction. The damping can be estimated using discrete test points with a sufficiently long duration by averaging multiple identifications, increasing the identification confidence. Based on the previous test points, the decision is made to proceed to the next test point. However, predicting critical damping at, e.g., higher flight speeds is not accurately possible. Therefore, transitioning from one test point to the next remains dangerous. Several studies for online or real-time modal parameter identification for FVT have been developed to tackle these dangers [54, 43, 24, 101]. The excitation frameworks mentioned above enable the utilization of input-output system identification

methods. The effect of excitation from aerodynamic turbulence is considered noise in this approach; therefore, turbulent airflow should be avoided. The different excitation types have different disadvantages, namely:

- Control surfaces: Mainly excitation of low-frequency modes. Those can be well identified from turbulence, and the additional excitation leads to overlay and hiding of responses of modes with higher frequencies.

- Additional hardware such as inertia exciters, thrusters, or oscillating vanes add masses to the structure, and oscillating vanes change the aerodynamics of the aircraft.

- The inevitable aerodynamic turbulence reduces the identification accuracy in the input-output framework [101].

In [68], the application of output-only methods for FVT has been compared to the conventional input-output framework. This paper concludes that the identification of damping ratios shows, in general, high uncertainties. Another comparison of output-only and input-output in-flight modal parameter identification is presented in [57]. Here, the authors state that the results identified from input-output data show higher accuracy for short data sets, but the advantage decreases with bigger data sets. However, in [47], the authors state that OMA and excitation from turbulence are suitable for real-time flutter assessment. In [39], a combination of unknown and partly known excitation is described as OMAX. The output-only framework is applied at DLR to avoid the disadvantages mentioned above of artificial excitation [79, 78, 37, 83, 49]. In [4], the continuous identification and tracking of modal parameters are tested with simulation data as an alternative test procedure to step-wise air speed increases. The authors conclude that tracking eigenfrequencies and damping ratios is possible for slowly varying systems. Still, estimating the damping ratios is difficult and, therefore, shows significant uncertainties. Similar findings are in [48], here LTV system formulations are presented, which can be used for simulation. It is shown that a slowly time-varying system can be identified using a LTI identification method if the system variation can be considered as "slow". It is shown in [48] that an aircraft during FVT can be assumed to be slowly time-varying and identified by continuous OMA. Analytical solutions for system identifications of LTV structures result in complex formulations that cannot be solved in real-time. Therefore, the iterative identification of LTV systems using LTI identification method is the state-of-the-art to enable real-time monitoring of aeroelastic behavior. The main challenge of online identification and monitoring of modal parameters for LTV systems remains the low reliability and high identification uncertainty.

The conduction and analysis of FVT remains an ongoing research topic. In this thesis, artificial excitation hardware is not applied to keep the test object as close as possible to the real aircraft. Therefore, real-time system identification using OMA methods will be the basis for this thesis. In current certification processes, artificial excitation is required. However, the OMA framework can also be applied if the excitation is a broadband random signal.

2.4 Automated Modal Parameter Identification

Automatic modal parameter identification, or autonomous modal analysis (AMA), describes the process of evaluating measurement data from a vibration test without user intervention. In modal analysis, most user interaction typically involves selecting appropriate hyperparameters (e.g., model orders, Hankel matrix sizes) and interpreting the stabilization diagram. In literature, the automated evaluation or interpretation of the stabilization diagram is primarily conducted following the steps:

1. Distinction of physical from spurious poles

2. Clustering of unique and physical modes

3. Improvement and selection of mode clusters

4. Selection of a representative mode per cluster

As there are now numerous publications in this field, the literature is summarized below based on how they address the aforementioned steps. An alternative approach to reviewing the literature regarding AMA is presented in [42]. In this work, the authors categorize AMA methods into different grouping categories, including hierarchical clustering, partitioning, and histogram analysis. However, this categorization primarily pertains to the second step of the overall AMA process.

Before poles in the stabilization diagram are clustered, so-called mode validation criteria are applied pole-wise to discriminate between spurious poles and potentially physical poles, as described in [100]. Commonly used validation criteria are modal phase collinearity (MPC) [64], mean phase deviation (MPD) [75] and the mode shape mode indicator function according to Breitbach [11]. Since a mode indicator function (MIF) exists as a function for spectra to indicate the location of a mode, the mode shape-related function is indicated by MIF_ψ. The MPC describes the degree of complexity of a mode shape by the linear relation between the real and imaginary parts

$$MPC(\psi) = \frac{\left(\Im(\psi)^T\Im(\psi) - \Re(\psi)^T\Re(\psi))^2 + 4(\Re(\psi)^T\Im(\psi)\right)^2}{(\Im(\psi)^T\Im(\psi) + \Re(\psi^T\Re(\psi))^2} \ . \tag{2.32}$$

The MPD describes the complexity of a mode shape by the standard deviation of the phase angles of the complex mode shape coefficients

$$MPD(\psi) = \sqrt{\frac{\sum\limits_{j=1}^{M}\left[w_j\left(\varphi_j - \frac{\sum\limits_{k=1}^{M}w_k\varphi_k}{\sum\limits_{k=1}^{M}w_k}\right)^2\right]}{\sum\limits_{j=1}^{M}w_j}} \ , \tag{2.33}$$

where w_j is a factor to weight the importance of individual degrees of freedom (DoFs), in this thesis $w_j = |\psi_j|$. The phase angle φ_j of each component is given by

$$\varphi_j = \begin{cases} \arctan\left(\frac{\Re(\psi)}{\Im(\psi)}\right) & , if \quad \arctan\left(\frac{\Re(\psi)}{\Im(\psi)}\right) \geq 0 \\ \arctan\left(\frac{\Re(\psi)}{\Im(\psi)}\right) + \pi & , if \quad \arctan\left(\frac{\Re(\psi)}{\Im(\psi)}\right) < 0 \end{cases} \ . \tag{2.34}$$

The MIF$_\psi$ is usually used during phase resonance testing to detect the eigenfrequencies of a structure. In that application, the function is applied to the complex response amplitudes. However, it can be applied to complex mode shapes to provide a measure of the mode shape complexity

$$MIF_\psi(\psi) = 1000 \cdot \left(1 - \frac{|\Im(\psi)|^T |\psi|}{\psi^H \psi}\right) \quad . \tag{2.35}$$

Two common methods for this discrimination are using a threshold or employing 2-means clustering. Table 2.1 provides an overview of different methods. In general, quality metrics assess the stability of modal parameters with increasing model order or checking the mode shape complexity. Setting thresholds for these metrics requires user expertise. Some methods utilize 2-means clustering (c-means clustering with c equal to 2) to automatically distinguish between spurious and physical poles to avoid the limitations of threshold-based discrimination. However, it is important to note that 2-means clustering divides the solution space into two convex clusters. The suitability of convex clusters for the distinction between physical and spurious poles cannot be guaranteed. Additionally, c-means clustering is sensitive to outliers, as outliers can pull the cluster centers away from the desired centers. Such outliers are expected for spurious poles.

Methods	Quality metrics	Reasoning	Drawbacks	Ex.
Threshold	Stability of f, ξ and ψ for increasing model order	• Structural modes appear similarly at different model orders • Reliability	Thresholds depend on the type of the structure and test conditions.	[34, 59, 93, 81, 91]
Threshold	MPC or MPD	Spurious modes tend to be highly complex	• Structure dependent • Weakly excited modes may vanish • ψ changes for LSCF with pole selection	[91, 16]
2-means	MPC or MPD	Group modes of low and high complexity	• Modes that are more complex than others vanish • Weakly excited modes may vanish • ψ changes for LSCF with pole selection	[75, 5, 98, 23]

Table 2.1: Distinction of physical from spurious poles

In the second step, the poles which belong to the same physical mode are clustered. The clustering methods are summarized in Table 2.2. Some methods apply a sort of hierarchical clustering with different distance criteria. The similarity of distinct mode shapes is often calculated with the modal assurance criterion (MAC). The MAC describes the collinearity of mode shapes

$$MAC(\psi_i, \psi_j) = \frac{(\psi_i^T \psi_j)^2}{(\psi_i^T \psi_i)(\psi_j^T \psi_j)} \quad . \tag{2.36}$$

The methods differ slightly from classical hierarchical clustering. However, their overall logic can be described as follows: In the beginning, each pole is its own cluster. Clusters

are merged until no pair of clusters has a distance less than a threshold. This threshold can be set manually; another approach is to extract it from the previous distinction of spurious and physical poles. For example, in [75], the mean and standard deviation of the change of the eigenvalue λ and the modal assurance criterion (MAC) [1] value between physical poles with increasing model orders are used to define the distance threshold for hierarchical clustering. This approach saves one hyperparameter at this stage, but it ties the distinction of modes to the stability criteria. Consequently, it limits further fine-tuning and creates an interdependence between two hyperparameters. For complex structures, physical modes may split into two or more vertical lines in the stabilization diagram for high model orders. The stability thresholds would split these lines into distinct mode clusters. A second type of grouping method is based on fuzzy c-means clustering (see partitioning methods in [42]). Poles are assigned to the closest center point based on initial cluster centers. After the cluster centers are adjusted with respect to the new samples, the next poles are iteratively assigned. The enhancement of fuzzy c-means clustering with respect to standard c-means clustering is that it allows all poles to have probabilities of being part of a specific cluster instead of an absolute membership. Nevertheless, the main drawback is that the number of clusters (i.e., physical modes) needs to be known beforehand, and the success of the method depends on the initial centers since bad initial clusters lead to local optima. In [80], an enhanced version of fuzzy c-means clustering can merge similar clusters, thus reducing the number of initial clusters. In addition, the initial points are optimized using a genetic algorithm to reduce the dependency on the initial cluster centers. The additional steps could improve the results for [80]. However, the computation time was significantly increased from 15 seconds for the classic fuzzy c-means clustering to about 45 seconds. This is expected since genetic algorithms are known to have a long run-time. The third clustering method is based on histograms in frequency. The idea follows the rule: the more poles accumulate at a small frequency range, the more likely they belong to a physical mode [34]. This method is time efficient but cannot distinguish modes with almost the same eigenfrequency. The last clustering approach applies density-based clustering for applications with noise (DBSCAN) [27] to λ and ψ [91]. DBSCAN is usually faster than, e.g., hierarchical clustering. It requires a threshold to define the maximal distance between points to be placed in the same cluster and a threshold of minimal points per cluster. It is difficult to find these hyperparameters in such a way that no physical mode is removed, but most spurious modes are removed. In [31], a manual modal analysis result is used to learn one threshold for hierarchical clustering. This optimization of one hyperparameter is a good approach. However, no further hyperparameters have been addressed.

In the third step, the clusters of modes are further investigated. In many papers, the clusters are removed that have fewer members than a threshold value (see, e.g., [49, 75, 100, 93, 16]). Clusters with very few poles are certainly not physical, but clusters of weakly excited physical modes may also have significantly fewer poles than well-excited ones. Of course, this also depends on the choice of identification bands (i.e., whether the mode is centrally located in the identification band) and the model order (at lower model orders, only the dominant modes are present in the identification band). Therefore, this threshold should be used with caution. Some papers apply 2-means clustering of cluster sizes to distinguish physical and spurious clusters similar to the approach in the first clustering step [75, 23]. However, in this case, 2-means clustering does not guarantee the finding of an optimal

Methods	Distance metrics	Reasoning	Drawbacks	e.g.
Hierarchical clustering	λ, ψ	Each mode is unique combining λ and ψ.	• Complex structures show higher scatter of λ in the stabilization diagram which requires a low threshold • Closely spaced modes require a high threshold	[49, 75, 5]
Hierarchical clustering	f, ψ	In reality, each mode is unique for most applications, combining f and ψ.	See above for λ, ψ, although the scatter of damping is assumed to be higher than for f only	[93, 16, 23, 65, 56]
Partitioning methods, i.e. Fuzzy c-means	f, ξ	Easy to use with a limited amount of sensors, i.e. poor mode shape information	• Problematic for closely spaced modes • Depends on good initial points	[18, 80, 98]
Histograms	f	Modes appear as vertical lines in stabilization diagram	Problematic for closely spaced modes	[34, 59]
DBSCAN	λ, ψ	Each mode is unique combining λ and ψ	Difficult to find optimal hyperparameters, see drawbacks of hierarchical clustering	[91]

Table 2.2: Clustering of unique modes

threshold. The clusters themselves are often not further improved. An exception can be found in [5]. To remove outliers, the authors perform DBSCAN on eigenfrequencies and damping ratios for each cluster. This approach is reasonable but relies on λ (eigenfrequency and damping ratio) only.

The fourth step has often been neglected in the literature so far. For the final modal model, most papers choose a pole close to the median damping ratio and eigenfrequency (see e.g. [91, 16, 5]), highest MPC [75] or stable damping increasing the model order [34, 59, 81] for each cluster. Since some MIDs can be biased in the presence of noise [8, 6], one can assume that the clusters based on these estimates are also biased. This means that the median values cannot be considered optimal either. In [50], the authors present a method that optimizes the modal model such that the synthesized spectra fit best to the measured spectra. The optimization is gradient-based by changing all modes simultaneously. This gradient-based approach can lead to local optima, as Section 3.3.1 shows. The optimization of well-excited modes has a more significant impact on the gradient-based spectral optimization than weakly excited modes. However, this approach can potentially overcome a bias of MIDs.

2.5 Automated Modal Parameter Tracking

Identifying modal parameters based on measured signals is a major part during GVT and FVT. In FVT, tracking the identified modal parameters is also important since the modal parameters change with the flight condition, such as, e.g., the altitude and flight speed. A modal model is identified based on measured signals at a specific point in time. At a later point in time, the identification is repeated to assess the change of modal parameters. To evaluate the change of modal parameters, modes of a modal model at time $t = k$ have to be correlated to modes identified at previous times $t < k$. This is usually done by evaluating a distance between two modes with a threshold, where the distance is calculated based on λ, the MAC-value, expanded modal assurance criterion (MAC-XP)-value [94] or a combination of the characteristics mentioned above (see examples in [22, 100, 56, 73, 30, 78, 49, 17]). The main challenges named in literature regarding modal parameter tracking of a varying structure are:

1. Limited number of sensors leads to poor mode matching using MAC

2. Some modes might be missing in the identification for some time-steps

3. Some modes cross in frequency due to changing conditions

4. Modal parameters identified from OMA show significant scatter

While some of the methods compare newly identified modes with a static reference modal model (mainly for structural-health-monitoring) [56, 30], others adjust the threshold or distance metric [17, 73] or compare new modes with an updating reference modal model, i.e. from the near past [78, 49]. The mode matching problem has received attention, which led to appropriate methods for aircraft FVT using a sliding reference set of each mode family for e.g., the MAC-XP comparison [48]. Unfortunately, the challenge of high scatter in modal parameter tracking from OMA has been addressed inadequately so far. An exception can be found in [70], where the authors use the standard deviations of the identification to remove highly uncertain identifications from the tracking. However, the uncertainty is used only for cleaning. In [87], a system is presented that incorporates information on previous time steps and builds a statistical model of the environmental influences on the structure. A KF is applied to fuse the statistical model, the current environmental information, and the current identification output. The system has its strength in long-term monitoring, i.e., months or years, of changing structural behavior because sufficient data is required to build a good statistical model. The method is applied to the structural dynamics of a ship and differs from applications in this work. Nevertheless, using formerly gained information about the structure is noteworthy.

2.6 Conclusion and Research Questions

In conclusion, the literature review has highlighted several key aspects of aircraft modal parameter identification, with a particular focus on GVT and FVT techniques. The state-of-the-art GVT analysis has proven to be a valuable tool for efficient structural identification, offering valuable insights into the dynamic behavior of an aircraft structure. However, it is worth noting that GVT analyses can still be user-dependent and time-intensive.

Additionally, the reproducibility of GVT analyses remains an area of consideration, and achieving high accuracy in damping estimation can be challenging using state-of-the-art methods. Online OMA as a real-time identification method for FVT is an interesting avenue for structural assessment. However, significant scatter in FVT results and the absence of precise and online-capable automation solutions (requiring computations within a two-second time frame) emphasize the need for further research and innovation in this domain.

Building upon the insights from the literature review, this research seeks to explore the potential advancements in aircraft modal parameter identification using AMA for GVT and FVT. The research questions that arise from this investigation are as follows:

1. How can AMA be optimized to achieve a high identification accuracy for efficient aircraft modal parameter identification during GVT and FVT?

This question addresses the potential for optimizing AMA by tuning all relevant hyperparameters, specifically for aircraft testing, to achieve more reliable and efficient identification of modal parameters.

2. How can the application of optimized AMA in the analysis chain enhance the automation and standardization of GVT analysis, minimizing user-dependency and increasing reproducibility?

This question focuses on the hypothesis that applying optimized AMA methods in GVT can result in faster results and less reliance on the expertise of individual engineers, ultimately leading to more consistent outcomes across different users and tests.

3. Can optimized AMA be applied in real-time FVT analysis to identify and track all relevant modes with reduced scatter?

This question investigates whether a unified AMA-driven approach enables the fusion of results from multiple MIDs, thereby identifying all relevant modes, reducing the scatter, and improving the confidence in the identified modal parameters in FVT.

By addressing these research questions, this study aims to contribute to the advancement of automated structural dynamic and aeroelastic system identification techniques, with a particular emphasis on improving accuracy, reproducibility, and efficiency in both GVT and FVT analyses.

3 Autonomous Identification and Fusion of Modal Parameters

3.1 Introduction to AMA

Modal analysis is a core application within experimental structural dynamic and aeroelastic identification. The data obtained through GVT and FVT can be analyzed for modal parameters using EMA and OMA techniques, respectively. Increased utilization of AMA is proposed to enhance the efficiency and user-independency of these analyses. In the state-of-the-art, this primarily pertains to the interpretation of the stabilization diagram, aimed at extracting the physical modes and establishing a consistent modal model.

To apply these methods in safety-critical contexts such as GVT and FVT, several challenges identified in Section 2 concerning AMA need to be effectively addressed. These challenges, still underrepresented in the literature, encompass the following:

- Ensuring the completeness of modal models, including weakly excited modes, while minimizing the retention of spurious modes

- Maintaining the analysis accuracy at a level equivalent to that of an experienced engineer

- Precise identification of the damping ratio by optimization of the synthesized spectra

- Establishing a methodology for achieving high reproducibility across numerous tests without the need for manual adjustments of several hyperparameters

- Consideration of significant uncertainties of the identifications in tracking

Hence, this chapter introduces a multi-tier clustering tailored for aircraft identification, explicitly focusing on comprehensive modal identification and precise damping estimation. Moreover, an additional step is incorporated to optimize the modal models, mitigating potential biases introduced by the MID. The modal models are optimized either using particle swarm optimization (PSO) and the synthesized spectra for EMA or using estimated identification uncertainties and data fusion approaches, i.e., inverse-variance mean (IVM) and Kalman filter (KF), for OMA. The data flow of the method is visually depicted in Figure 3.1.

The individual steps of the AMA method are shown with an example data set of the DLR laboratory aircraft model (AIRMOD) [34]. This beam model with structural properties similar to an aircraft was extensively tested in [34], so reference is made to this work for further information. A raw stabilization diagram of a measurement run with measured random broad-band excitation force is given in Figure 3.2. As with actual modal tests, there are different identification bands with different model orders, e.g., the lowest identification band below 14 Hz has a lower maximum model order than the others. This example is analyzed step by step using the presented AMA method in the following sections.
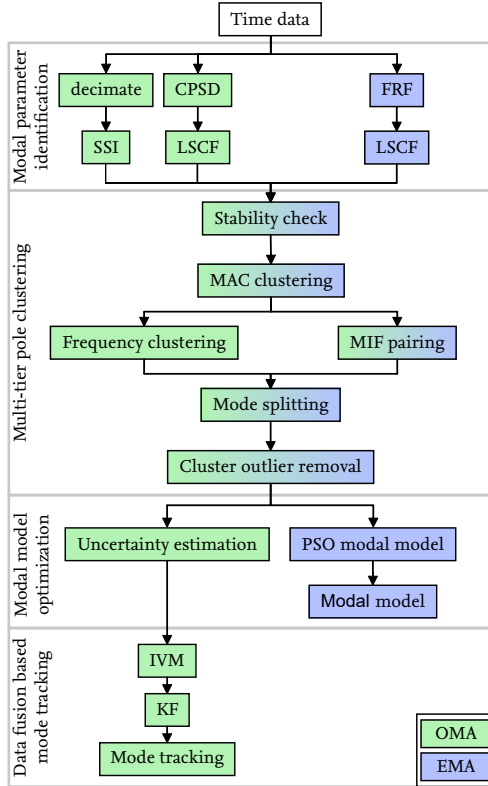
Figure 3.1: Data flow diagram of the presented method

3.2 Multi-tier Pole Clustering

The clustering of poles in the stabilization diagram is the core task of most AMA methods (see Section 2.4). Most methods are used to identify mainly the dominant modes. Often, the focus is on identifying the eigenfrequencies. Therefore, the clustering in this work consists of several clustering steps to carefully fulfill the first three of the four steps from Section 2.4. The fourth step, i.e., the modal model optimization, is explained in Section 3.3.

3.2.1 Distinction of Physical from Spurious Poles

The initial step of AMA clustering involves identifying and discriminating spurious poles. Spurious poles manifest in the stabilization diagram due to over-fitting caused by high model orders. The basic assumption of the stabilization diagram is that poles of physical modes show similar modal parameters with increasing model orders. This stabiliza-
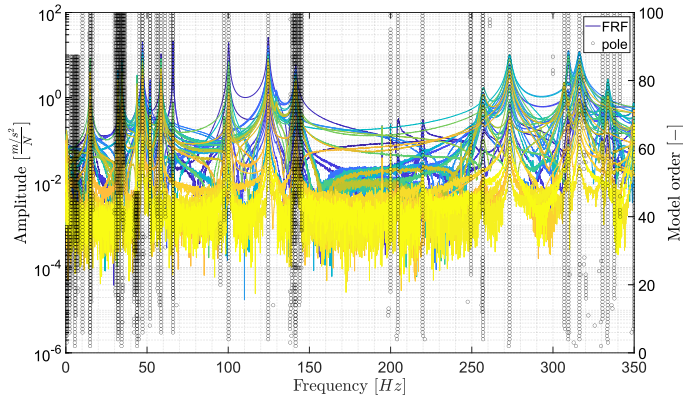
Figure 3.2: Example raw stabilization diagram based on pLSCF from laboratory aircraft model (AIR-MOD)

tion criterion has become an established standard by common practice. Therefore, this is also applied in the automated analysis chain. Starting with the lowest model order, it is checked when increasing the model order that a corresponding pole in the previous model order has similar modal parameters, including eigenfrequency, damping ratio, and mode shape vector. In literature, the tolerated deviation often is 1% in eigenfrequency, 5% in damping ratio, and 2% in mode shapes [95]. The stabilization diagram of the example data set cleaned by those stability thresholds is shown in Figure 3.3. Compared to Figure 3.2, spurious poles are removed at, e.g., about 300 Hz. However, some potentially spurious poles remain, e.g., at 330 Hz and model order 20, which are cleaned in subsequent steps.

3.2.2 Clustering of Physical Modes

In the second step, the stable poles are categorized into clusters based on their similarity in mode shapes, potentially indicating their association with the same mode. This grouping is achieved through the application of DBSCAN, where the distance measure between two poles relies on the MAC value of the corresponding mode shapes as $(1-\mathrm{MAC}(\psi_i, \psi_j)$. When applied to the example data, this results in the creation of expansive clusters, as illustrated in Figure 3.4. Mode clusters are illustrated as different colors. Notably, this approach combines columns of poles with differing eigenfrequencies; a situation typically avoided in the existing literature by incorporating eigenvalue information in this clustering step. However, this thesis uses the eigenvalue explicitly in the subsequent step. The rationale behind this choice is that poles featuring complex mode shapes and slight variations in eigenfrequency and damping would otherwise necessitate small threshold values for clustering. Furthermore, a mode that splits into two columns as the model order increases would be inaccurately distributed into two distinct mode clusters.

Since different modes with similar mode shapes have been falsely grouped, a further step is required to separate them. One approach is to conduct additional clustering based on
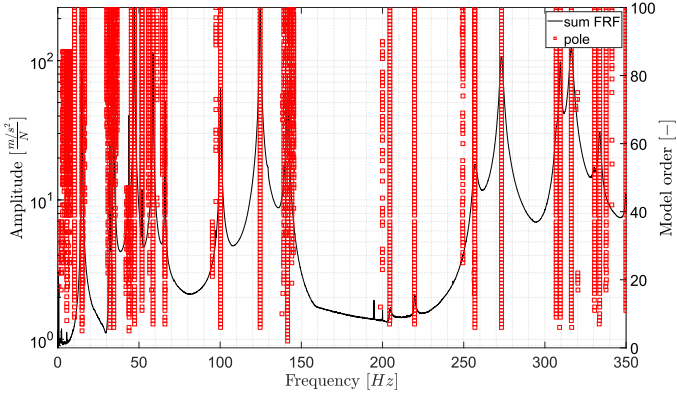
Figure 3.3: Removed unstable poles from stabilization diagram
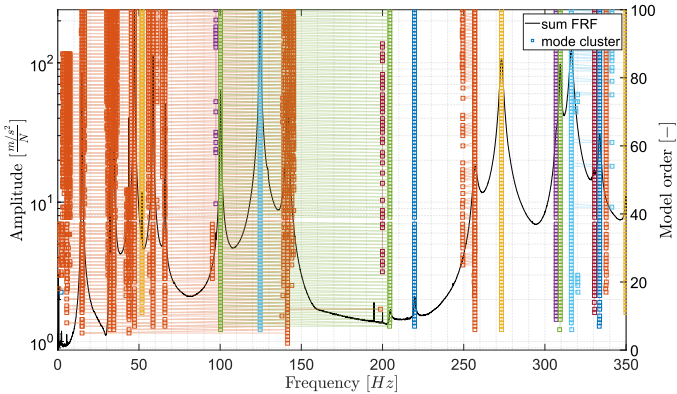
Figure 3.4: Stabilization diagram after clustering based on MAC

either frequency or the complex eigenvalue. It allows for a subsequent clustering to be performed for each cluster. This approach is well suited for the OMA application. For application in the EMA case, the so-called mode indicator function (MIF) [44] can be utilized, a method commonly employed in manual stabilization diagram analysis. In Figure 3.5, the example dataset is shown with the multivariate MIF (MMIF)[107]. Within a cluster, all poles must be closest to the same local MIF minimum and within a small region around the minimum. Therefore, if an entire cluster is located too far from any MIF minimum, it is identified as spurious and removed. The approach is, in fact, similar to the manual workflow for modal analysis. This step separates different clusters with similar mode

shapes and eliminates poles or entire clusters that cannot be associated with any MIF minimum. For example, in Figure 3.4, a second column of poles is assigned to the mode at approximately 256Hz. However, since the left column of this cluster lies outside the MIF minimum range, it is removed as shown in Figure 3.5a. In Figure 3.5b, the frequency range between 30 and 55 Hz is shown which has a high modal density, demonstrating that the modes can be effectively separated by the MIF minimums in this area as well. Besides
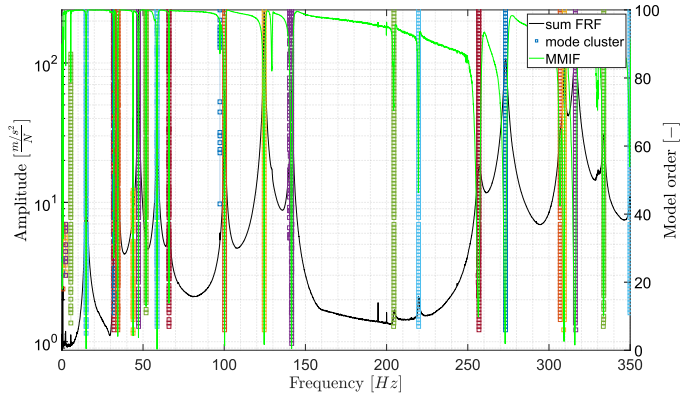
(a) Full frequency analysis band
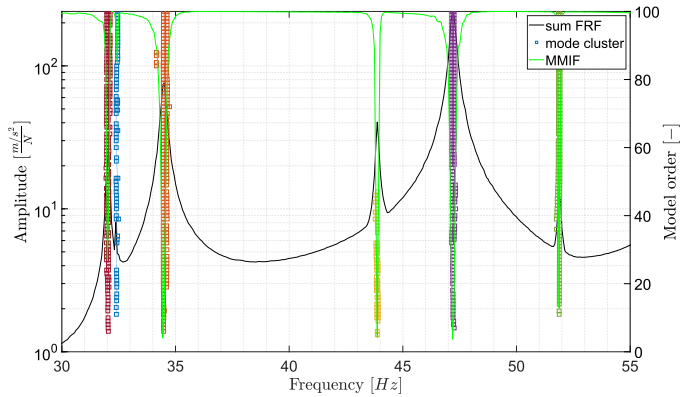
(b) Zoom to frequency band with high modal density

Figure 3.5: Stabilization diagram after cluster MIF peak pairing

the MMIF, there exist other MIF functions like the complex MIF (CMIF)[82] or real MIF (RMIF)[72], which can be applied in an analog manner, each with its strengths and weaknesses. This thesis employs multiple MIF functions in parallel. While the MMIF can be

applied to EMA solely, the CMIF can be utilized for both EMA and OMA. However, the results obtained with CMIF-peak-pairing in OMA data are not always optimal. Depending on the structure and data condition in the OMA case, the re-clustering using eigenvalues or pairing with CMIF-peaks can be more suitable. In contrast, EMA yields highly reliable results when paired with multiple MIF functions.

3.2.3 Improvement of the Physical Mode Clusters

Depending on the excitation situation (artificial or ambient), specific modes may experience stronger excitation than others. Consequently, weakly excited modes are often identified only at high model orders. The necessarily high model orders can lead to some modes being identified multiple times per model order. The redundant identification, in turn, leads to the fragmentation of mode clusters into two or more columns within the stabilization diagram, exemplified by the mode at approximately 47.2 Hz in Figure 3.6a. As in manual analysis, this split must be detected, and the mode must be determined from a model order below the split-up point. In the provided example, all poles exceeding model order 31 are removed (as denoted by the red dashed line). In a second step, the internal

(a) Mode splitting with high model orders

(b) Multi-dimensional outlier detection for each mode cluster
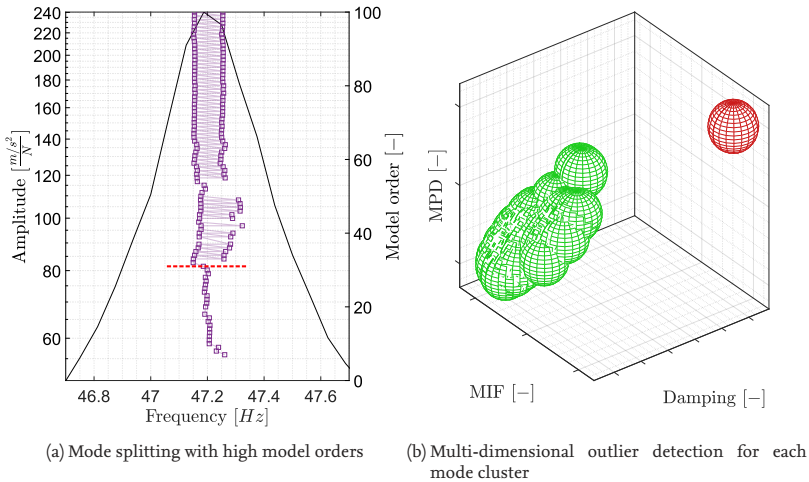
Figure 3.6: Cleaning steps of each physical mode cluster

consistency of each cluster is assessed in detail by explicitly conducting another DBSCAN analysis using multiple dimensions for each cluster. This new clustering can involve dimensions like damping ratio, MIF_ψ, and mean phase deviation (MPD). For instance, in mode cluster 18 at about 140 Hz of the example dataset, certain outliers can be effectively removed, as demonstrated in Figure 3.6b. While this additional clustering may seem redundant in theory compared to previous clustering steps, it intentionally introduces additional hyperparameters, adding fine-tuning mechanisms to enable the careful detection of

outliers. After this step, mode shapes can be checked with respect to their complexity using MIF$_\psi$, MPC, MPD, and corresponding thresholds. Highly complex mode shapes can be assumed to be spurious. However, this should be checked cautiously, as complex mode shapes can be physical for some structures. After the multi-tier clustering, very small clusters can be removed, a practice commonly found in various existing methods. The notable advantage of the proposed method lies in its accurate cleaning process, permitting the selection of a very low cluster size threshold. The outcome of the mode clustering process
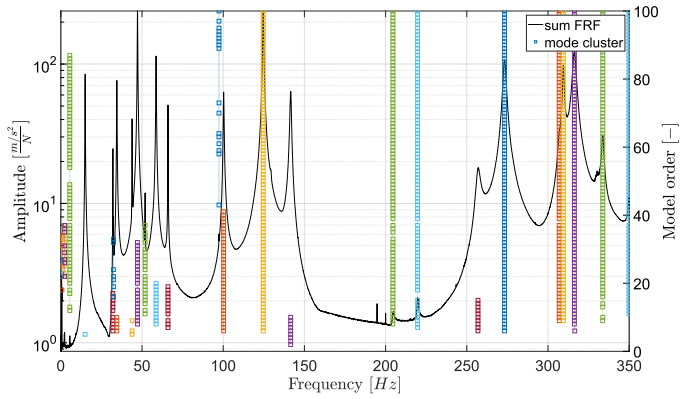
Figure 3.7: Stabilization diagram after multi-tier clustering

is illustrated in Figure 3.7. Some clusters consist of only a few poles due to the cut at a low model order to avoid the splitting of the cluster; see Figure 3.6a. Nevertheless, this is not a significant concern, as the modal model will undergo further optimization in Section 3.3.

3.3 Modal Model Optimization

In literature, the modal model is built using the median values of a cluster [16, 5, 91], high MPC values [75] or modes with most stable damping over the model order [34, 59, 81]. Since some MIDs can have a bias in the presence of noise [8, 6], also cluster centers can be biased. Therefore, the final modes should be chosen more carefully. Optimization of the modal model is an ongoing research topic. In principle, the goal is that an identified modal model should represent the structural dynamic properties of the physical structure as closely as possible. Therefore, the spectra synthesized from the modal model should match the measured spectra from the physical structure. Another aspect is that the modal parameters identified from measurement data should have as little uncertainty as possible. Although measurements are always noise-related, multiple identifications of the same system should result in similar modal models. Since different assumptions are made for EMA and OMA during the identification, two approaches are presented in the following subsections for optimizing the modal model.

3.3.1 Spectra Synthesis Optimization

For EMA, the measurement uncertainties are low thanks to complete control over the excitation and, consequently, good signal-to-noise ratio of excitation and response signals in a laboratory environment. Therefore, it can be assumed that the measured time signals and subsequent FRFs calculated from them are reasonably accurate. Thus, for EMA, the modal model is adapted so that spectra synthesized from the identified modal model match as closely as possible to the FRFs of the measured data. The synthesis of the spectra is carried out by LSFD [96]. A pole-residue model is fitted to the estimated spectra. The residuals can be calculated in the least-squares sense if the poles are known. For the mathematical formulation, reference is made to [96]. In practice, poles are chosen from the stabilization diagram, and spectra are synthesized using the LSFD method. Two examples of synthesized spectra for the AIRMOD dataset are given in Figure 3.8. Here, the summed FRFs from the measured data (in blue) and the summed FRFs synthesized using LSFD (in green) are shown. The absolute difference between the two curves is highlighted in red. Hereafter, the absolute value of this area is referred to as spectra synthesis error. In Figure 3.8a, the pole of the right-hand side mode is selected with a too-low eigenfrequency and too-high damping ratio. Therefore, the synthesis error is high. In the second example in Figure 3.8b, the mode selection is optimized, and the synthesis error becomes negligible. One can reformulate the problem so that the difference between the FRF_{synth} and

(a) The pole of the right hand side mode is non-optimally selected.

(b) The pole of the right hand side mode is optimally selected.
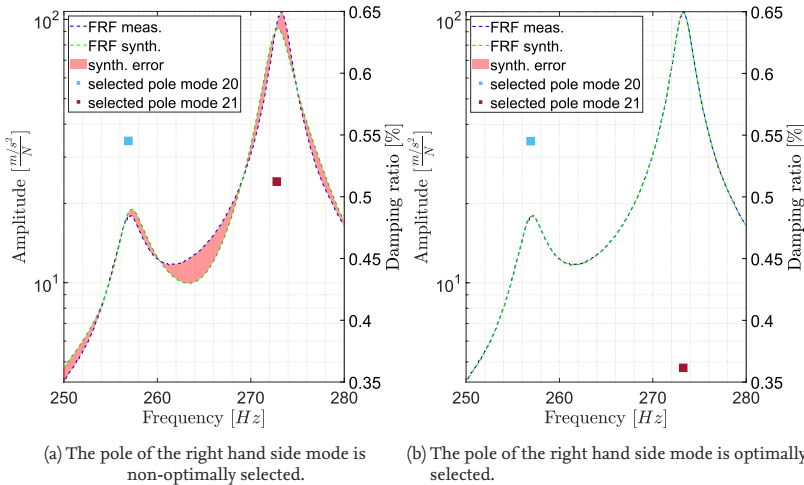
Figure 3.8: Synthesized FRFs using LSFD

FRF_{meas} is minimized gradient-based by adjusting all modes of the modal model. This method is called the maximum likelihood modal model (ML-MM)[50]. In this method, all poles are adjusted together to optimize the spectra of the entire frequency range. Figure 3.9a shows a mode cluster of a seven DoFs simulated data set based on LSCF. The simula-

tion system is described in more detail in Section 3.6.1. The synthesis error of eigenvalue estimates for this mode is shown on the z-axis. It can be seen that the analytical solution is not found by the LSCF mode cluster. Additionally, a grid is plotted for theoretical eigenfrequency and damping ratio points (i.e., theoretical poles) in the surrounding area. It can be seen that the eigenfrequency and damping ratios close to the analytical solution have minimal spectra synthesis errors. Since noise is added to the simulation data, the synthesis error is always greater than zero. Nevertheless, the solution can be found if the poles are optimized to minimize the synthesis error. This example is also shown in two dimensions in Figure 3.9b. One can see that the variation of the damping ratio has the most significant effect on the spectra synthesis error because the variation of eigenfrequency is negligible. In these plots, however, it is assumed that the other modes of the modal model are from the analytical solution. In reality, however, these are also estimated from the stabilization diagram, i.e., from non-optimal mode clusters. If one now calculates the synthesis error for the same mode with random poles of the other mode clusters for the synthesis of the spectra, one obtains the plot in Figure 3.10. While the global minimum of the synthesis error is close to the analytical solution, many local optima exist. Therefore, a gradient-based method would lead to a local optimum.

In this thesis, the modal model is therefore optimized using a gradient-free approach. In

(a) 3D view of a grid with changing eigenfrequencies and damping ratios

(b) 2D view with constant eigenfrequencies
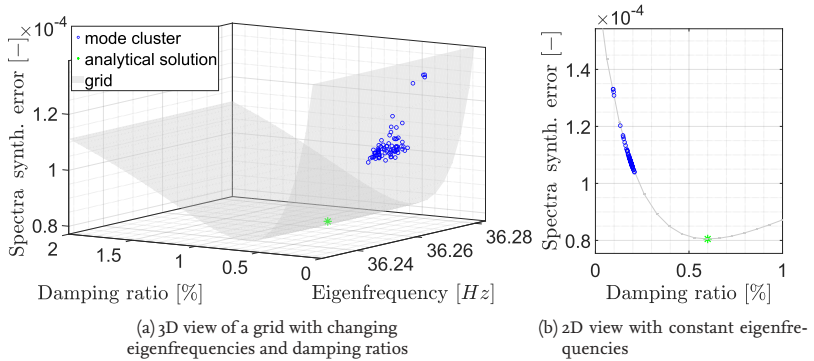
Figure 3.9: Spectra synthesis error for one mode cluster if all other modes of the modal model are from the analytical solution

addition, only the relevant frequency ranges close to the eigenfrequencies are optimized instead of the whole frequency band. In frequency ranges without modes, the signal-to-noise ratio is generally poor (smaller signal amplitudes), and therefore, curve fitting is less meaningful. The $-6\,dB$ range around the spectra peak can be chosen as the relevant range around the mode. An example is shown in Figure 3.11. The synthesis errors for the local and whole frequency ranges are calculated and displayed in the upper right corner of the plot. The area outside the peak strongly influences the synthesis error of the entire frequency range since it is more than twice as big as the local error. The total synthesis error of a modal model is the sum of all local synthesis errors of the modes. The local synthesis errors of the modes can be normalized using the amplitude of the spectra peak to avoid domination of well-excited modes. Based on the synthesis errors of all poles,
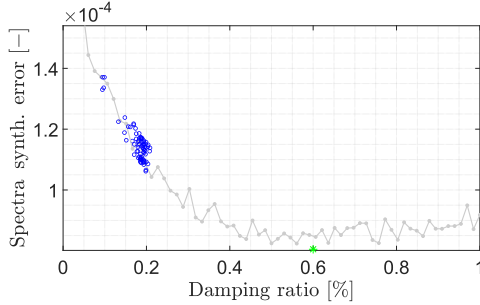
Figure 3.10: Spectra synthesis error for one mode cluster if all other modes are experimentally identified
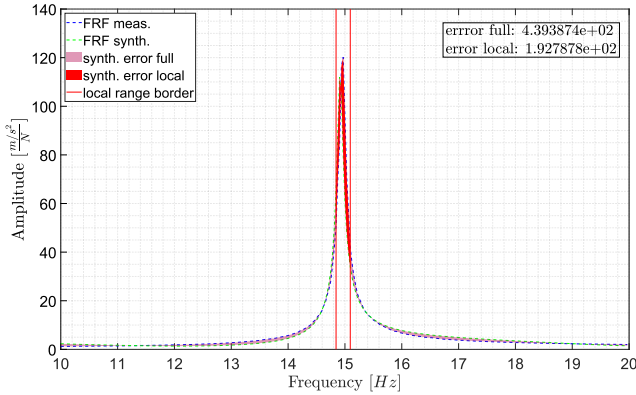
Figure 3.11: Local range for cluster-based synthesized error calculation

the modal model is now optimized with particle swarm optimization (PSO) [53]. PSO is a swarm intelligence-based optimization algorithm. It simulates the social behavior of particles in a population, where each particle adjusts its position based on its own experience and the experiences of its neighbors, collectively exploiting swarm intelligence to converge towards the global optimum in the search space. For modal model optimization, each particle consists of two dimensions for each mode, i.e., for the eigenfrequency and damping ratio. Figure 3.12 shows an example in which the parts of one mode of a particle are shown. One can see that different particles have different paths to explore the solution space. However, the swarm converges towards the analytical solution in total. In principle, this procedure is also possible with CPSDs and thus also suitable for OMA. In this work, however, it is assumed that the data quality for OMA in FVT is poorer than for EMA in GVT for various reasons. Therefore, optimizing the modal models for FVT is

(a) 3D view of the particles optimizing the modal model

(b) 2D view
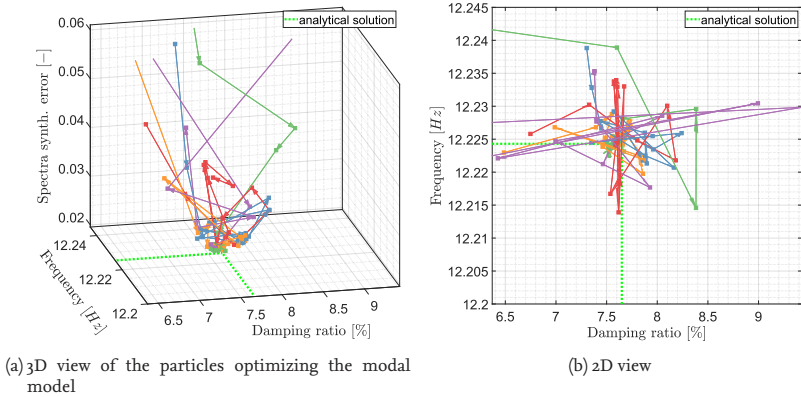
Figure 3.12: PSO modal model optimizing the spectra synthesis error

realized by combining several identifications with the help of estimated uncertainties instead of optimizing a single data set based on measured data. The uncertainty estimation is described in Subsection 3.3.2.

3.3.2 Qualitative Uncertainty Estimation of Modal Parameters

Because of a low signal-to-noise ratio, non-stationary excitation, and high differences in modal damping when approaching the flutter stability boundary (e.g., one percent for one mode and 30 % for another mode), the overall data complexity in FVT is higher than in GVT. Therefore, an alternative perspective for modal model optimization is described for application in the OMA framework. Moreover, the iterative approach of modal model optimization in PSO is not applicable for real-time application in FVT. However, in FVT, the identification results are continuously available, and multiple MIDs can be used in parallel. The uncertainties of the modal parameters are valuable in allowing the assessment, comparison, and, eventually, combination of multiple identification results. For SSI and LSCF, there are different approaches in the literature to calculate uncertainties. For example, in [76], the uncertainties of SSI are calculated based on the covariances of the identified system matrices. Although in [25] the computational speed of this method was increased, it is still not fast enough to be used for near real-time system identification. In [102], the uncertainties of LSCF are estimated in terms of standard deviations of a mode cluster in the stabilization diagram. The authors have compared these uncertainty estimates with statistical uncertainties obtained empirically with a Monte Carlo simulation. The uncertainties do not exactly match the statistical uncertainties, but the authors state that the approach "provides useful uncertainty bounds"(p. 7 [102]). Additionally, the calculation of cluster-based uncertainties is fast. With the new multi-tier clustering approach of this thesis, clusters can be assumed to be well-conditioned for uncertainty estimation. Even though the uncertainties are not quantitatively exact, the uncertainties of two modal models are comparable when identified with uniformly optimized hyperparameters (e.g.,

model order, size of the Hankel matrix, etc.).

Figure 3.13 shows identified eigenfrequencies and damping ratios from a time-invariant laboratory aircraft structure. The laboratory aircraft structure is presented in [105], the mode shown in Figure 3.13 is the 2n wing bending at 26 Hz. The modal parameters of the system are identified 1000 times based on small time sequences, i.e., 40-100 s, with small time shifts of two seconds. In theory and without noise, all those identifications should result in the same modal parameters. Because of the noise of, e.g., the measurement, the identifications show scatter. The identification results are black dots, forming an ellipsoid of empirical scatter or variance. The uncertainty is additionally estimated using the cluster-based approach for each of these identifications. The uncertainty is estimated by the dimensions of the cluster after AMA. Those uncertainty estimations are averaged and illustrated using the green ellipsoid. The empirical scattering and estimated uncertainty ellipsoids have a similar shape with different scaling. Suppose the time buffer length for modal analysis is increased. In that case, the amount of information (i.e., periods of each vibration) is increased, and therefore, the uncertainty can be decreased, as shown in Figures 3.13b to 3.13d. The uncertainty reduction is well estimated using the cluster-based approach. The same data is plotted in Figure 3.14 to demonstrate the quantitative

(a) Time length $40\,s$ (b) Time length $60\,s$ (c) Time length $80\,s$ (d) Time length $100\,s$
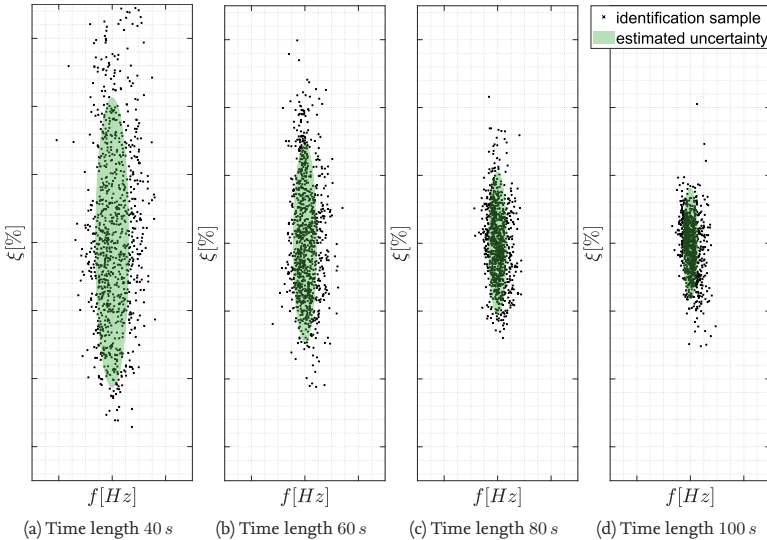
Figure 3.13: Qualitative comparison of empirical and estimated modal parameter uncertainties

difference of the uncertainties. The upper plots show uncertainty comparisons of eigenfrequencies and damping ratios. The green shaded area shows the standard deviation of all uncertainty estimations. The scaling of the uncertainties differs between the empiric and cluster-based methods, e.g. the uncertainty of the eigenfrequency identification is underestimated. This underestimation is indeed the case for both SSI and LSCF, while the underestimation of the uncertainty is higher for LSCF. Theoretically, such an underesti-

mation can be corrected using a re-scale factor. Nevertheless, the empirical and estimated uncertainties changes are very similar, as seen in the bottom plots. Here, the uncertainties are normalized to the one from the 40 s time buffer. This example shows that the cluster-based uncertainty estimation can be used for modal parameter assessment and fusion in Section 5, but not for exact predictions of confidence bounds.

(a) Eigenfrequency uncertainty comparison

(b) Damping ratio uncertainty comparison

(c) Normalized eigenfrequency comparison

(d) Normalized damping ratio comparison
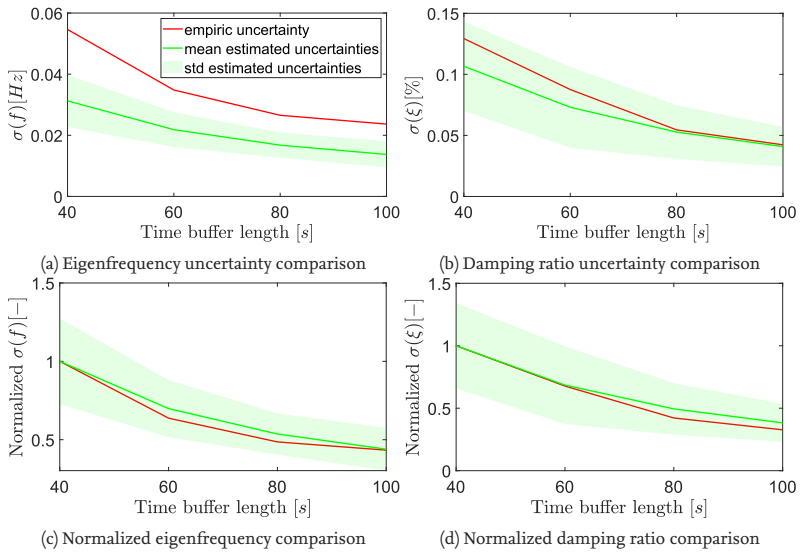
Figure 3.14: Quantitative comparison of empirical and estimated modal parameter uncertainties

3.4 Data Fusion for Uncertainty Reduction

A drawback of the real-time identification in OMA is the presence of significant identification uncertainties. Some challenges are described in Section 2.3 from literature and in Section 5.1 for the developed methods presented in this thesis. A novel method is presented in this section to reduce these uncertainties by applying data fusion methods. In OMA, it is challenging to identify all modes of the structure because not all modes are well excited, but also because an individual MID does not identify all modes equally well. Therefore, Section 3.4.1 presents the application of several MIDs and the fusion of their results. This fusion of methods is assumed to achieve comprehensive modal models and to reduce the uncertainties of individual MIDs. To further reduce the remaining uncertainties, a KF is implemented to fuse subsequent estimations of the modal parameters. This method is presented in Section 3.4.2. The example application in the following subsections is the real-time FVT of aircraft. However, implementing the fusion methods for identified modal parameters applies to general OMA applications.

3.4.1 Fusion of Modal Parameter Estimators

Several identification methods exist in OMA to estimate modal parameters. Since different assumptions are made for those estimators, they have different strengths and weaknesses. In [9, 37], two different MIDs, namely SSI-DAT and LSCF, are tested in a wind tunnel test, and the one with more consistent modal parameters is chosen to predict the flutter boundary. Nevertheless, in some circumstances, the other MID might lead to better results, which are difficult to supervise manually and close to real-time. The optimal MID differs not only for different circumstances, such as, e.g., the excitation level and signal-to-noise ratio, but also some modes are better identified using the one MID while others are better identified using another, e.g., modes with low damping vs. modes with high damping.

Choice of Identification Methods

In this thesis, three MIDs are used in parallel, and their results are combined to exploit the different advantages. The choice of the MIDs is made to include different approaches for identification and, therefore, exploit the different strengths. However, the presented systems (AMA, BO of hyperparameters and the fusion of MIDs) work with all MIDs, which allow the construction of a stabilization diagram. Different MIDs might be better suited for other applications. However, the state-of-the-art methods for real-time aircraft modal parameter identification from flight tests are SSI and LSCF. OMA methods can be distinguished by the domain used for identification: time- or frequency-domain. SSI belongs to the time domain methods and is a direct method, and LSCF works in the frequency domain and is an indirect, modal method. Since many different types of SSI exist, two well-known types are applied in this thesis, namely covariance-based SSI (SSI-COV) and data-driven SSI (SSI-DAT). A simple yet helpful comparison of some advantages and disadvantages concerning FVT identification is given in Table 3.1. The advantages and disadvantages mentioned are related to identifying aircraft modes in flight. In other applications, the methods might perform differently. From experience in wind tunnel testing, it is known that LSCF is well suited to identify modes with high damping ratios, while SSI is well suited to identify low damping ratios[9]. A typical example of flutter is the coupling of a wing bending and wing torsion mode. In this example type of coupling, the damping of one mode becomes very large, and the damping of the other modes becomes zero or negative. Therefore, simultaneously tracking two or more modes with low and high damping ratios is important. In general, the SSI-based methods show a larger scatter than LSCF, but LSCF can be biased in the presence of high noise. All three methods rely on well-chosen hyperparameters and some preprocessing, such as time data decimation or spectra calculation.

Bias Compensation

A significant disadvantage of LSCF is a potential bias in eigenfrequency and damping ratio estimation in the presence of high noise. Examples from applications to aircraft of this bias can be found in [8], and a mathematical explanation is given in [6]. In this thesis, LSCF as well as SSI-COV and SSI-DAT are optimized using BO before they are applied. During this optimization, a first check should be done to determine if the bias of LSCF is significant or negligible. If the bias is significant, it should be corrected. Under the

Name	Advantages	Disadvantages	Domain	Preprocessing
SSI-COV	no bias, good identification of low damping	large scatter, single identification band	time	decimation
SSI-DAT	no bias, good identification of low damping	large scatter, single identification band	time	decimation
LSCF	small scatter, good identification of high damping, multiple identification bands	biased in the presence of high noise	frequency	CPSDs calculation

Table 3.1: Comparison of MIDs chosen for real-time modal parameter tracking in FVT

assumption that an estimation using SSI has no bias, the averaged result of a LTI system identified over a long time range is unbiased, too. Therefore, the bias of LSCF can be determined empirically given a long data sequence analyzed using LSCF and SSI. A simple approach to determine the bias at time t is given as

$$bias_t(LSCF, \Theta) = \frac{1}{n-1} \sum_{i=t-n}^{t-1} \Theta_i^{LSCF} - \tilde{\Theta}_{t-n:t-1} \quad , \tag{3.1}$$

$$\tilde{\Theta}_{t-n:t-1} = \frac{1}{n-1} \sum_{i=t-n}^{t-1} \Theta_i^{SSI} \quad , \tag{3.2}$$

with Θ is the estimation and $\tilde{\Theta}$ is the averaged unbiased estimation. The empirical bias of LSCF estimating Θ is given by the difference of the averaged estimation of Θ_i^{LSCF} using LSCF in the close past and the averaged unbiased estimation of $\tilde{\Theta}$ from the same time. The unbiased estimation is the average of estimations Θ_i^{SSI} by SSI. In this thesis, n is chosen to be 15, meaning the bias of LSCF is determined from the last 15 analysis blocks, i.e., 30 s. The larger n is, the better the averaged SSI-estimate for a LTI system. Since the system and excitation vary over time in the presented study, the bias is assumed to vary, too. Therefore, the trade-off $n = 15$ is made. This bias can be calculated separately for the eigenfrequencies and damping ratios or directly using the complex eigenvalue.

Weighted Mean of Modal Parameters
Considering different modes identified by three MIDs (SSI-COV, SSI-DAT and LSCF), a combined modal model has to be built. If all MIDs are well suited for the test case, all three MIDs should lead to three almost complete modal models at each time step. Because of the optimization of all MIDs using the method described in Section 3.5.3, all estimators will probably identify the main modes. In this case, the modal parameters need to be fused. Of course, fusion should also be possible in real-time. A simple and fast way for estimation fusion is the inverse-variance mean (IVM)[41]. The more uncertainty the estimation of a specific mode has, the less it will influence the estimation of the fused mode. Unfortunately, an exact calculation of modal parameter identification uncertainties in real-time is not possible so far. However, one could assume the three MIDs as equally uncertain, or one can estimate the MIDs uncertainties using the cluster variances of AMA. Section 3.3.2 describes the cluster-based uncertainty estimation of identified modal parameters.

Modal parameters can be combined as weighted means using the estimated uncertainties. Since the eigenfrequency and damping ratio are of main interest for monitoring, they are calculated using IVM with

$$\hat{\Theta} = \frac{\sum_{i=1}^{M} \omega_i \Theta_i}{\sum_{i=1}^{M} \omega_i} \quad , \tag{3.3}$$

$$\omega_i = \frac{1}{\sigma^2(\Theta_i)} \quad , \tag{3.4}$$

$$\hat{\sigma}^2(\hat{\Theta}) = \frac{1}{\sum_{i=1}^{M} 1/\sigma^2(\Theta_i)} \quad , \tag{3.5}$$

with $\hat{\Theta}$ is the fused value, Θ_i is the estimation of the ith MID, M is the number of MIDs, and the weighting ω_i is the inverse of the variance σ^2. The variance of the fused estimation is $\hat{\sigma}^2$. This equation is applied to the eigenfrequencies and damping ratios of each modal model, i.e., at each time step. If one mode is found only by one MID, the formula leads to the same result as taking the mode directly.

3.4.2 Fusion of Subsequent Modal Models

Combining multiple different MIDs is important to obtain complete and unbiased modal models at each time step. The uncertainty of modal parameter identification is also reduced using IVM fusion; however, the uncertainty, i.e., scatter, remains too high for damping estimates even after IVM fusion. Therefore, further information is utilized to make assumptions about the estimated modal parameters, namely the variation over time. Considering the monitoring architecture, see Section 5.1, the information used for identification is stored in a time buffer of between 20 and 120 s, depending on the eigenfrequencies of interest and the excitation. The subsequent analysis takes place two seconds later. Therefore, the overlap of the FIFO buffer is between 90 and 98%. Assuming that the unknown excitation is stationary, the information about the aeroelastic system inside the buffer does not change significantly from time step k to $k + 1$. Since this assumption is an extension to the already violated classical OMA assumptions of stationary and random excitation signals in LTI systems, it should be considered with caution as described above. However, this leads to the simple yet feasible assumption that the aeroelastic state cannot change arbitrarily large from time step k to $k + 1$. Therefore, a previous estimation of modal parameters can be used to correct or smooth the subsequent estimation iteratively. A computationally efficient way to exploit these assumptions for a smooth estimation is using a linear transition model from k to $k + 1$. Even if the unknown change of modal parameters with operational conditions is nonlinear (e.g., damping with flight speed), it can be represented by a curve with piece-wise linear segments, provided that the spacing of the observation points is close enough. Based on the transition model and modal identifications by AMA with uncertainties, a KF can be implemented to fuse the subsequent modal parameter estimations optimally.

Kalman Filter-based Tracking
A KF will be used per mode. Therefore, the index r is omitted in the following paragraph

for the sake of simplicity. We define the KF state of a specific mode as

$$x = \begin{bmatrix} f \\ \xi \\ \Delta f \\ \Delta \xi \end{bmatrix} \quad , \tag{3.6}$$

with f is the eigenfrequency, ξ is the damping ratio, Δf is the change of the eigenfrequency from k to $k+1$ (two seconds later) and $\Delta \xi$ is the change of the damping ratio from k to $k+1$. The state at time step k is modeled as a Gaussian distribution $x_k \sim \mathcal{N}(\hat{x}_k, P_k)$ with P_k is the process covariance matrix. The identified modal parameters by AMA are provided as

$$z_k = \begin{bmatrix} f_{AMA} \\ \xi_{AMA} \end{bmatrix} \quad , \tag{3.7}$$

with z is called measurement. In addition, as part of AMA, the uncertainties of the eigenfrequencies and damping ratios are estimated; see Section 3.3.2. Those are transformed into a diagonal matrix R_k

$$R_k = \begin{bmatrix} \sigma(f_{AMA}) & 0 \\ 0 & \sigma(xi_{AMA}) \end{bmatrix} \quad , \tag{3.8}$$

with R_k is the measurement noise covariance matrix. Since the excitation from turbulence and the noise level change during flight, the measurement noise is also time-dependent. We can use R_k to define the noise of the measurement model as $m_k \sim \mathcal{N}(0, R_k)$. The measurement model follows as

$$z_k = \begin{bmatrix} 1 & 0 & 0 & 0 \\ 0 & 1 & 0 & 0 \end{bmatrix} x_k + m_k \quad . \tag{3.9}$$

Assuming the continuous analysis approach for FVT, the flight speed changes continuously. Therefore, the change of the system is also continuous. As mentioned above, we assume a linear transition from k to $k+1$, therefore the transition model is given as

$$A_k = \begin{bmatrix} 1 & 0 & \Delta t_k & 0 \\ 0 & 1 & 0 & \Delta t_k \\ 0 & 0 & 1 & 0 \\ 0 & 0 & 0 & 1 \end{bmatrix} \quad , \tag{3.10}$$

with Δt_k is the time interval between time step k and the previous one, in this thesis, two seconds. This transition model assumes a constant rate of change in the system. In the field of navigation and localization, i.e., if the state contains positions, this transition model is referred to as a "nearly constant velocity model" [2]. The process model is defined as

$$x_k = A_k x_{k-1} + v \quad , \tag{3.11}$$

with the process noise is $v \sim \mathcal{N}(0, Q)$. The process noise covariance matrix Q can be determined based on previous example measurement data, e.g., also used for HO. A linear KF can optimally solve such a process model.

Interacting Multiple Models

The constant change transition model is best suited if the system has a constant rate of change. In conventional FVT, stationary test points are used where the altitude and the flight speed are constant. The best transition model from k to $k + 1$ in such a case is to assume constant eigenfrequencies and damping ratios and to define the state as

$$x = \begin{bmatrix} f \\ \xi \end{bmatrix} \quad . \tag{3.12}$$

The transition matrix, in this case, is the identity $A = I_2$. The discrete test points are often performed subsequently, i.e., after a test point, the aircraft is accelerated to a higher flight speed, and test conditions are kept constant at the next test point. This stepwise flight speed increase might lead to smeared results of the KF-based monitoring during the transition phases. A hybrid filter is an alternative approach to react dynamically to those changes. A simple and cost-effective variant is the interacting multiple model KF (IMM-KF)[3]. The core idea of IMM-KF is that multiple filters are used in parallel with different transition models. Two filters could be used for a stepwise flight speed variation: one with a constant change model and one with an identity model. An overview of the IMM-KF process is shown in Figure 3.15a taken from [3]. At each step, the probability for each filter is calculated. The final fusion of the IMM-KF is then taken as a weighted mean of all filters. The filter probabilities are adjusted for the next time step depending on the individual filter performance. The estimate of each filter is mixed with the estimates of the other filters taking into account the filter probabilities (called interaction) to avoid a filter diverging while another filter is more probable. In this thesis, the IMM-KF structure

(a) IMM-KF from [3]   (b) Adjusted IMM-KF
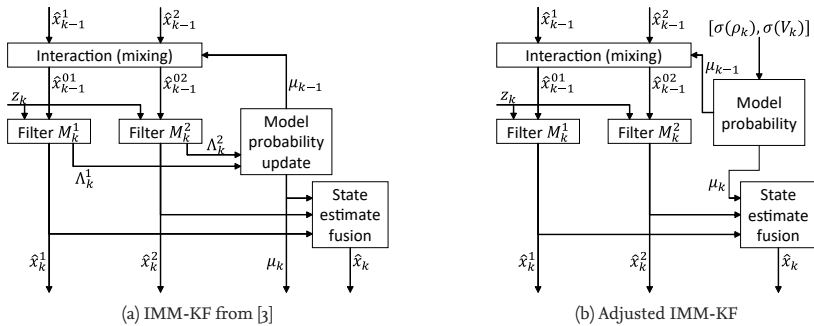
Figure 3.15: IMM-KF process

is adjusted slightly since the probability of the filters can be derived based on the standard deviation of the external parameters (air density and air speed). If the standard deviation is small, the constant transition model is better suited and, therefore, more probable. The higher the standard deviation is, the more likely the constant change transition model is. Other approaches have been tested, in which the process noise of the KF is adjusted with respect to the flight speed changes [103]. This approach works well for simulated cases, but the IMM-KF is more robust for real flight test results as shown in Subsection 5.3.2

3.5 Hyperparameter Optimization

The presented steps of modal parameter identification with LSCF or SSI, multi-tier clustering, and modal model optimization allow a fine-tuned AMA to achieve high accuracy. In this case, fine-tuning is the setting of optimal hyperparameters for a specific test condition, e.g., test structure, excitation type and position, sensor layout, and boundary conditions, such as, e.g., the suspension. The influence of the selected hyperparameters on the modal analysis results is evident, but in most cases, they are chosen as general, generic values or determined based on subjective experience. In [17], the identified eigenfrequencies and damping ratios are systematically investigated as a function of the selected Hankel matrix blocksize for SSI. It can be seen that the identification results of the physical modes converge for a specific block size. A stabilization diagram based on varying hyperparameters is shown in Figure 3.16 to illustrate the importance of the hyperparameters of both the MIDs and the AMA process. A simple structural dynamic system with seven DoFs and random excitation is simulated, and the time data with added noise is used for identification with varying hyperparameters. In the plots on the left side, i.e., Figures 3.16a, 3.16c and 3.16e, the Hankel matrix blocksize (for SSI) is varied between 20, 40 and 60. The analytical eigenfrequencies of the simulated system are marked with green lines. One can see that most modes are well-identified independent of the block size. However, for example, the mode at 25 Hz is not well identified. This mode shows the clearest stabilization using the highest block size. Nevertheless, in this case, also spurious modes seem to stabilize. In the plots on the right side, Figures 3.16b, 3.16d and 3.16f, the blocksize is set to 40 and a frequency stability threshold of 0.2, 1 or 2 % is applied for the cleaning. In this example, the stability threshold of 0.2 % leads to the best cleaning result. Since the optimal hyperparameters are challenging to determine and several hyperparameters are interdependent, it is not feasible to optimize them manually. In this section, the relevant hyperparameters of AMA for EMA and OMA are described. Furthermore, the Bayesian optimization (BO) method is introduced, which is well known for efficient machine learning hyperparameter optimization using Gaussian process (GP). A novel objective function is presented, which can be used to optimize all required AMA hyperparameters using BO and manual results of an engineer.

3.5.1 Hyperparameters of AMA

One of the main challenges in EMA and OMA is the determination of the optimal hyperparameters of, e.g., LSCF or SSI. For example, in [17], it is shown that the chosen Hankel blocksize has a strong influence on the identified eigenfrequencies and damping ratios. However, this is only one out of several hyperparameters which should be considered. The number of hyperparameters increases in the automation of modal analysis, including clustering, etc., especially with the AMA chain presented in this thesis. Which of those overall hyperparameters needs to be optimized depends on the specific measurement condition, test structure, and user experience. An experienced user might choose some hyperparameters himself, while an inexperienced user might want to optimize all hyperparameters automatically. The method presented in Section 3.5.3 can optimize all hyperparameters. Manually predefining some hyperparameters can reduce training time, but the risk of non-optimal hyperparameters increases. Based on the analysis chain described in Section 3.2 and 3.3, the hyperparameters listed in Table 3.2 are identified as
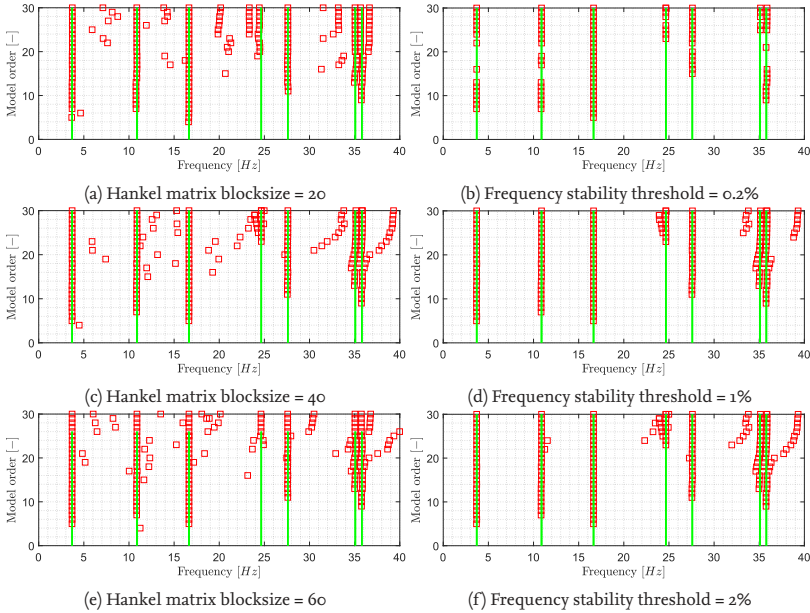
Figure 3.16: Stabilization diagrams of varying hyperparameters Hankel matrix block size and frequency stability threshold

most relevant. In analogy to [104], the hyperparameters are referred to as using a bold P and a number (e.g., **P1**), while the overall set of hyperparameters to run AMA is referred to as **P**. For simplicity, all hyperparameters are listed in the table. However, only a subgroup is relevant for OMA or EMA, respectively. In addition, for each hyperparameter, an initial range is given, which experience has shown to be suitable for optimization.

For EMA, the basic signal processing hyperparameters, such as the windowing settings for FRFs calculation, are assumed to be optimally set by the engineer beforehand. Therefore, those are usually not adjusted from the system. However, the system can optimize those hyperparameters, too, if required. This also applies to the chosen frequency identification bands, i.e., in which frequency band modes should be identified. In this thesis, those are optimally determined by the engineer. However, a more exhaustive optimization of these parameters is interesting for future research since some MIDs assume modes to be centered in the frequency identification band and not located closely to the border of an identification band. Since those hyperparameters are feasible to be well set by the engineers, they are not further discussed in the following section. LSCF and other MIDs require a range of model orders to be identified for the stabilization diagram. In LSCF, this defines the orders of the polynomials fitted to the measured FRFs. Since the highest model order for the stabilization diagram is unknown and cannot be chosen trivially,

ID	Description	Impact on	Range	Field
P1	CPSDs reference	which DoFs are used as references	bool	OMA
P2	CPSDs window length	the CPSDs frequency resolution	$[2^9; 2^{14}]$	OMA
P3	CPSDs window overlap	the CPSDs averaging	$[0; 1]$	OMA
P4	Time decimation	the sample rate for SSI	$[1; n]$	OMA
P5	Time buffer length	the time length in seconds	$[20; 120]$	OMA
P6	Hankel blocksize	identified modes from SSI	$[2; 30]$	OMA
P7	Model order	identified modes from LSCF	$[20; 150]$	both
P8	Frequency stability	stable poles in stabilization diagram	$[0; 1]$	both
P9	Damping stability	stable poles in stabilization diagram	$[0; 1]$	both
P10	MAC tracking	first step clusters of poles	$[0.2; 0.8]$	both
P11	Freq. clustering ϵ	clusters separation	$[0; 0.4]$	OMA
P12	Freq. clustering size	min. size of a mode cluster	$[0; 1]$	OMA
P13	MIF peak height	how strong the MIF has to drop to indicate a mode	$[0; 0.5]$	EMA
P14	MIF peak width	how far away can a mode be from a MIF peak	$[0; 1]$	EMA
P15	MIF peak accuracy	how strict the MIF peak borders are	$[0; 1]$	EMA
P16	Mode splitting	whether splitting of clusters is cleaned or not	bool	EMA
P17	Outlier detection ϵ	consistency of each mode cluster	$[0; 0.5]$	both
P18	Outlier detection cluster size	mode cluster size after outlier detection	$[0; 1]$	OMA, EMA
P19	MAC-XP double poles	maximal similarity of distinct modes in the modal model	$[0.5; 1]$	both
P20	MIF_ψ	allowed mode shape complexity	$[0; 1]$	both
P21	MPC	allowed mode shape complexity	$[0; 1]$	both
P22	MPD	allowed mode shape complexity	$[0; 90]$	both
P23	PSO exploration factor	how far PSO expands the search space for each cluster	$[0; 5]$	EMA
P24	PSO swarm size	the number of individuals in PSO	$[5; 30]$	EMA

Table 3.2: Hyperparameters of AMA

this hyperparameter is optimized using the presented method. The stabilization diagram is built based on the modal parameters identified from the selected model orders. The variation of eigenfrequencies and damping ratios over the increasing model order can be used to discriminate spurious poles using thresholds. The variation (or stability) thresholds should also be optimized, as shown in Figure 3.16. The following steps described in Section 3.2 and 3.3 require some thresholds for spurious pole discrimination as well as hyperparameters for the clustering steps using DBSCAN and the modal model optimization method using PSO.

For OMA, the hyperparameters of the signal processing are more difficult to determine. Therefore, the CPSDs calculation parameters, the length of the used time buffer, and the

potential decimation of the time data should be optimized for the output-only case. As for EMA, the hyperparameters of the clustering are part of the optimization. Since the online identification during a FVT is a particular case of OMA, the multi-tier clustering can be merged into a clustering with fewer tiers, see in Section 5. However, optimizing the according hyperparameters, such as, e.g., the DBSCAN distance, is important, too.

3.5.2 Bayesian Optimization

The term hyperparameter optimization (HO) is well known in the field of machine learning (ML) and applied artificial intelligence (AI). It is a challenge to tune the settings of a potentially expensive black box function to work best for a specific problem. Examples of such a hyperparameter are the learning rate in neural networks or the kernel type in a support vector machine. Hyperparameters define the architecture of the ML method and must be set before the training. Since manually chosen hyperparameters are often non-optimal and their results are difficult to compare and reproduce, automated optimization of hyperparameters is performed [45]. Different methods exist for HO like, e.g., grid search, random search, gradient-based optimization, or Bayesian optimization (BO) [108]. Training of a ML method is usually time-consuming and expensive, but still HO requires several repetitions of the training and evaluation phase. Therefore, HO has a long execution time that increases with the number of hyperparameters, the size of the training data sets, and the number of samples the HO needs. Unlike the other mentioned methods, BO chooses the next hyperparameter sample based on the knowledge of previous evaluations iteratively. Therefore, sample evaluations can be reduced significantly compared to exhaustive search or gradient-based optimization schemes. An obvious disadvantage of BO is that the optimization cannot be parallelized. However, in this thesis, the overall reduction of the number of evaluations is most important. Therefore, BO was found to be the most efficient and appropriate HO method.

The basic idea of BO is to use a few observations to build a computationally efficient surrogate model, which can be used to estimate the accuracy of the black box function and to find the next sample reasonably. Based on the observations, an a priori probability distribution of the accuracy of the function is defined. An a posteriori probability distribution can be calculated using the a priori probability distribution and the simple but potentially nonlinear surrogate model. Therefore, the accuracy probability distribution of unknown hyperparameters can be estimated. An optimum can be chosen as the next sample for evaluation using the probability distribution. For further information on the basics of BO, the reader is referred to [58], the application of BO to HO in the field of ML is described for example in [63, 85]. The two main parts of BO are, firstly, the surrogate model and, secondly, the acquisition function. Possible surrogate models for BO are a Gaussian process (GP), random forest, or the tree Parzen estimator, which have different advantages. In this thesis, GPs are chosen as the surrogate models because of the fast convergence speed for continuous hyperparameters [108]. This choice corresponds to the common application of BO and GP in the field of ML, see e.g. [63, 85].

A GP is a non-parametric statistical model over function spaces. A GP describes a prior probability distribution which can be used to calculate a posterior probability distribution given some observations. The GP is defined using a mean function $m(x)$ and a covariance function $k(x, x')$. The covariance function of a GP is often called the kernel.

(a) GP kernel functions

(b) A posteriori distribution example of GP
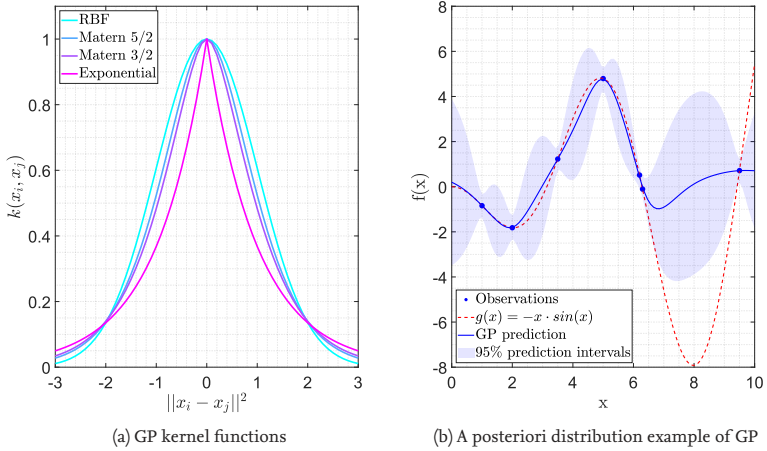
Figure 3.17: Gaussian process example

Formally, in [74] a GP is defined as

$$f(x) = GP(m(x), k(x, x')) \ . \tag{3.13}$$

The mean function is usually set to zero. Therefore, the kernel mainly defines a GP. Hence, the correct choice of a kernel function for a specific objective function is necessary. Since the tuning of kernel functions and more detailed insights into GPs exceed the scope of this thesis, the reader is referred to [74, 85]. Nevertheless, well-known kernel functions have been tested for the objective function presented in Section 3.5.3. Those kernel functions, namely squared-exponential kernel (or radial basis function, RBF), Matern 5/2, Matern 3/2, and the exponential kernel function are plotted in Figure 3.17a. The plot shows how much similarity is assumed given the distance of two parameters, x_i and x_j. The tests with example data have demonstrated that Matern 5/2 is the most promising kernel function for the application in this thesis. The kernel might have to be adjusted with a changing objective function. The a posteriori distribution of GP with a Matern 5/2 kernel of an one-dimensional example problem with seven observations is shown in Figure 3.17b. One can see that the target function $g(x)$ is well predicted near the observations and more uncertainty is present in regions without observations. An acquisition function chooses the best next sample based on the predicted function values. This evaluation incorporates the predicted mean values as well as the uncertainties. Assuming the function shall be minimized, one approach would be to select the minimal mean value of the predicted function values. This approach would result in a value close to $x = 2$. The uncertainty, however, is already relatively small in this area because the point $x = 2$ has already been observed. A better approach in this example is to explore the ranges in which the uncertainties are high. Figure 3.18 shows two example acquisition functions. Figure 3.18a plots the acquisition function lowest confidence bound (LCB). One can see high values of the

acquisition function where the bounds of the confidence intervals show the lowest values. Figure 3.18b shows the acquisition function expected improvement (EI). EI considers the best values so far observed and the confidence intervals. Therefore, the search for the global optimum is very efficient, and EI is often applied in BO [85].

(a) lowest confidence bound (LCB)   (b) expected improvement (EI)
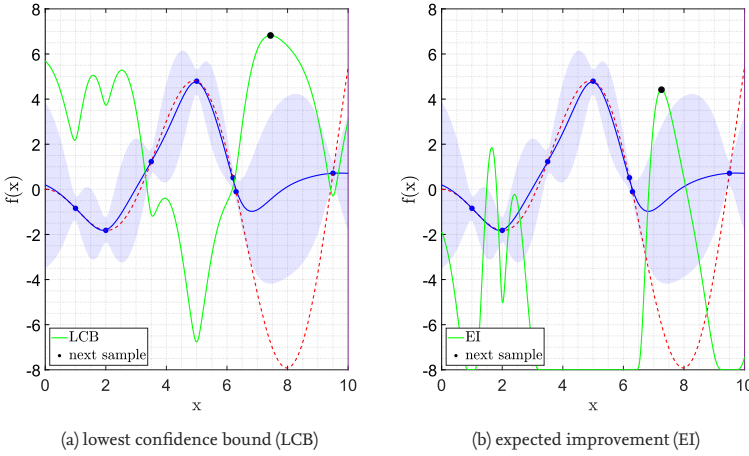
Figure 3.18: Bayesian optimization acquisition functions

3.5.3 Learning AMA Hyperparameters

In Sections 3.2 and 3.3, the analysis chain of AMA is described, which is capable of fully automated modal parameter identification and optimization of the identified modal model. However, the MID as well as AMA need to be fine-tuned using hyperparameters, which are described in Section 3.5.1. BO with GPs and EI is a promising method to optimize an expensive black-box function efficiently. The objective function to be optimized by BO takes hyperparameters and should return a numerical value indicating the accuracy of the AMA process. The open question is how optimal modal parameters are defined based on experimentally measured data. One option would be to use the modal parameters of a simulation model. This option has the advantage that no user input is required. However, a GVT is used to validate the simulation model; therefore, another approach is introduced in this thesis. Up to now, the best result of modal analysis for complex structures has been produced manually by trained modal analysis experts. Therefore, the AMA method learns how the analysis should be done by comparing it to an expert. Simply put, the results of AMA are compared to that of an expert. The results are the identified modal models of the autonomous method or manually identified by an expert. The modal parameters of a modal model are hereafter indicated as $\lambda_{AMA,j}$ and $\psi_{AMA,j}$ or $\lambda_{MAN,i}$, $\psi_{MAN,i}$, respec-

tively. The comparison results in a quality $q(\mathbf{P})$ using the objective function:

$$q(\mathbf{P}) = -N_{Sp} \cdot r_{Sp} + \sum_{i=1}^{N} w_{M,i} \cdot q_i \;\; , \tag{3.14}$$

with q_i is the quality of mode i, $w_{M,i}$ is an optional weighting of the impact of each mode in the optimization, N_{Sp} is the number of spurious modes in the AMA modal model, r_{Sp} is a penalty value for regularization avoiding too many spurious modes and $\mathbf{P}$ contains the hyperparameters. The default penalty for a spurious mode is $r_{Sp} = 0.5$. The individual quality of each mode q_i with $i \in N$ and N is the size of the manually identified, i.e., the target modal model is calculated by

$$q_i = \begin{cases} c_j \cdot w_c^T, & if \quad MACXP(\lambda_{AMA,j}, \psi_{AMA,j}, \lambda_{MAN,i}, \psi_{MAN,i}) > 0.5 \\ -r_{Mis}, & otherwise \end{cases} \;\; , \tag{3.15}$$

$$c_j = \begin{bmatrix} \Delta S & MIF_\psi(\psi_{AMA,j}) & MPC(\psi_{AMA,j}) & MPD(\psi_{AMA,j}) \end{bmatrix} \;\; , \tag{3.16}$$

with c_j is a vector of quality criteria of j-th mode from the AMA modal model, w_c is a weighting of the quality criteria, and r_{Mis} is a penalty of a missing mode. If a mode j of the AMA modal model matches the i-th mode of the manual modal model, the quality criteria of the mode are calculated, weighted, and used as the quality of this mode. The quality criteria in this thesis are based on the synthesis error ΔS, i.e., the difference of the synthesized and measured spectra (see also in Section 3.3), the mode shape MIF_ψ, the MPC and the MPD. Each criterion is normalized to become 1 for an optimally identified mode. The weighting of the quality criteria is by default $w_c = [0.5\,0.3\,0.1\,0.1]$. If there is no mode of the AMA modal model that matches the i-th mode of the manual modal model, i.e., the MAC-XP values are below a threshold (in this thesis 0.5), a penalty value is applied. The penalty of a missing mode is set to $r_{Mis} = 10$. The objective function sets the priorities for the optimization as follows:

1. Find all modes ($r_{Mis} = 10$)

2. Improve the quality of each mode ($q_i \leq 1$)

3. Avoid spurious modes ($r_{Sp} = 0.5$)

The presented equation in 3.14 can be used to test the quality of a set of hyperparameters $\mathbf{P}$. A modal analysis expert can create the required manual modal model. Consequently, the fine-tuned AMA can be used fully autonomously for additional measurement runs. The biggest advantage of AMA lies in the repetitive analysis of different data sets of the same structure with a similar test setup. This scenario can be found in GVT and FVT. In a GVT, an aircraft is tested with different excitation locations, levels, types (e.g., random, sweeps), and in different configurations. In a FVT, the aeroelastic system is continuously identified (repeatedly every 2 seconds) in a monitoring setup or at multiple distinct measurement points in the envelope. In both cases, an initial analysis by a modal analysis expert practically makes sense in the beginning to check the whole test setup for plausibility. To speed up this initial analysis, the expert can run AMA with default hyperparameters, adjust the modal model where necessary in a semi-automated modal analysis, and run the BO using the objective function in Equation 3.14. Further data sets can be analyzed autonomously
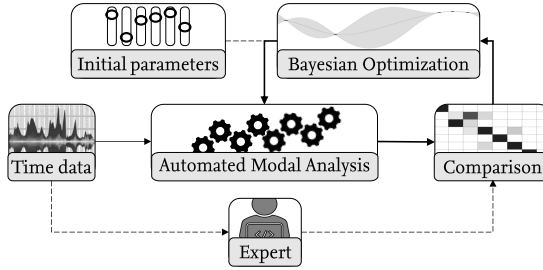
Figure 3.19: BO AMA concept

with high accuracy.

The general workflow to learn AMA hyperparameters from a modal analysis expert is shown in Figure 3.19. Based on time data and initial hyperparameters AMA creates a modal model that is compared to the results of an expert. The hyperparameters are iteratively optimized using BO until the hyperparameters converge or a maximal execution time is reached. It should be noted that this HO does not lead to the identification of specific target modes but instead results in an optimal set of hyperparameters. Those can be used to analyze further data sets as accurately as an expert but fully reproducible, user-independent, and much faster. The HO phase using BO is time-consuming because it reevaluates the AMA hundreds of times. Since the modal model optimization using PSO for EMA is the slowest part of AMA, the clustering and modal model optimization can be split into two tasks with subsets of hyperparameters. Running subsequent HOs for clustering and modal model optimization can significantly increase the training speed because most hyperparameters are part of the clustering phase. Therefore, the number of iterations required for PSO is reduced. In the shown applications, the training of hyperparameters was limited to ten minutes. Sometimes, the optimization converges faster. If the optimization does not converge for a specific test case, the allowed training time should be increased to ensure good hyperparameters.

3.6 Results

The presented AMA method aims to achieve high accuracy in identifying modal parameters in both experimental and operational applications. In this thesis, the accuracy of modal parameter identification is defined as:

- Complete identification of all physical modes,

- Minimal retention of spurious modes,

- High agreement between the measured and synthesized spectra and

- Reasonable uncertainties in modal parameter tracking.

Two simulation examples demonstrate the high analysis accuracy of the presented method, comparing the analytical solution with the identification results. One example involves a LTI system with and without noise, illustrating the accuracy of AMA for a single dataset. The second example involves a simple aeroelastic system with varying air speed to demonstrate data fusion methods for modal parameter tracking.

3.6.1 Accuracy of Modal Parameter Identification

The seven DoFs LTI system is taken from [19]. Simulated acceleration time data is transformed into FRFs and analyzed using LSCF. The LSCF estimates are analyzed manually with a stabilization diagram and with AMA. The system is simulated both without noise and with Gaussian white noise. The added noise has an amplitude of 0.5 times the average amplitude of the time signal and is added to the time data. Figure 3.20 shows the stabilization diagram of the noise-free example. The simulated spectra are seen to be noise-free. Due to the high model orders, the system is highly overfitted, forming many spurious modes. However, the pole clusters of the simulated modes are clearly visible, allowing the correct identification of the seven modes. Figure 3.21a shows the identified and an-
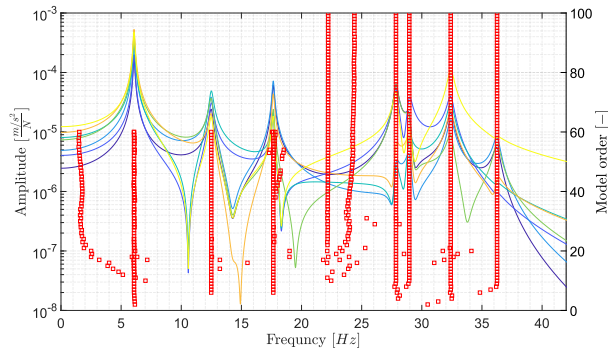
Figure 3.20: Stabilization diagram of noise-free example

alytical modal parameters. On the left y-axis, the sum of the simulated spectra (referred to as 'measured') and the sum of the synthesized spectra for the two results (manual and AMA) are displayed. The modal parameters are shown as eigenfrequency and damping. It is evident that the spectra and the modal parameters match well. The errors in eigenfrequency and damping are also compared in Figures 3.21b and 3.21c (manual in red and AMA in blue). The error bars for AMA are generally smaller, but the errors overall are negligible. In reality, data always contains noise. Figure 3.22 shows a stabilization diagram of the same simulation example, but this the noise is added to the time data. The noise is visible in the spectra. However, the seven modes are still well identified by LSCF, forming distinct clusters. It should be noted, however, that the seventh mode in this example is only identified at a model order higher than about 30. The identification results are shown in Figure 3.23. Due to the noise, the identified modal parameters of modes with smaller amplitudes deviate slightly from the analytical solution. In particular, the damping of the

(a) Identification comparison

(b) Eigenfrequency error

(c) Damping error
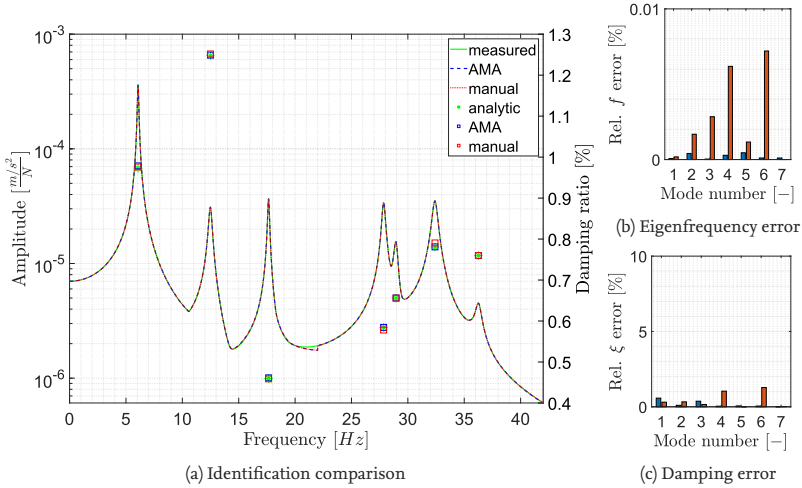
Figure 3.21: Identification comparison manual and AMA for simulated data without noise
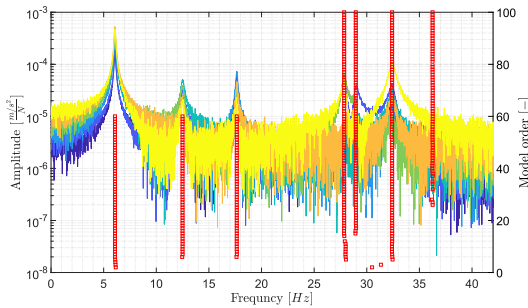
Figure 3.22: Stabilization diagram of simulation example with noise

seventh mode is underestimated in the manual analysis with LSCF. The comparison of identification errors in Figure 3.23b shows that the eigenfrequency error of all modes remains small despite the noise. However, in Figure 3.23c, the damping estimation of the seventh mode in manual modal analysis with LSCF is poor. By optimizing the synthesized spectra, AMA significantly reduces the error in damping estimation.

3.6.2 Uncertainty Reduction for Aeroelastic Modal Parameter Tracking

The data fusion methods for modal parameter tracking are demonstrated using a LPV system. The three DoFs system was initially described by [92]. A 2D linear aeroelastic sim-

(a) Identification comparison

(b) Eigenfrequency error

(c) Damping error
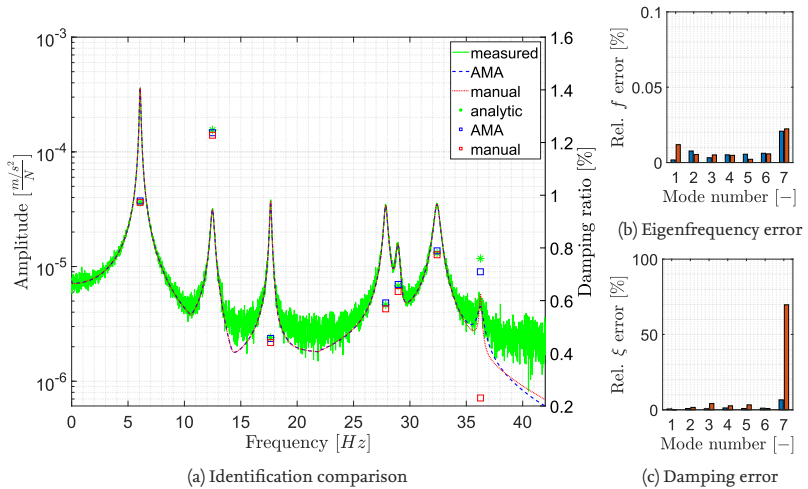
Figure 3.23: Identification comparison manual and AMA for simulated data with added noise

ulation was described in [77] and is used in the following. The airfoil is shown in Figure 3.24a. It can undergo heave, pitch, and flap motions, resulting in three structural dynamic degrees of freedom. There is no structural damping in the model. Combined with aerodynamic forces, the structural model leads to an aeroelastic model that exhibits different aeroelastic phenomena depending on the structural parameters. Two examples can be found in [48]. In the application shown here, heave and pitch couple at higher air speed, with the damping of the heave mode becoming negative. The density in this example remains constant over time. The air speed is initially constant and then increases linearly, as shown in Figure 3.24b. This results in a variation of eigenfrequencies and damping ratios as shown in Figure 3.25. The heave mode couples with the pitch mode. The damping of the pitch mode increases during mode coupling, and the damping of the heave mode decreases. Based on the analytical modal parameters (eigenfrequency and damping ratio),

(a) Three DoFs airfoil example

(b) Air speed variation
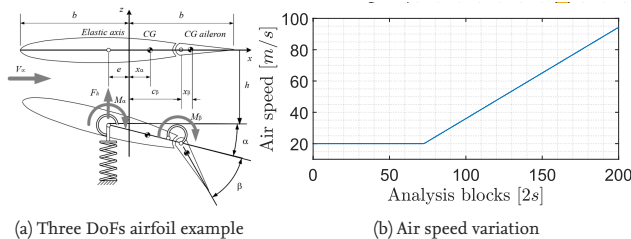
Figure 3.24: Aeroelastic simulation example

(a) Eigenfrequencies tracking

(b) Damping ratios tracking
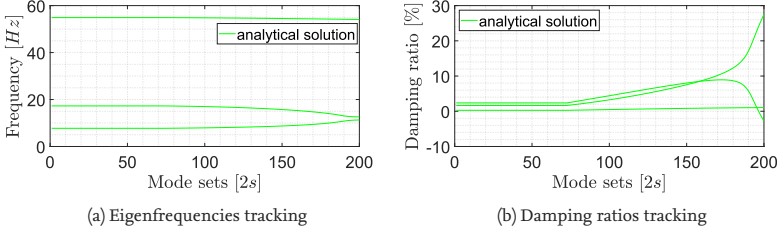
Figure 3.25: Simulated flutter curves

the identification results of the three MIDs are simulated. For this, the analytical modal parameters are assigned uncertainties corresponding to a relative standard deviation, as given in Table 3.3. A relative bias is also added to the eigenfrequencies and damping ratios identified by LSCF. In addition to the added uncertainties and bias, about 20% of

MID	$\sigma(f_r)/f_r^*$	$Bias(f_r)/f_r^*$	$\sigma(\xi_r)/\xi_r^*$	$Bias(\xi_r)/\xi_r^*$
SSI-COV	0.1	0	0.5	0
SSI-DAT	0.1	0	0.5	0
LSCF	0.05	0.02	0.2	-0.1

Table 3.3: Uncertainties added to aeroelastic simulation

the identifications were randomly removed. All MIDs have the same probability of being removed, but the identification of a mode is more likely to be removed if

- the eigenfrequency is higher than 20 Hz, as excitation in the lower frequency range is often better,

- the damping is higher than 10 % and the MID is SSI, or

- the damping is less than 1 % and the MID is LSCF.

These assumptions do not yield exact estimates of the MIDs but serve as a simple approach to generating typical flutter curves for different MID. The simulated identification results for the MIDs are shown in Figure 3.26. These results do not claim to evaluate SSI or LSCF but form a basis for validating the data fusion methods. For example, it can be seen that the SSI methods identify the pitch mode (in orange) less frequently at higher mode sets because the damping of this mode increases, as shown in Figures 3.26b and 3.26d. The flap mode at 57 Hz is generally identified worse due to the high frequency, and additionally, LSCF performs worse than SSI because the damping of this mode is very low. These simulated identification results are then further processed using data fusion methods. Figures 3.27a and 3.27b show the results of IVM fusion. It can be seen that all three modes are identified more reliably than by the individual MIDs. However, the curves still show scatter. This scatter is subsequently smoothed by the KF. The KF results are shown in Figures 3.27c and 3.27d. Apart from the region around the first mode sets and the very high damping, the KF curves closely follow the analytical curves. The deviations at the beginning of the tracking are as expected, as the KF improves with subsequent

(a) Eigenfrequencies SSI-COV

(b) Damping ratios SSI-COV

(c) Eigenfrequencies SSI-DAT

(d) Damping ratios SSI-DAT

(e) Eigenfrequencies LSCF

(f) Damping ratios LSCF
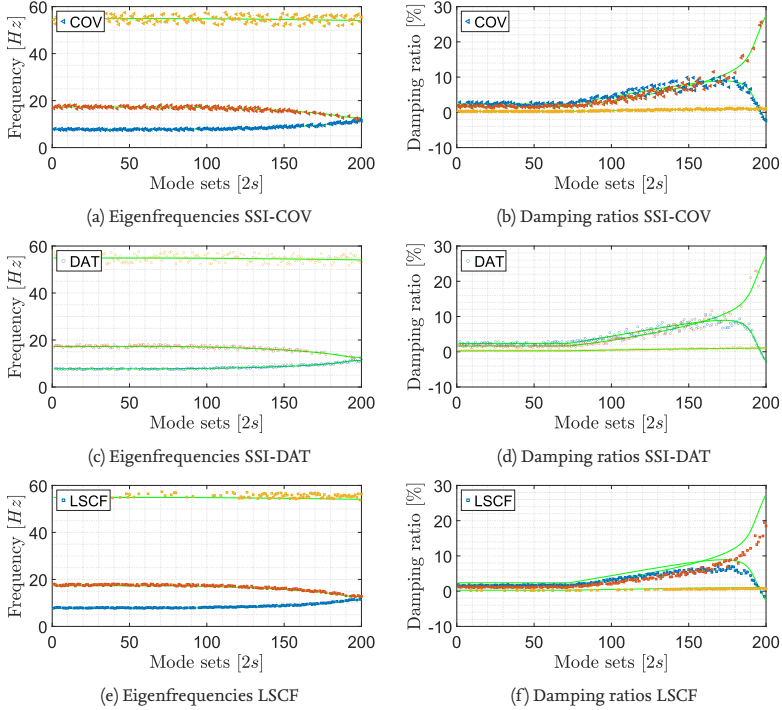
Figure 3.26: Simulated identification results

estimates. The remaining uncertainties in the very high damping region result from the lack of good identifications. The linear constant velocity model from Equation 3.10 is used as the KF transition model, however, the nonlinear behavior of the flutter curves is well approximated. The mean distance between the analytical and identified flutter curves quantifies the scatter. The RMS error is calculated as:

$$RMS(f_r) = \sqrt{\frac{\sum\limits_{k=1}^{N}\left(f_{r,k} - f_{r,k}^*\right)^2}{N}}, \tag{3.17}$$

with f_r^* is the analytical eigenfrequency, and N is the number of identifications, i.e., ideally $N = 200$ if a mode is identified in each analysis block. The $RMS(\xi_r)$ is calculated analogously. Figure 3.28 shows the RMS errors for the three eigenfrequencies and damping values for all identification methods. The results indicate that for LSCF, the bias significantly influences the mean error. The two SSI methods lead to comparable errors, as the same uncertainties were used. Notably, the application of IVM fusion reduces mean errors, with further improvement achieved by using the KF. The reduction of the mean
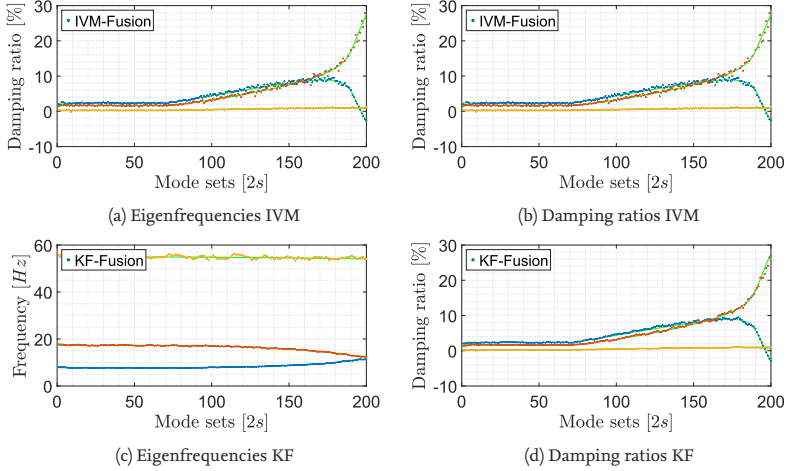
Figure 3.27: Data fusion tracking results

errors is particularly noteworthy, as the uncertainties in the fusion methods are derived from a larger number of identification points than the individual MIDs, where modes were occasionally removed in challenging scenarios.
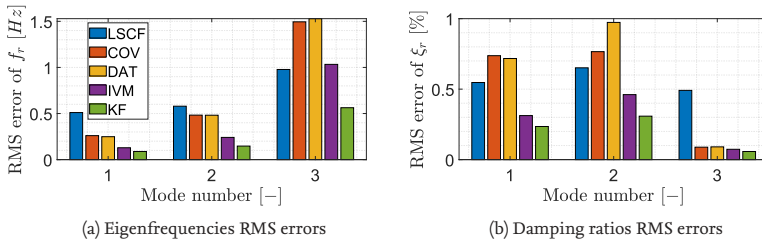
Figure 3.28: RMS errors comparisons

4 Semi-Autonomous Ground Vibration Test Analysis

4.1 Introduction to SAGVT

The GVT is a central component in the certification process of new aircraft prototypes or significantly modified aircraft, see Section 2.2. A GVT is usually performed a few weeks before the maiden flight. The test and data analysis are therefore highly time-critical. Over the last decades, the DLR has developed and iteratively improved the entire GVT realisation, including: suspension, excitation, acquisition, signal processing, EMA and data correlation [89, 36, 15]. However, EMA remains a major challenge in terms of optimal identification of damping, the required analysis time and user-dependency. This is also due to the difficulty of defining simple target functions for modal analysis and modal correlation. In comparison, the definition of cut-off frequencies or the selection of the required frequency resolution for signal processing, for example, have a clear and simple objective. Therefore, EMA and correlation are parts of the GVT analysis which can be improved semi-autonomously by AMA. Nevertheless, some other parts of the GVT analysis chain can be automated, too. The automated analysis chain is described in Subsections 4.2.1 and 4.2.2. A key feature of the presented AMA method is the optimization of hyperparameters to ensure high accuracy. With regard to GVTs of aircraft the training of hyperparameters must be repeated under significantly changed measurement conditions. This semi-automated relearning system is described in Section 4.2.3. The semi-autonomous GVT analysis (SAGVT) was tested twice on-site in GVTs of a small fixed-wing unmanned aerial vehicle (UAV) and a business jet, respectively. The results are presented in Section 4.3.

4.2 Semi-Autonomous Analysis chain

The application of AMA to the GVT analysis automates a fundamental part of the analysis chain. The data flow of the GVT data analysis is shown in Figure 4.1. The blocks in Figure 4.1 represent the analysis stations described in Section 2.2. The main analysis tasks are mentioned within the blocks, where the black tasks are performed autonomously by the presented system. However, some tasks are feasible to be carried out manually by an engineer. These tasks are therefore not automated and are shown in grey in the data flow illustration. In addition to AMA, the automated detection of faulty sensors and the automated correlation are presented in this thesis. Some remaining tasks are also automated (e.g. the FRF estimation or the plotting of non-linearities), but only the state of the art is implemented here without significant further new developments.

4.2.1 Faulty Sensor Detection

The first station in the DLR GVT processing chain after the acquisition is called signal processing in Figure 2.3b. The engineer at this station checks each sensor signal for plausibility and afterwards the data of accepted sensors is transformed into FRFs. Those are
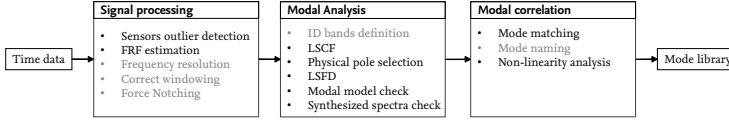
Figure 4.1: Data flow diagram of the semi-autonomous GVT analysis chain

again checked before they are passed to the EMA station. Obviously, the main user interaction is the visual check of each time signal and spectra signal. For the automated analysis chain an automated outlier detection method is applied. The basic idea is that all valid sensors show similar data characteristics in the time and frequency domain. The time data is checked using the kurtosis. The kurtosis is defined as

$$K(X) = \frac{E\left[(X - \mu)^4\right]}{(E\left[(X - \mu)^2\right])^2} \quad , \tag{4.1}$$

where X is a random variable, μ is the mean value of X and E is the expected value. Here, X is the time data series of a sensor. The kurtosis value of a corrupt acceleration sensor is assumed to be significantly higher than the one of a valid sensor (see page 83 in [10]). The check of the data in the frequency domain is done using the coherence (see page 291 in [10]). The coherence is defined as

$$\gamma_{yx}^2(f) = \frac{|G_{yx}(f)|^2}{G_{xx}(f)G_{yy}(f)} \quad , \tag{4.2}$$

where G_{yy} is the APSD of an output signal (response), G_{xx} is the APSD of an input signal (excitation) and G_{yx} is the CPSD of an input and output signal. The coherence is defined to be $0 \leq \gamma_{yx}^2(f) \leq 1$. If the coherence is almost one for a frequency, the output is linearly dependent on the input. For frequencies which are not close to the anti resonances, this should be the case. If the coherence is small over the whole frequency range, the sensor might be corrupt or the excitation is bad. For each sensor a kurtosis value and a mean coherence is calculated and normalized and a simple outlier detection using DBSCAN or local outlier factor (LOF) [27, 13] is applied to identify the outliers. Figure 4.2 shows an example outlier detection of a faulty sensor in a GVT. In this example, the data of the faulty sensor does not show a conspicuous kurtosis value, however, the mean coherence is significantly lower compared to the other sensors. For more variability, further characteristics of faulty sensors might be used to enrich the outlier detection. In this thesis, the two mentioned characteristics are found to be reliable for GVTs.

4.2.2 Automated Modal Correlation

The correlation of modal models from different measurement runs is a time consuming and cognitively complex task. DLR has developed a software tool for correlation with a tailored graphical user interface (GUI) to support this task, which is presented in [15]. The goal of the correlation is a complete library of all modal parameters sorted into so-called mode families. In order to build a full modal model of the aircraft, all distinct modes from different measurement runs have to be included. However, to avoid multiple entries of the

(a) Coherence outlier

(b) Outlier detection example
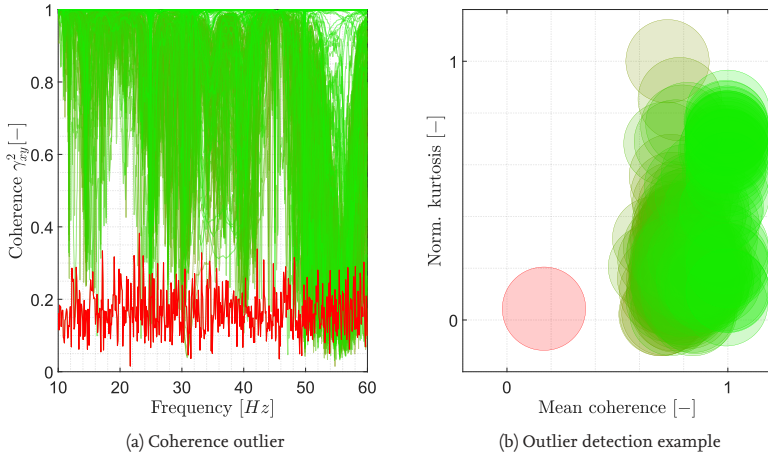
Figure 4.2: Faulty sensor detection using outlier analysis of coherence and kurtosis

same physical mode from different measurement runs in the final modal model, they are correlated into the same mode family. From all mode families one representative master mode is in the end selected to be in the final modal model. For example, the symmetric 2n wing bending mode is usually identified from many different excitation conditions, like e.g. symmetric or random wing excitation, symmetric or random fuselage excitation or even an empennage excitation. Each identification of the 2n wing bending mode needs to be correlated with the mode families and sorted into the corresponding family. The symmetric and anti-symmetric excitations are repeated with increasing force levels to investigate nonlinearities. A complete library of mode families allows the construction of nonlinearity plots which show a potential change of eigenfrequency and damping ratio of a mode with increasing excitation force.

A high modal density and complex mode shapes, especially in the higher frequency range, makes the correlation a time consuming and cognitively complex task. In this thesis, the correlation is replaced by an automated MAC-XP tracking. The modal model of the first measurement run defines the initial mode families. That means that each mode of the first measurement run becomes a mode family. For every new modal model for each new mode the following simple, yet robust tracking algorithms is applied:

1. calculate the MAC-XP value between the new mode and every mode in a family

2. select the highest MAC-XP value as the similarity for the family

3. repeat 1 and 2 for all mode families

4. assign the mode to the mode family with the highest similarity, if the similarity is high, otherwise create a new family

The simple algorithm sorts new modes into the family with the highest similarity in terms of MAC-XP. If the highest MAC-XP value is smaller than a threshold, in this thesis 0.5, a new mode family is created. AMA results can include some spurious modes, therefore some quality criteria, like e.g. MIF_ψ or MPC, are checked in order to include physical modes only. Since the number of measured degrees of freedom is limited, some mode shapes of actually distinct modes result in high MAC values. If those modes are additionally similar in eigenvalue, they might be sorted into wrong mode families. However, in this thesis, this simple approach is applied and the presorted mode families can be modified using a GUI. Some user interaction remains required here, but the amount of interaction is reduced significantly. However, this is an open point that can be investigated in future research.

4.2.3 Relearning Hyperparameters in a GVT

The optimization of AMA hyperparameters is a key feature of increasing the accuracy of AMA results. In a GVT, the excitation location, the excitation type (e. symmetric, anti-symmetric or unsymmetric or random) and the aircraft configuration (e.g. unfueled or fueled) are varied. The optimal hyperparameters for different measurement conditions vary, therefore they need to be retrained during a GVT. Figure 4.3 shows the procedure of handling and retraining the hyperparameters. Challenges of retraining the hyperparam-
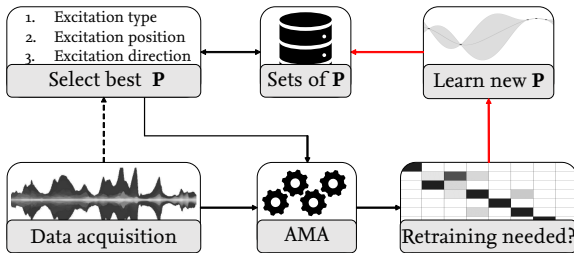
Figure 4.3: Framework of retraining hyperparameters **P** of AMA during a GVT

eters for AMA in GVT are:

- Retraining requires a manual analysis by an expert (time consuming)

- Many different sets of hyperparameters for very similar conditions might introduce non-physical variation of modal parameters (i.e. for different force levels)

- Non-optimal hyperparameters lead to non-optimal modal identification

The goal is to keep the number of retrainings as small as possible, while ensuring accurate modal identification results. The SAGVT system stores hyperparameter sets **P** together with the excitation conditions, such as the excitation type, position and direction. For every new measurement run, the system searches for the most similar measurement condition and analyses the data using the corresponding **P** of that reference measurement run. The result is compared with the modal model of the reference measurement run. If

the modal models differ significantly, new hyperparameters **P** should be retrained (indicated by red arrows in Figure 4.3). Small differences in modal parameters, however, have to be accepted. The modal model comparison function described in Equation 3.14 in Section 3.5.3 is used to compare the current modal model with the corresponding reference modal model. A difference of the modal models can be a result of non-optimal hyperparameters, but also optimal hyperparameters might lead to different modal models because of a different excitation condition. Therefore, the system asks the expert to retrain the hyperparameter, if the identified modal models differ significantly, presumably because the hyperparameters are non-optimal or the excitation condition changed significantly. The decision whether a retraining should be done more often or less often depends also on the size of the structure and therefore different excitation variations during a GVT. Therefore, the two examples in this thesis in Section 4.3 show applications of this system to a GVT of a small UAV and of a large aircraft, respectively, with a different number of retrainings.

4.3 Application and Results

The SAGVT has been verified in two GVTs. The first GVT has been performed on a research aircraft, i.e. a modified business jet. The main validation of SAGVT is shown using these results in Subsection 4.3.1. In the second example in Subsection 4.3.2, the system was verified in the GVT of a small fixed-wing UAV. This example is shown to demonstrate the ability of SAGVT to correct sub-optimal manual modal analysis during the hyperparameter training process.

4.3.1 Business Jet Research Aircraft GVT

The SAGVT has been tested in the GVT of the DLR research aircraft ISTAR (in-flight systems and technology airborne research). ISTAR is a Dassault Falcon 2000LX, which has been modified for the research activities in aeronautics of the DLR. Because of these modifications a GVT was performed before first test campaigns. ISTAR is an unique, experimental aircraft, therefore the following results refer exclusively to this modified version. A photo of the aircraft in GVT together with the manual and semi-autonomous data analysis chain is shown in Figure 4.4. The conventional (manual) analysis chain consists of the stations: 1) data acquisition; 2) signal processing; 3) EMA; 4) correlation, see also Section 2.2. The first station controls the excitation signals and measures the data (input forces and output acceleration signals). At the signal processing station the engineer checks the signals in order to detect a faulty sensor. This check is performed using the time acceleration signals, statistics, as well as spectra. Additionally, FRFs are calculated and prepared for the next station, i.e. EMA. Usually, two EMA stations are used in parallel, since this processing step is most time consuming. However, even two engineers working in parallel can not always keep up with the measured time data in complex situations. At the last station, called correlation, the modal models from different runs are correlated in order to build mode families and a final modal model. The novelty at this GVT is station 5). Here, the new SAGVT system was implemented and tested. The SAGVT system is tested as a potential alternative to manual stations 2)-4).

  The test setup typically involves a comprehensive arrangement of sensors and excitation points to accurately capture the vibration behaviour of the structure under investi-

Figure 4.4: ISTAR in GVT with manual analysis chain (1-4) and SAGVT (5)

gation. In this specific GVT setup, more than 200 acceleration sensors are strategically placed across the structure to measure the responses, see Figure 4.5a. The excitation is introduced at 17 distinct points, see Figure 4.5b, with some points used simultaneously with two shakers to ensure effective excitation of symmetric and anti-symmetric aircraft modes. While most global modes are well excited from multiple excitation points, some local modes require specific excitation points for accurate identification. The test consists of anti-symmetric as well as symmetric sweeps with a rate of 0.5 octaves per minute, allowing for a detailed analysis of the structure's response over the critical frequency ranges. The sweeps are performed in two distinct frequency bands: the lower band ranges from 3 to 10 Hz, and the higher band spans from 8 to 64 Hz. Additionally, a random excitation is performed within a broader band of 0.1 to 64,Hz to capture the full dynamic responses as well as the low frequency rigid body modes. The random excitation is used as well to

(a) Sensor plan

(b) Excitation positions
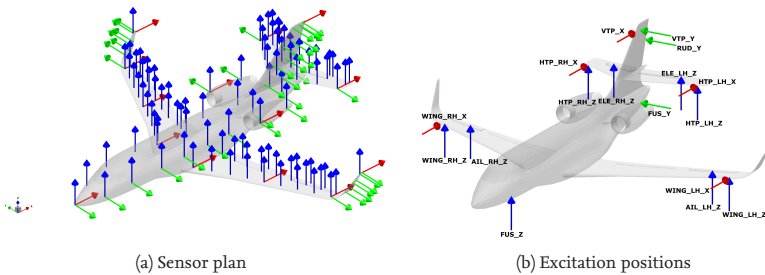
Figure 4.5: Acceleration sensor plan and excitation positions in ISTAR GVT

notch the force signals of the shakers for the sweep runs in order to comply to the acceleration limits of the structure. Overall, the GVT consists of 115 measurement runs, ensuring a comprehensive data set that provides insights into the dynamic characteristics of the structure.

To enable the usage of SAGVT on-site at a real GVT a GUI has been developed to provide an interface to train hyperparameters and supervise the overall semi-automated analysis process. The GUI is shown in Figure 4.6. It consists of the twelve individual displays:

1. AMA GUI

2. Console output

3. Stabilization diagram of a measurement run

4. Auto-MAC of a measurement run

5. Mode list of a measurement run

6. Mode shape comparison for a measurement run

7. Stabilization diagram GUI settings

8. Tracking/Correlation diagram

9. Cross-MAC of a mode family

10. Mode shape comparison of a mode family

11. Nonlinearity plot of a mode family

12. Cross-MAC of all mode families
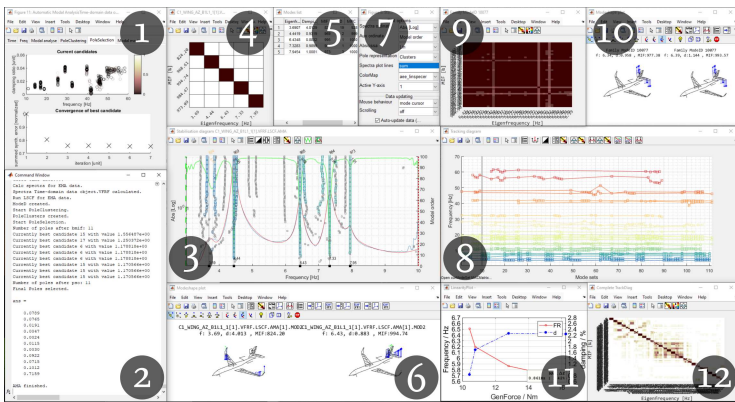
Figure 4.6: SAGVT GUI in ISTAR GVT

A new GUI for GVT analysis should be intuitive and provide easy access to all the necessary functionalities ideally at the same time. One disadvantage of the conventional analysis

chain is that the engineer at the correlation station cannot adjust a potentially wrong mode selected at the EMA station, i.e. remove a spurious mode or select an alternative pole. A detailed description of how each component can be integrated into one interactive GUI is given in the following. The first window of the GUI shows the progress of AMA of the currently analysed measurement run (**1**). The different steps are shown such as faulty sensor checks, modal identification using LSCF, pole clustering, PSO-based modal model optimization and the final modal model. Below the AMA window, there is a console output panel (**2**). This console displays real time logs, error messages, and status updates, providing feedback to the user on the progress and results of the running analysis. The central window shows a stabilization diagram (**3**). The stabilization diagram provides a graphical representation of the stability of identified modes across different model orders or across damping ratios, the selected mode as well as the measured and synthesized spectra. The poles can be colored according to the stability of the modes as well as according to the mode clusters they belong to. Greyed out poles were discriminated by AMA. Nevertheless, they are shown to allow the user to include them manually if wanted. The stabilization diagram is framed by windows which provide additional functionalities to assess the results of the specific measurement run. Examples are an auto-MAC matrix to compare the linear dependency of the mode shapes of the selected modes (**4**) or a geometry plot to compare the mode shapes side-by-side in a 3D view (**6**). There is also a settings window (**7**) which offers configuration options for the stabilization diagram, such as color schemes (e.g. stability vs. clusters) and axis parameters (e.g. modal order vs. damping ratio). The main window on the right side is the tracking or correlation diagram (**8**). This diagram shows the tracking of modes over different measurements. This window features interactive tracking lines of eigenfrequencies or damping ratios and includes filter options for specific modes or excitation types or positions. Using the tracking diagram a measurement run is selected which is shown in the central windows (**4**)-(**7**). This allows efficient adjustments of EMA results. Above the tracking diagram a specific mode family can be investigated. The cross-MAC matrix window is dedicated to analyze a chosen mode family (**9**). It includes a matrix visualization and an interactive selection of one or two family members for the mode shape comparison (**10**). The mode family eigenfrequency and damping can also be visualized over the generalized force (**11**). This plot can be used to find nonlinearities in mode families if the eigenfrequency or damping changes with excitation force. Lastly, the MAC matrix in window (**12**) provides comprehensive cross-MAC analysis across all mode families. For each mode family up to five modes are shown in order to check if different mode families should be merged into one family. This GUI layout ensures that all essential functionalities are accessible and organized in a user-friendly manner. Each component has specific features to support the postprocessing of EMA results in a stabilization diagram, from real time feedback in the console output to detailed mode shape comparisons and tacking diagrams. In addition, the hyperparameter relearning is triggered by this GUI and the manual modal analysis can be performed directly in the stabilization diagram.

The hyperparameter retraining is triggered based on an automated review of the AMA results. The basis of the review is the comparison function used for HO given in equation 3.14. If the new AMA result is too far away from the training reference, new hyperparameters should be trained. The threshold for the review comparison is set to -40 in this study.

Retraining	Position	Direction	Type	Frequency band
1	WING	X	anti-symmetric sweep	band 2
2	WING	X	multi-point random	band 3
3	WING	X	symmetric sweep	band 2
4	WING	X	anti-symmetric sweep	band 1
5	WING	Z	anti-symmetric sweep	band 2
6	WING	Z	symmetric sweep	band 1
7	WING	Z	multi-point random	band 3
8	FUS	Y	anti-symmetric sweep	band 2
9	FUS	Y	anti-symmetric sweep	band 1
10	FUS	Y	random	band 3
11	RUD	Y	anti-symmetric sweep	band 2
12	HTP	Z	anti-symmetric sweep	band 2
13	HTP	Z	multi-point random	band 3
14	HTP	X	anti-symmetric sweep	band 2
15	ELE	Z	anti-symmetric sweep	band 2
16	VTP	Y	anti-symmetric sweep	band 1

Table 4.1: Measurement runs used for retraining of hyperparameters
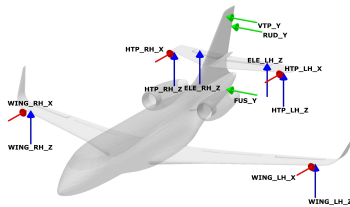
Figure 4.7: Excitation positions used for hyperparameter retraining

This leads to a library of different hyperparameter sets **P** associated with a specific reference measurement run. If a new measurement run is available, the best hyperparameter set has to be chosen from the hyperparameters library. From experience the following order is chosen as descending relevance for hyperparameter changes:

1. Excitation type

2. Excitation position

3. Excitation direction

4. Frequency band

This means that most important for the choice of hyperparameters in GVT is the excitation type (i.e. random, anti-symmetric sweep or symmetric sweep). If multiple hyperparameter sets are available for the excitation type, the excitation position of the new measurement run is chosen and so on. This scheme should find the hyperparameter set from

the most similar measurement run, e.g. the same excitation type at a similar excitation position. The result of AMA using hyperparameters from the most similar measurement run are reviewed again autonomously. If the result is accepted, the system waits for the next measurement run. As described above, the best hyperparameter set differs for the excitation type, position, direction and frequency band. This is confirmed by Table 4.1. In this table all measurement runs are listed for which a retraining of hyperparameters was performed. It is evident that all excitation types are present multiple times. Also many combinations of excitation positions and directions are present. Those are also visualized in Figure 4.7. For most, but not all excitation points at least one training was required. For some cases, also the different frequency bands require different hyperparameters. In total 115 measurement runs have been analyzed using SAGVT and 16 retraining were required. The manual analysis of one measurement run takes between 45 and 60 minutes from time data to the correlated modes. The SAGVT needs about ten seconds for the whole analysis. Therefore, the overall analysis time could be reduced by about 86 %. Sometimes, the automated correlation was corrected by the engineer in SAGVT, however this was feasible before the next measurement run was acquired.

The main comparison between the conventional or manual GVT analysis and the SAGVT system, however, is with respect to the identification accuracy, namely the final modal model and mode families. The engineer could use the presented GUI to postprocess the SAGVT results. However, the results shown in this chapter have not been postprocessed, but are the original results identified by AMA. Figure 4.8a shows a MAC matrix between the manual and SAGVT results. Most importantly, the diagonal should result in almost dark squares in order to indicate the same identified mode shapes from both methods. The lighter the values are, the more linear independent are the mode shapes. The off diagonal modes indicate that using the chosen sensor setup, some mode shapes of distinct modes have a linear dependency. This makes the automatic correlation more difficult. This topic of sensor placement optimization is not further discussed in this thesis. In Figure 4.8b the MAC-XP matrix between both modal models is shown. Here, the eigen-

(a) MAC matrix   (b) MAC-XP matrix
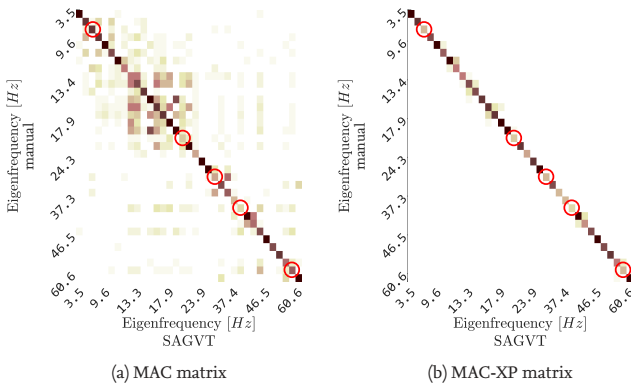
Figure 4.8: Modal model comparison between AMA and manual GVT analysis chain

(a) APU mode SAGVT #17 at 19.0 Hz   (b) APU mode manual #17 at 19.0 Hz

(c) elevator rotation SAGVT #22 at 30.1 Hz   (d) elevator rotation manual #22 at 30.2 Hz

(e) 3n wing in-plane bending SAGVT #26   (f) 3n wing in-plane bending manual #26
    at 38.4 Hz   at 38.4 Hz
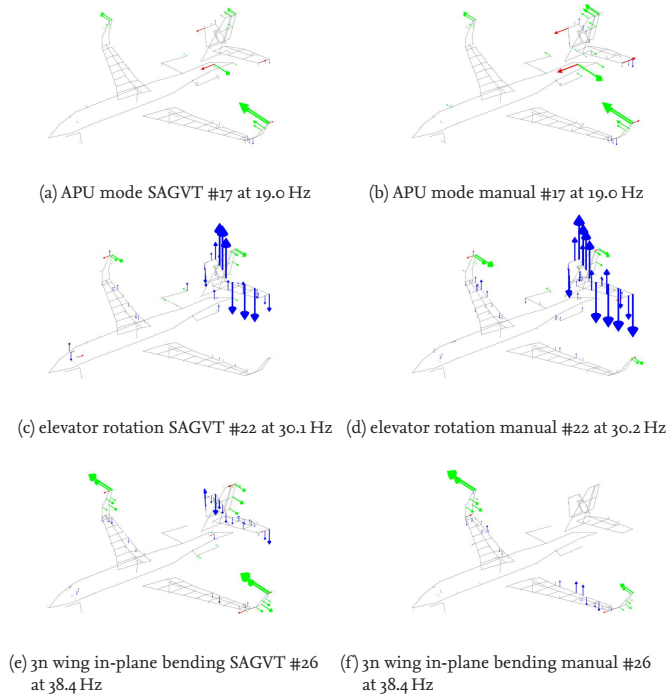
Figure 4.9: Mode shape comparison of modes with low MAC values

value is used to further weight the MAC values. A first result is that all modes are identified by SAGVT. For most modes, the comparison is good. However, some modes differ. The modes with lowest agreement are encircled. Since some modes show a low MAC value, the mode shapes of these modes are shown in Figure 4.9. These modes are with respect to the auxiliary power unit (APU), the elevator rotation and the 3n wing in-plane bending. One can see for example in Figures 4.9a and 4.9b the APU mode identified by SAGVT and manual analysis, respectively. The main component of the mode is the x-and y-direction of the APU DoF. Since this mode is a local mode, the contribution of other components, e.g. the winglets, are out of phase. These complex mode shapes with a significant phase shift lead to a small MAC value. Nevertheless, both mode shapes show the same physical mode. Similar differences can be seen for the other two modes in Figure 4.9. For example, the main contribution of the 3n wing in-plane bending mode is the x-direction (red arrows), however additional contribution can be seen in the other directions.

The first and last red circle highlight the HTP-roll mode and a higher winglet bending mode. Since the MAC value of these two modes are high, the main differences of the MAC-XP value results from the eigenvalue differences. Figure 4.10 shows the relative deviation
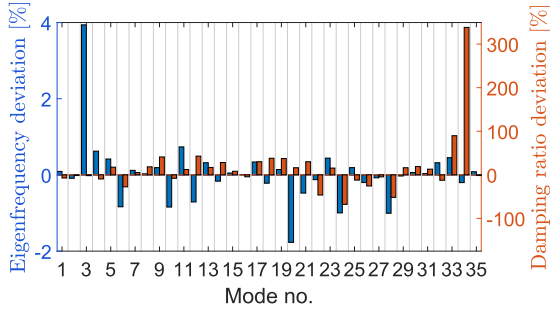
Figure 4.10: Eigenfrequency and damping ratio deviation between AMA and manual GVT analysis chain

in eigenfrequency and damping ratio of each mode in percent. One can see that the third mode, HTP-roll, has a significant deviation in eigenfrequency of 4 %. The last encircled mode shows a high deviation in damping ratio. A significant change of the damping ratio can be a result of the synthesis optimization using PSO. LSCF is known to underestimate the damping in the presence of noise. The manual result of this mode is based on pure LSCF and shows 0.6 % damping while the result from SAGVT is 2 % damping using the optimized spectra synthesis. The eigenfrequency deviation of the third mode however cannot be explained using the synthesis optimization.

In order to investigate the eigenfrequency deviation of the HTP-roll mode, the corre-

(a) SAGVT, 39 modes

(b) manual, 26 modes
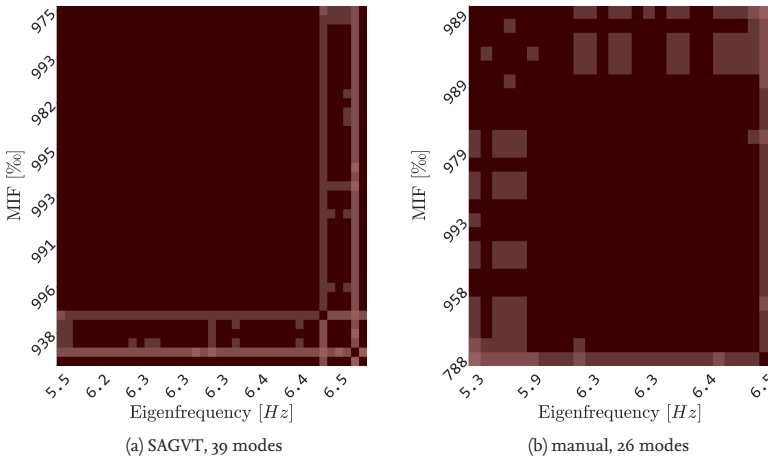
Figure 4.11: Auto-MAC matrix HTP-roll mode families comparison
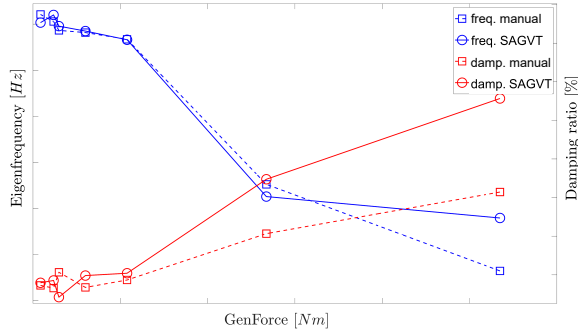
Figure 4.12: Nonlinearity plot comparison for HTP-roll mode
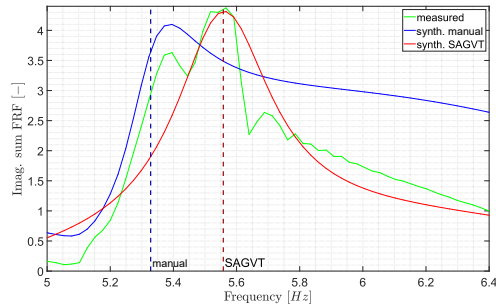
Figure 4.13: Spectra synthesis based on selected modes for HTP-roll mode

sponding mode families are analyzed. Figure 4.11 shows the MAC matrices of the mode family by SAGVT and the manual analysis. Both matrices show overall high coincidences, the mode is identified clearly several times. The MIF$_\psi$ values along the y-axis indicate that the mode is identified with low mode shape complexity. However, the eigenfrequencies, shown at the x-axis, spread over a wide range from 5.3 to 6.5 Hz. This high eigenfrequency range indicates a nonlinear mode. The range is similarly identified by both methods, however the final selection seems to be different. Figure 4.12 shows a comparison of the mode nonlinearity. One can see that the eigenfrequencies and damping ratios match well for low levels of generalized force. With a higher force level the deviation between the manual analysis and SAGVT becomes larger. For nonlinear modes, the selection of the mode for the final modal model is usually chosen from the highest force level sweep of the best excitation. In this case, the best excitation is an anti-symmetric sweep at the HTP in the z-direction with the highest force level. A comparison of the modes selected from this measurement run is shown in Figure 4.13. The measured spectra is shown as the green line and shows the typical form of a nonlinear mode from a sweep excitation. In manual EMA, the mode is chosen at the left point of the spectra peak due to the decreasing

eigenfrequency with force. Therefore, it is chosen at this specific position having the effect of the nonlinearity in mind. AMA selects the mode usually close to the highest point of the spectra peak. This leads to the discrepancy for the high force levels of this nonlinear mode. Nevertheless, the nonlinearity plot in Figure 4.12 shows that the nonlinearity is identified by SAGVT, but should be further investigated with additional methods or manual postprocessing.

4.3.2 Fixed-Wing UAV GVT

(a) Front view   (b) Side view
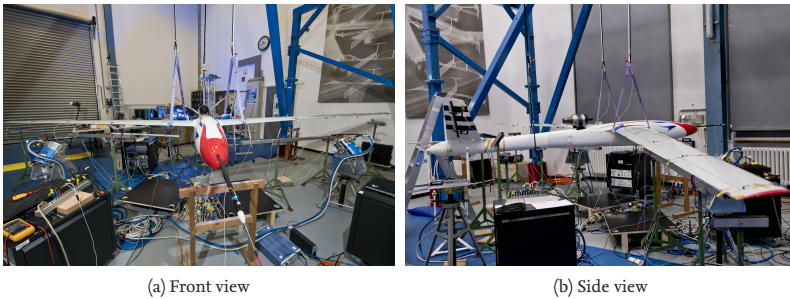
Figure 4.14: UAV during GVT

The fixed-wing UAV has been developed in a project called FLEXOP (Flutter Free FLight Envelope eXpansion for ecOnomical Performance improvement), funded within the Horizon 2020 framework programme of the European Union (grant agreement ID 636307). The UAV in the GVT is shown in Figure 4.14. The aircraft demonstrator shows many complex structural dynamic and aeroelastic phenomena similar to full-scale aircraft. Therefore, the GVT of this aircraft provided data well suited to test the SAGVT. The GVT was conducted in Göttingen, Germany at DLR in March 2019. For further general information about the GVT, the reader is referred to [88]. Since the main findings match the ones from Section 4.3.1, in this section the manual modal analysis for hyperparameter training is performed by different engineers with different modal analysis experience. Therefore, the manual reference modal model might be sub-optimal in some cases. A complex situation in this GVT was the suspension of the UAV. In Figure 4.14 one can see that the UAV is suspended using bungees in order to decouple the aircraft from the environment. The rigid body modes of the UAV are decoupled from the flexible modes, however the suspension itself has lateral modes in the frequency range of interest. If those modes are close to flexible modes of the UAV, the suspension modes might influence the identification of the UAV modes. Therefore, the correct and accurate identification of the UAV structural behaviour requires the adequate identification of the suspension modes.

The manual EMA by different engineers with different experiences in modal analysis led to differences in identified modes especially with respect to the suspension. In general, most engineers identified most of the suspension modes, but some engineers identified only few suspension modes. An example manual modal model for hyperparameter training is shown in Figure 4.15. Based on the HO, SAGVT has reanalyzed the measurement

run. The red arrows show the modes with respect to the suspension. One can see that six suspension modes are identified by the manual analysis together with nine UAV structure modes. One suspension mode at 16.4 Hz is not identified by the manual analysis, however SAGVT identified this mode. One could expect that AMA is tuned in order to find the exact same modes as given by the manual analysis. This is indeed not the case. The training of good modal analysis leads to hyperparameters which enable a well suited modal analysis procedure. Therefore, physical modes are identified, even if they have not been selected in the manual analysis which is used for the training. Of course, the manual modal analysis must find most of the physical modes and must not select many spurious modes, however some small mistakes can be corrected by SAGVT. For each mode, qual-
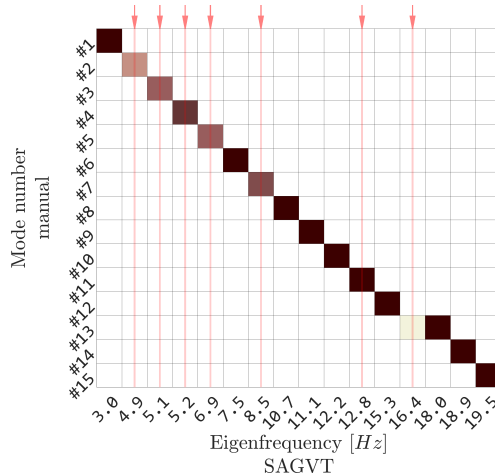
Figure 4.15: MAC-XP comparison manual training reference and SAGVT result

ity indicators can also be calculated, such as how well the synthesized spectra match the measured ones or mode shape complexity indicators like MIF_ψ, MPC, or MPD. Figure 4.16a shows comparisons of accuracy of the manual and automated modal models. The specific quality indicators are normalized so that a green bar to the top means a better value for SAGVT and a red bar to the bottom means a better value for the manual results. In Figure 4.16b, only the elastic modes of the aircraft are shown, as the optimization of the suspension modes is greater because these modes are observed with fewer sensors only. Since the correct identification of the elastic modes of the aircraft is the objective of the analysis, these comparisons are more important than the suspension modes comparisons. One can see that some quality indices are better for the SAGVT result and some are better for the manual result. It is particularly noteworthy that the spectra synthesis is invariably better in the SAGVT solution. Since the spectra synthesis is the best evidence for a good damping estimation, this quality indicator is most important. Using the trained hyperparameters, additional measurement runs were automatically analyzed and compared with manually analyzed modal models by different engineers. Results of two example measurement runs from other configurations are shown in Figure 4.17. It is ev-

(a) Full modal model

(b) Aircraft structure modes
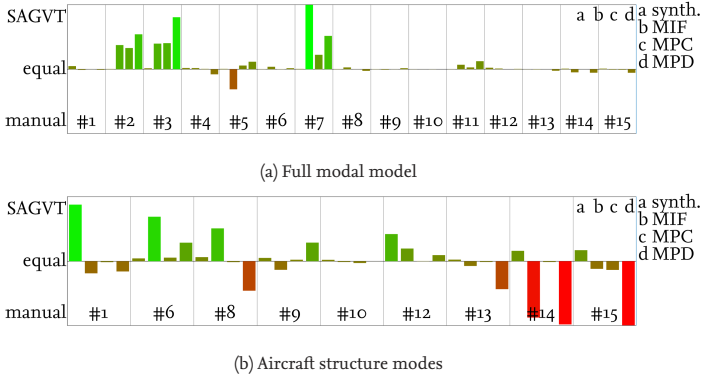
Figure 4.16: Accuracy comparison manual training reference and SAGVT result

ident that not all the suspension modes are picked in both manual analyses. In contrast, SAGVT performs the analyses consistently and reproducibly, ensuring reliable detection of the suspension modes. The optimization of the synthesized spectra also ensures that the SAGVT damping estimations are more accurate than the manual ones in this case.

(a) MAC-XP C2 WING XZ

(b) MAC-XP C3 Wing XZ

(c) Accuracy C2 Wing XZ

(d) Accuracy C3 Wing XZ
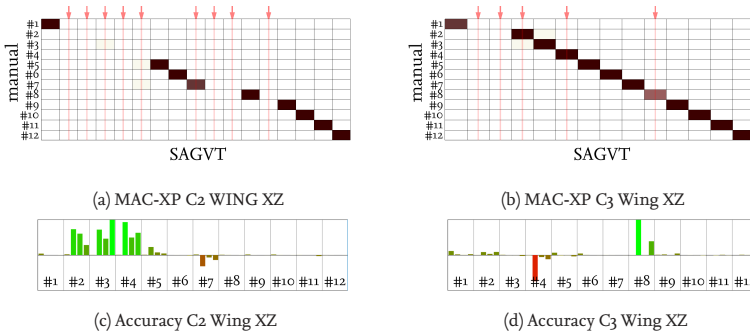
Figure 4.17: Accuracy comparison validation manual modal models and SAGVT result

4.4 Discussion

The implementation of AMA into SAGVT has significantly enhanced the efficiency and moreover the accuracy of GVT analysis. One of the foremost advantages of SAGVT is the considerable reduction in analysis time. Errors can be detected immediately rather than only after subsequent measurement runs have been recorded, enabling quicker iterations and adjustments.

Additionally, even with sub-optimal training, SAGVT produces reliable results. It has the

capability to correct small errors made during manual modal analysis for the reference model, ensuring that the outcomes are at least as good as the manually produced results, if not better. This robustness highlights the effectiveness of SAGVT, as it compensates for potential inaccuracies introduced during manual analysis.

The thoroughness of AMA surpasses that of manual analysis due to its user-independent and fully reproducible nature. The automated process eliminates the variability and subjectivity inherent in manual modal analysis, leading to a more consistent and optimized modal model. This consistency enhances the reliability of the results, making SAGVT a good choice for GVT analysis. In addition, the accuracy of the eigenfrequency and damping identification using AMA is higher than the one based on manual identification with LSCF. This is demonstrated by the invariably lower spectra synthesis error based on the modal models identified using AMA.

Despite these advantages, SAGVT does encounter challenges, particularly in accurately identifying nonlinearities. While these nonlinearities are recognized, they are not ideally identified and require postprocessing. Identifying nonlinearities in a GVT remains an active research area, as highlighted in literature [8, 33, 90].

Frequent retraining is necessary for large GVTs. In this study, for approximately 14% of the measurement runs a retraining was required for the research aircraft and the automated correlation must be postprocessed sometimes. Advanced AI techniques hold promise for further improving these aspects. Reducing the frequency of training sessions can further speed up the analysis process. However, for large GVTs, a solution where one person occasionally correlates and retrains the model seems acceptable. In contrast, for smaller GVTs, minimal retraining is required. In the shown UAV GVT example, hyperparameter training was performed three times only out of 54 measurement runs, which led to sufficient accuracy. This approach balances maintaining accuracy with reducing the workload associated with frequent retraining.

In conclusion, while SAGVT presents some challenges, particularly with nonlinearities, its benefits in terms of analysis speed, error detection, result quality, and reproducibility make it a valuable tool in modern GVT analysis. With ongoing research, these remaining challenges can be further addressed, enhancing the overall efficiency and reliability of the testing process.

5 Continuous Aeroelastic Identification in Flight Vibration Tests

5.1 Introduction to Aeroelastic Monitoring in FVT

The aeroelastic behavior of an aircraft is defined by the structural dynamics of the aircraft and the aerodynamic forces that act on the aircraft. The structural dynamic behavior of the aircraft is simulated, and the simulation model is validated using the results from the GVT. The validated structural dynamic simulation model is coupled with a model of the unsteady aerodynamic forces in the flutter calculations. The main interest is the flutter boundary, i.e., the lowest air speed for a specific air density for which the damping of one mode becomes negative. In detail, the change of eigenfrequencies and damping ratios of all modes in the frequency range of interest is monitored with changing altitude (air density) and velocity (air speed). If the flutter calculations predict an aeroelastic stable behavior in the envelope, the stability is demonstrated in a FVT. The changes in eigenfrequencies and damping ratios can be experimentally identified in flight and tracked over changing flight conditions to predict the flutter boundaries for ideal model validation. The conventional procedure is to fly to discrete points in the envelope and to iteratively expand the envelope after analyzing the quasi-constant conditions. An example is given in Figure 5.1a. In this example, discrete measurement points with constant conditions are

(a) Conventional FVT

(b) Continuous identification of FVT

(c) Discrete damping estimates

(d) Continuous damping estimates
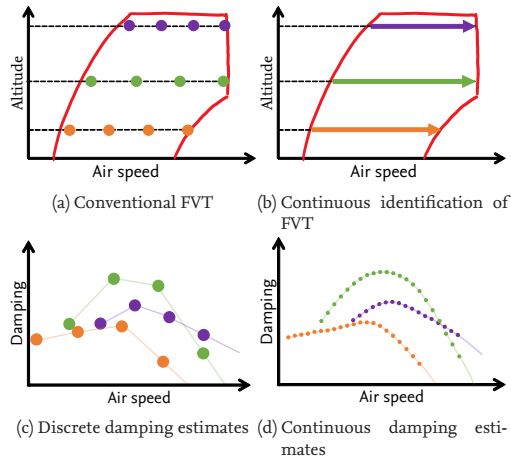
Figure 5.1: Flight envelope and resulting damping trends with FVT measurement points

chosen at four air speeds at three altitudes. This results in three damping curves of an example mode; see Figure 5.1c. Modal analysis is performed between the measurement points, and the aircraft stays on hold at a lower flight speed. The next test point is de-

fined based on the modal parameter trends, and the aircraft accelerates to the next flight speed. Unfortunately, the extrapolation of the overall damping curve relies only on a few measurement points. DLR proposes an approach of continuous analysis and slow change of flight speed. The advantage is to exploit the expensively produced flight data more and provide more accurate curves of modal parameters and extrapolations. The trend of modal parameters can be monitored during flight using real-time OMA and tracking of modes. Real-time monitoring can increase safety because a drop of damping is detected immediately. On top of that, the efficiency of a FVT is improved because less landing between measurement points and offline analysis is necessary. The continuous change
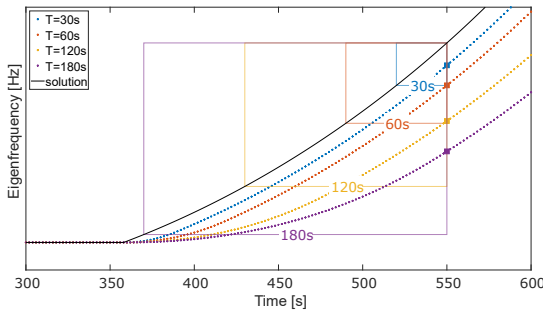
Figure 5.2: Time buffer length effect on continuous identification of LTV systems

of the flight velocity introduces some additional challenges to OMA. The correct and un-biased identification of the LTV system is possible if the system variation is "slow" [48]; however, the violation of the LTI assumption adds uncertainty to the identification results. To counteract the effect of the system variation, i.e., the smearing of varying parameters, the time buffer utilized for a single modal analysis should be as small as possible. Figure 5.2 illustrates the ideal identification of a LTV system using a sliding time buffer. The black line shows an analytical solution of a time-varying eigenfrequency. In this theoretical example, the excitation level is constant, and thus, the MID identifies the exact mean value of the information in the time buffer. The blue dotted line is identified if the system is identified based on a 30 s time buffer. The curve of the identified parameter lags behind the curve of the analytical solution by a certain distance, and a small smearing effect is noticeable at the kink. If the time buffer is increased to 60, 120, or 180 s this effect becomes more significant. However, MIDs like SSI or LSCF have less uncertainty using longer data sets since more periods of each vibration are present in the data. This effect is also shown in Figure 3.13. This means that continuous modal parameter identification requires a trade-off between the time lag of identification and identification uncertainty. In addition, OMA methods assume the excitation signal to be random and stationary. That means that the excitation level must not change in time, i.e., from the beginning of a time buffer to the end of the time buffer 50 s later. In addition, the excitation is assumed to be randomly distributed over the whole structure. Neither of the assumptions mentioned above can be ensured in actual flight tests. To conclude, the uncertainty of the modal parameters identified with OMA in FVT is increased by the non-exhaustive list:

1. poor signal-to-noise ratio

2. short time buffer length to counteract the LTV effect

3. non-stationary excitation over time (i.e. within a time buffer)

4. sub-optimal excitation over space and frequency content

5.2 Optimized Real-Time Modal Parameter Monitoring

The real-time modal parameter monitoring consists of preprocessing, MID, AMA, and modal tracking. This procedure and plots of example data are shown in Figure 5.3. In the state-of-the-art methods, the automation of modal parameter identification for FVT is highly simplified and focused on very fast processing [49]. However, the basic data flow is similar to the new one, shown in Figure 5.3. The novel AMA system does not only optimize the reliability of identifying all relevant modes and the accuracy of the identification but also provides estimated uncertainties of the identified modal parameters.

The first step of the monitoring process is a preprocessing in which the time data is

(a) Data flow   (b) Examples
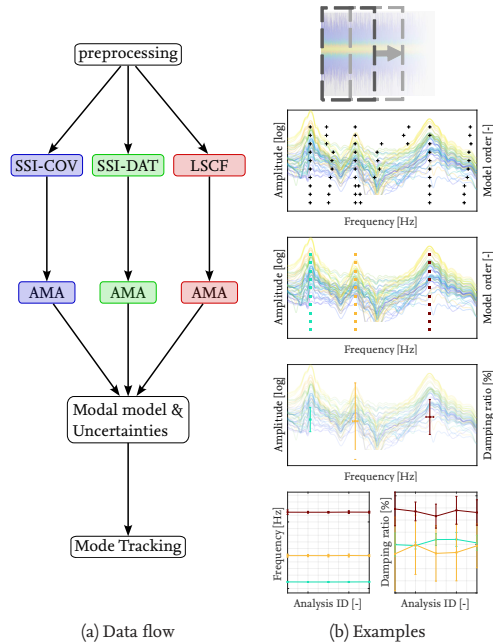
Figure 5.3: Data flow of real-time modal parameter monitoring

buffered, eventually decimated (SSI), and spectral densities are calculated (LSCF). In the

second step, MIDs estimate eigenfrequencies, damping ratios, and mode shapes for several model orders. Theoretically, any MID can be used, which creates a stabilization diagram. The chosen MIDs in this thesis are described in Section 3.4.1. The AMA method described in Chapter 3 is used to identify the physical and unique modes and to estimate uncertainties based on the mode clusters. As discussed in Section 3.5, the hyperparameters have a significant influence on the identification accuracy of MIDs like SSI-COV, SSI-DAT or LSCF and AMA. Concerning modal parameter monitoring, additional hyperparameters are of interest, e.g., the time buffer length, the time decimation, or spectra windowing parameters, see Table 3.2 for OMA. Since the run time of the whole identification should not exceed two seconds, AMA needs to run in less than two seconds on one CPU core to have enough resources for preprocessing, tracking, and background processes like GUI handling on the other cores. The multi-tier clustering described in Chapter 3 is simplified into a two-tier clustering of poles identified in only ten subsequent model orders:

1. Clustering of eigenfrequencies and damping ratios (stability analysis)

2. Clustering using a combination of eigenvalue and eigenvector information (physical mode clustering) from the following dimensions: MAC, MAC-XP, hyperbolic distance metric (HDM)[55], λ, f, ξ, MIF_ψ, MPD

3. Cluster variance calculation

The more sophisticated clustering of physical modes using additional tiers and PSO modal model is not used in the real-time AMA version. Often, the modal parameter identification is performed well also using the reduced AMA method; however, the accuracy, especially in GVT, can be increased using the more sophisticated version, since a resulting processing time of about 10 seconds is feasible in GVT.

The optimization of hyperparameters, which are relevant for OMA, are optimized for monitoring purposes using the scheme shown in Figure 5.4. Multiple sequences of an overall long time data set are used to optimize the modal parameters for various test data conditions (e.g., the time data of a flight with varying conditions). This is feasible since the FVT takes place usually later than the maiden flight and some other flight tests. Since the reference modal model for AMA result comparison is defined only once, the mode matching threshold for the mode quality comparison (see Equation 3.14) should be lower for MAC-XP, e.g., 0.3, or the matching metric can be simplified by using the MAC function. In this thesis, both metrics are used in parallel, and if one value indicates a match, the mode is assigned to the family. An additional penalty term discriminates hyperparameters, which would lead to a longer run time than two seconds, to ensure real-time capability. This leads to an updated objective function

$$q_{FVT}(\mathbf{P}) = -N_{Sp} \cdot r_{Sp} + \sum_{i=1}^{N} w_{M,i} \cdot q_{FVT,i} - r_{\Delta t} \ , \tag{5.1}$$

$$r_{\Delta t} = \begin{cases} 30, & if \quad runtime > 2\,s \\ 0, & otherwise \end{cases}, \tag{5.2}$$

$$q_{FVT,i} = \begin{cases} c_j \cdot w_c^T, & if \quad MACXP(\lambda_{AMA,j}, \psi_{AMA,j}, \lambda_{MAN,i}, \psi_{MAN,i}) > 0.3 \\ c_j \cdot w_c^T, & if \quad MAC(\psi_{AMA,j}, \psi_{MAN,i}) > 0.7 \\ -r_{Mis} & otherwise \end{cases}, \tag{5.3}$$

with $r_{\Delta t}$ is the penalty for a high run time. The presented HO can be applied to a combination of each MID with AMA. Therefore, the ideal hyperparameters for SSI-COV, SSI-DAT, and LSCF are most likely different. Since they build the basis for the clustering, the AMA hyperparameters will also be different depending on the MID. Because of that, the scheme in Figure 5.4 should be applied to each included MID. However, the applied time buffer lengths of different MIDs have to be identical since the investigated system might differ otherwise in the case of a LTV system. To fuse the results of multiple MIDs, they must identify the same quasi-stationary system.

The outcome of AMA for every analysis block is appended to a so-called mode library
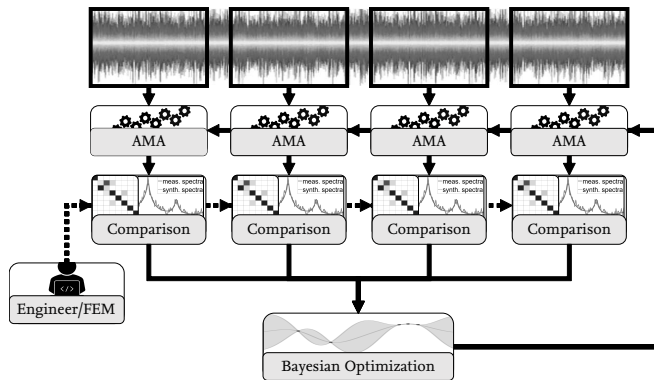
Figure 5.4: HO using BO for real-time modal parameter monitoring

comparable to the correlation step at GVT: a mode family is a group of re-identifications of the same physical mode from different conditions. In addition, all relevant external parameters, such as, e.g., air speed and altitude, are stored in the mode library to link the modal parameters to flight conditions. This process is often called mode tracking (see an example algorithm in [48]). In this thesis, the resulting mode library holds all relevant data in tabular form to ensure efficient read and write operations, which are used to fuse different MIDs within one time step and to fuse subsequent time steps. Those fusion methods are described in Section 3.4.1 and 3.4.2.

5.3 Application and Results

The real-time modal parameter monitoring using AMA and data fusion approaches is verified in two flight test activities. First, the method was applied and tested at a FVT of a research aircraft business jet. In this FVT, continuous acceleration maneuvers at constant flight levels could be realized. The results are shown in Section 5.3.1. Additionally, the method was tested using flight test data from a fixed-wing UAV, in which the flight speed was changed conventionally, i.e., stepwise, from discrete flight speed measurement points to the next discrete point. In this flight test, the aircraft was accelerated up to the flutter speed.

5.3.1 Business Jet Research Aircraft FVT

The monitoring system was verified in the FVT of the DLR research aircraft ISTAR. A photo of the ISTAR before the FVT is shown in Figure 5.5a. The business jet has a wing span of 21.4 m, a maximum take-off weight of 19.1 t, and a maximum cruise speed of about 519 kn (961 km/h). The uniqueness of ISTAR is the high-density instrumentation of 62 acceleration sensors, many other sensors such as, e.g., strain sensors, and a measurement system. The measurement system is the CRONOSflex from imc Test & Measurement[46], which is capable of recording data continuously in every flight of the aircraft and streaming the data online every two seconds to an analysis computer in the cabin over Ethernet. Figure 5.5b shows the acceleration sensor plan. The flight test campaign took place at the airport Brunswick/Wolfsburg, Germany, in May 2023 as part of the DLR internal project HighFly (high-speed inflight validation). In the flight test campaign, the boundaries of the flight envelope were approached, so that significant changes in the operating conditions were achieved; however, the aircraft was in a flutter stable regime for the whole flight. The FVT was not part of a certification process; therefore, the new real-time monitoring system could be tested and demonstrated in flight. The flight tests consisted of maneuvers at different constant altitudes while slowly increasing the flight velocity. During these maneuvers, real-time modal parameter identification was used to track the eigenfrequency and damping ratio changes. The monitoring system was implemented on two analysis computers in the cabin to be able to run the former DLR version [49] of the real-time modal parameter monitoring and in parallel with the novel version using AMA and data fusion. The data processing computers were mounted into racks inside the cabin and were connected to the measurement system using Ethernet. The data processing computers with the presented modal parameter monitoring system are shown in Figure 5.6.

The test consisted of ten flights on four flight levels and different level acceleration

(a) Photo at airport Brunswick/Wolfsburg   (b) Acceleration sensor plan
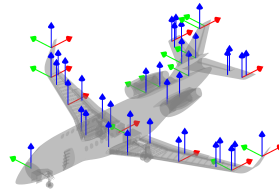
Figure 5.5: DLR research aircraft ISTAR at FVT

maneuvers, including fast and slow acceleration. In all level acceleration maneuvers, the aircraft stayed at a constant flight level, accelerated from a low air speed to a high air speed, and decelerated back to the initial flight condition. For example, for flight number five, the aircraft was on flight level 110, about 3335 m altitude, and was accelerated from about 180 kn to 430 kn. During the fast acceleration (full throttle), this resulted in 108 s duration from slow to fast or an average acceleration of 2.3 kn/s. The slow acceleration resulted in 395 s duration, i.e., an average acceleration of 0.64 kn/s. For this thesis, the slow level acceleration maneuver is of major interest. The time acceleration data of the slow acceleration

Figure 5.6: Analysis computers with real-time modal parameter monitoring system in ISTAR FVT
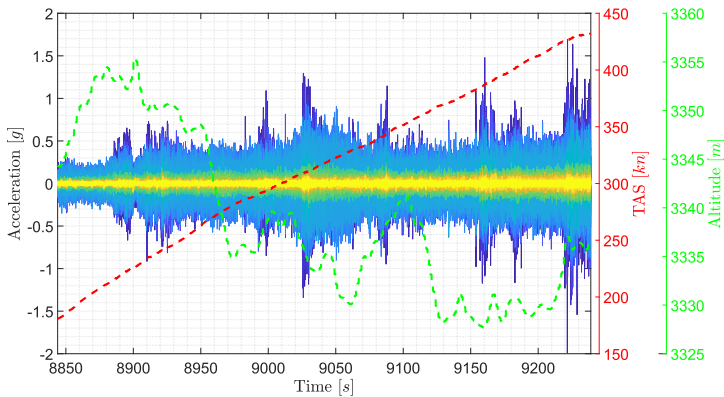
Figure 5.7: Acceleration time data with TAS and altitude from ISTAR FVT level acceleration maneuver

maneuver is shown in Figure 5.7. The true air speed (TAS) and altitude are plotted on the right axes of ordinates. The continuous and slow acceleration worked well for this maneuver since the air speed changes almost perfectly linearly. The altitude is kept between 3327m and 3355m; this variation is neglected in the following. The presented data fusion-based improvement of real-time modal parameter monitoring consists of two approaches: fusion of different MID and fusion of subsequent time steps. The flight maneuver is analyzed using the individual MIDs (SSI-COV, SSI-DAT and LSCF processed with AMA), fused by IVM and fused by KF to show the effect of both approaches. The first comparison is between the individual MIDs and IVM. Figure 5.8 shows an overview of the eigenfrequency tracking. In this maneuver, 15 modes are identified and tracked up to 20 Hz. Compared to the GVT results most modes are found and tracked, as seen in Table 5.1. Since the ac-

No. FVT	Name	GVT f	FVT f	GVT ξ	FVT ξ
1	2n wing bending S	3.5	3.9-5.4 Hz	0.51%	7.2-24%
2	3n wing bending A	4.4	4.6-6.1 Hz	1.31%	6.1-29%
3	HTP roll A	5.3	6.6-7.3 Hz	2.07%	4.8-19%
4	2n fuselage bending A	7.5	6.7-7.7 Hz	1.50%	2-6.7%
5	engine heave A	7.1	7.9-9.8 Hz	0.5%	4.6-21%
6	4n wing bending S	9.7	9.5-10.7 Hz	1.5%	2.9-7.2%
7	2n fuselage bending S	11.0	11.1-12.2 Hz	0.88%	3.2-9.7%
8	VTP bending A	12.8	11.6-13.3 Hz	3.0%	3-13%
9	5n wing bending A	11.9	13.3-14.9 Hz	2.2%	1.92-10%
10	2n HTP bending S	14.1	13.5-15.1 Hz	0.89%	0.79-5.4%
11	2n wing inplane S	14.0	14.0-14.3 Hz	0.89%	1.4-4.5
12	winglet S	16.9	16.5-17.3 Hz	2.3%	1.5-4.4%
13	winglet A	17.0	16.7-17.7 Hz	2.45%	2.7-7.4%
14	wing torsion A	17.8	18.4-20.3 Hz	1.1%	0.64-10%
15	wing torsion S	18.6	18.9-20.0 Hz	0.93%	0.86-8.6%
-	engine heave S	7.5	-	1.2%	-
-	HTP yaw A	9.7	-	0.5%	-
-	engine yaw A	9.9	-	2.5%	-
-	engine yaw S	12.0	-	2.2%	-
-	FTI rack A	13.8	-	1.4%	-
-	rudder A	16.9	-	1.3%	-
-	APU U	18.9	-	0.86%	-

Table 5.1: Comparison of identified eigenfrequencies and damping ratios from ISTAR GVT and FVT

celeration sensors installed closest to the engines for the flight tests are on the pylons and those in the Y direction are installed only on one pylon, only one out of four engine modes is identified. The HTP yaw mode and the rudder mode are difficult to observe since only a few sensors are installed at those components, and modes with similar frequencies and larger amplitudes superimpose the modes. The remaining local modes at the flight test instrumentation (FTI) rack and APU cannot be identified since no FTI sensors exist to observe these modes. Figure 5.9 shows some examples of the damping ratio tracking. Some modes are identified continuously by all MIDs, e.g. in Figure 5.9a, 5.9c and 5.9e. But for several modes, only a subgroup of all MIDs shows continuous identification results. For example, mode number four is well identified by SSI-DAT and LSCF only; see Figure 5.9b. However, the seventh mode is identified by SSI-DAT and SSI-COV only; see Figure 5.9d. In a third example in Figure 5.9f, one can see that the anti-symmetric winglet mode is identified mainly by SSI-COV only. In some examples, e.g., in Figure 5.9d and 5.9e, the damping estimated by different MIDs differs significantly. In these examples, the IVM fusion of the MIDs results can lead to a zick-zack of the damping estimates, which needs further processing. Nevertheless, the modes are clearly identified, as seen in the mode shapes of those six example modes in Figure 5.10. The combination of the three MIDs leads to almost continuous identification of all 15 modes.
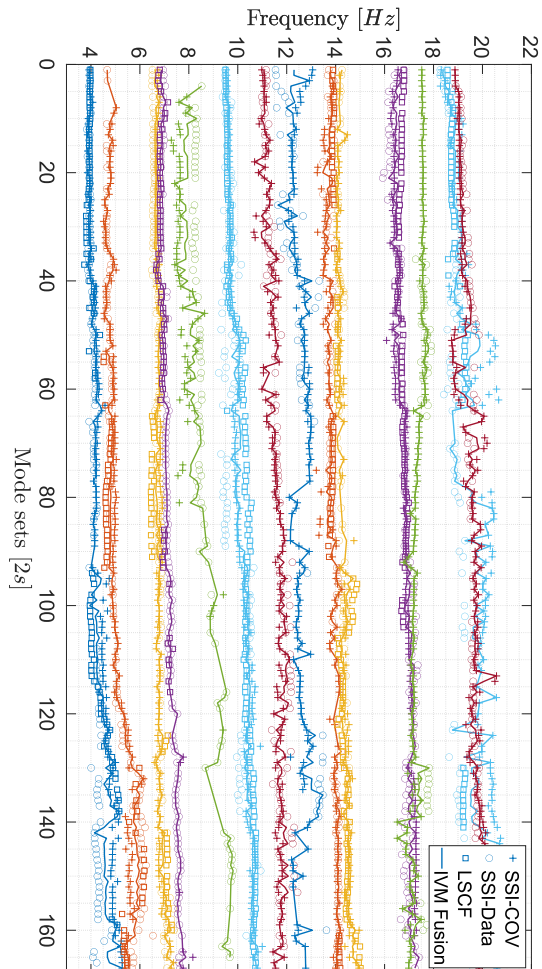
Figure 5.8: Eigenfrequency tracking using MIDs and IVM over time from ISTAR FVT
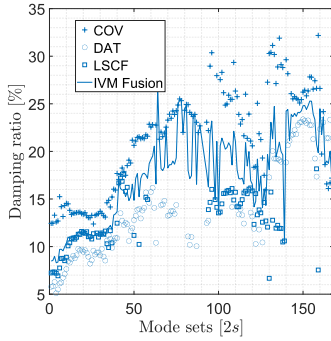
(a) 1st mode - 2n wing bending
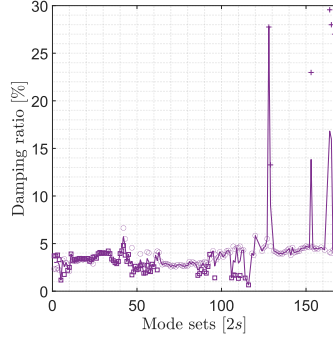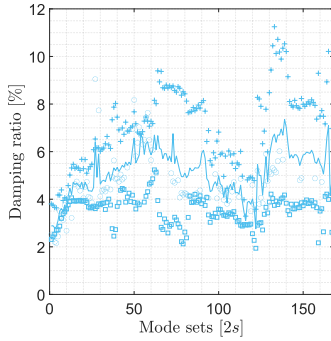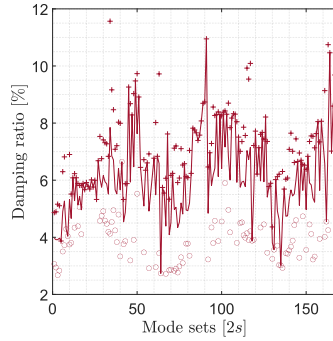
(b) 4th mode - 2n fuselage A

(c) 6th mode - 4n wing bending

(d) 7th mode - 2n fuselage S
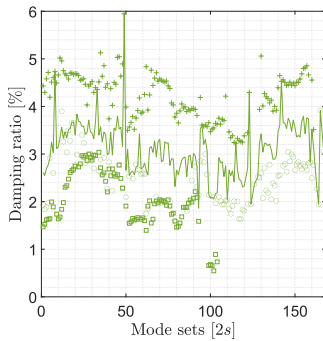
(e) 12th mode - winglet symmetric
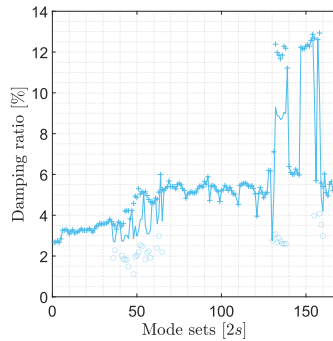
(f) 13th mode - winglet anti-symmetric

Figure 5.9: Damping ratio tracking of MIDs and IVM of example modes from ISTAR FVT.

(a) 1st mode - 2n wing bending

(b) 4th mode - 2n fuselage A

(c) 6th mode - 4n wing bending

(d) 7th mode - 2n fuselage S

(e) 12th mode - winglet symmetric

(f) 13th mode - winglet anti-symmetric
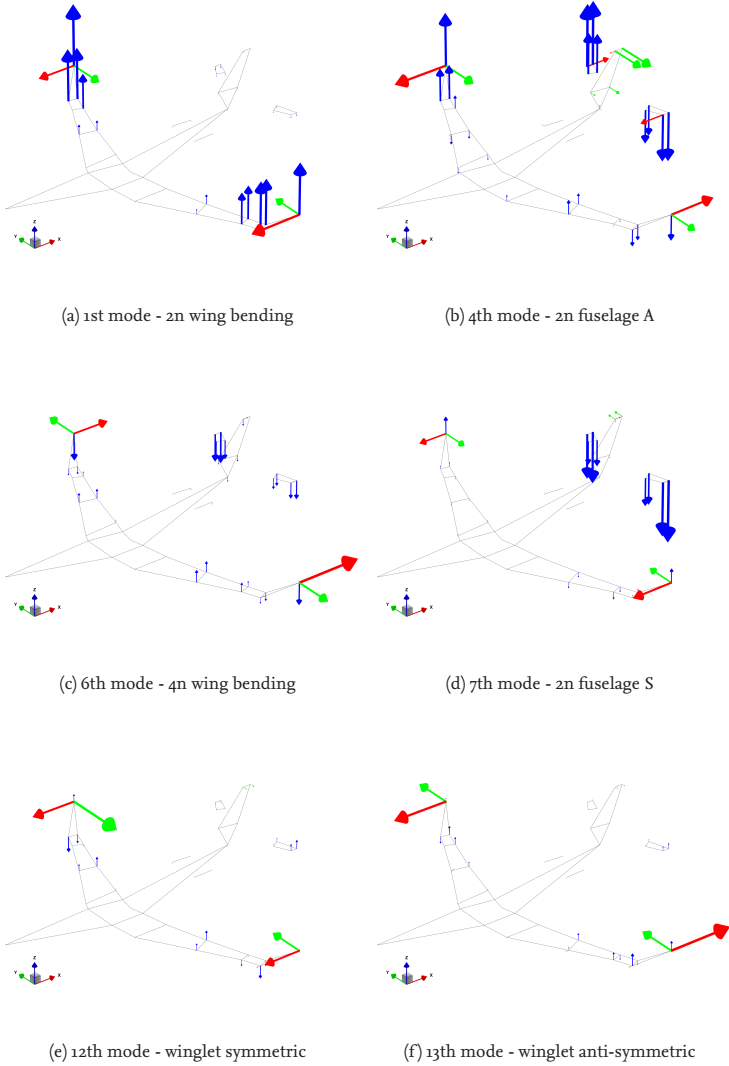
Figure 5.10: Mode shapes of example modes from ISTAR FVT.

In addition to the challenge that some modes are not found reliably by individual MIDs, two more examples are shown in Figure 5.11 and Figure 5.12. In Figure 5.11, one can see the eigenfrequency tracking of two modes using individual MIDs and a combined tracking of all MIDs. In Figure 5.11a, the tracking using LSCF results in one mode family since the mode shapes of the anti-symmetric mode (3n wing bend) are highly complex and therefore seem to be similar to the symmetric mode (2n wing bend) in terms of MAC-XP. However, if these LSCF results are identified in combination with SSI-COV and SSI-DAT, the modes identified by LSCF are tracked into the correct mode families, see Figure 5.11b.

Figure 5.12 shows the eigenfrequency and damping tracking of the 4n wing bending mode. This example shows that the MID, which gives the most promising eigenfrequency estimation, is not necessarily the same for the best damping estimation. The modes identified by individual MIDs are shown together with the IVM fusion as a line. Assuming that the fusion of those three estimators is a good overall estimate, the eigenfrequency is found best, i.e., closest to the IVM estimate, by SSI-COV and the damping ratio is identified best by SSI-DAT. The combination of different MIDs leads to more complete modal

(a) Mode tracking of individual MIDs

(b) Mode tracking of combined MIDs
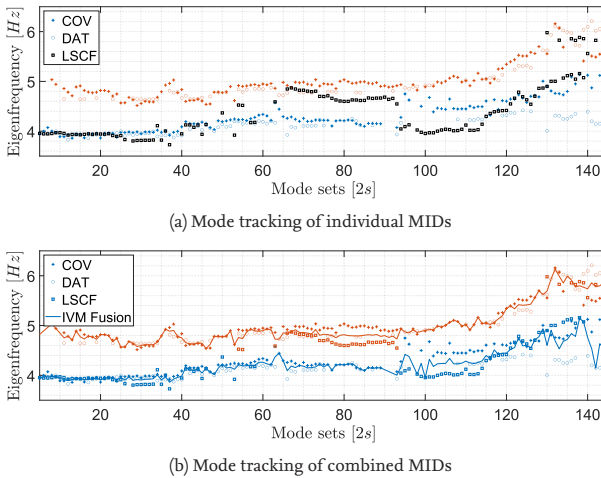
Figure 5.11: Mode tracking of individual MIDs can result in incorrect tracking, in this case merging of two neighboring modes

models, more reliability in re-identification of modes, and reduction of potential biases of individual MIDs. The scatter (or uncertainty) of the eigenfrequencies and especially the damping ratios is still significant. Therefore, the second step of data fusion, i.e., the KF, is applied, too. The maneuver of the FVT is an almost constant acceleration of the aircraft at an almost constant flight level. Therefore, the assumptions made for the KF in Section 3.4.2 are valid for this data. The dynamic behavior identified using the highly overlapping FIFO time buffer is assumed to change linearly from one time step to the next; therefore, the constant change transition model is used in this example. Figure 5.13 shows an overview comparison of the eigenfrequencies identified using the IVM fusion

(a) Eigenfrequency tracking

(b) Damping ratio tracking
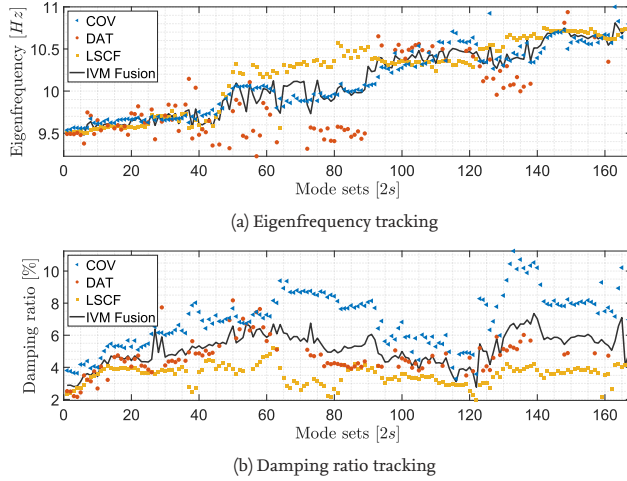
Figure 5.12: MIDs comparison for 4n wing bending: SSI-COV is closest to the IVM eigenfrequencies, but SSI-DAT is closest to the IVM damping ratios

as squares and the KF fusion as lines. One can see, in general, smoother curves and less scattering of the eigenfrequency changes. Notably, outliers of eigenfrequencies that remain in the IVM fusion are cleaned using the KF fusion. The KF shall decrease the scatter of the eigenfrequencies. However, it must not smear or manipulate the physical changes of the eigenfrequencies. The overall trend of modal parameters using continuous OMA in aeroelastic applications is often visualized as an interpolation using restricted cubic splines of mean values [78, 9]. This simplifies a subsequent comparison to the numerical flutter curves of the simulation model. The mean values along the flight speed are fit using a least squares method from [40]. The scatter of modal parameters over changing flight speed can be interpreted as the mean deviation between the identification points and the interpolation. However, the interpolation itself changes if calculated based on different identification points; therefore, it has to be proven that the interpolation does not change significantly. Figure 5.14 shows eigenfrequency tracking over true air speed (TAS) of example modes using IVM, KF and the corresponding interpolations. The first outcome is that the interpolation curves match well; therefore, the core information content of the data is not manipulated. The second outcome is a reduction in scattering using the KF in red, while local phenomena and changes in eigenfrequencies are kept. The damping ratios of the same example modes are shown in Figure 5.15. In general, the outcomes match the ones of the eigenfrequency tracking; however, in Figure 5.15b, the interpolations differ for low TAS because of different damping estimations of the used MIDs. In Figure 5.15d, the KF-based results are slightly further away from the interpolation than the IVM results for a small TAS range. The scatter is described as mean squared difference (MSD) between the identification points and the interpolation lines to compare the scatter of IVM and KF quantitatively.
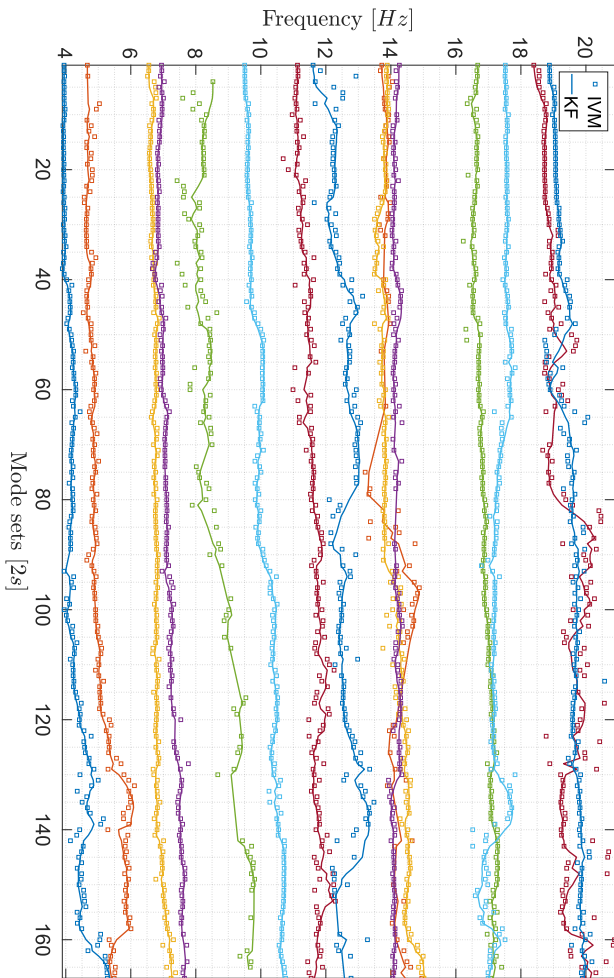
Figure 5.13: Overview of KF-based eigenfrequency tracking from ISTAR FVT

(a) 1st mode - 2n wing bending

(b) 2nd mode - 3n wing bending
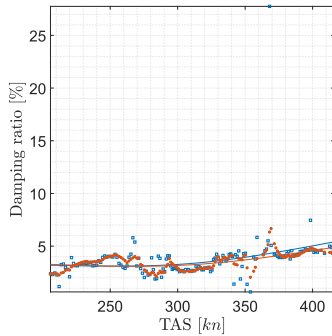
(c) 4th mode - 2n fuselage A
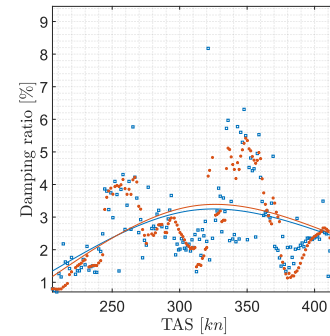
(d) 10th mode - 2n fuselage bending
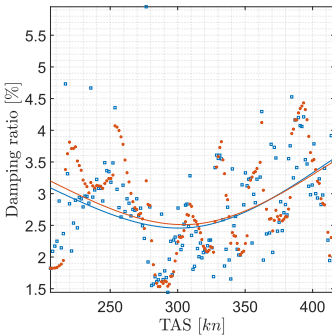
(e) 12th mode - winglet S
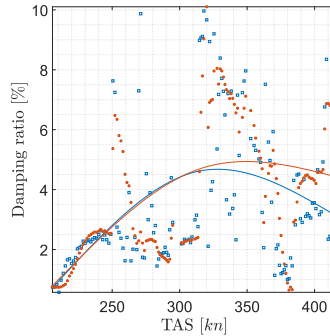
(f) 14th mode - wing torsion A

Figure 5.14: Interpolation of KF and IVM eigenfrequency tracking over speed of example modes from ISTAR FVT.

Figure 5.15: Interpolation of KF and IVM damping ratio tracking over speed of example modes from ISTAR FVT.

(a) Eigenfrequency

(b) Damping ratio
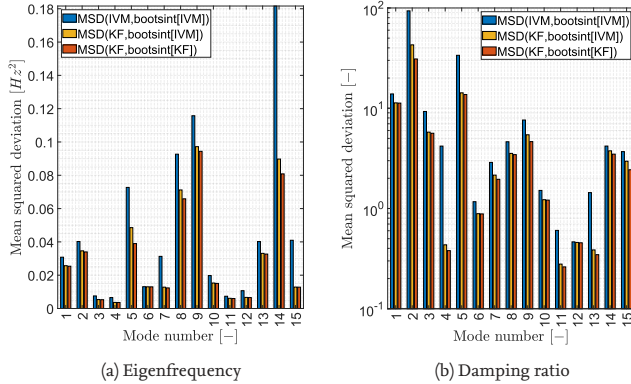
Figure 5.16: MSD between KF and IVM identifications and the overall interpolations

An overview of the MSD for all modes is given in Figure 5.16. Since the interpolation line itself might be different using the KF, the identification points of both IVM and KF are compared with respect to the interpolation of the IVM. In addition, the MSD of the KF points with respect to the KF interpolation is given. The blue bars indicate the MSD using the IVM points, the yellow bars indicate the MSD between the KF points and the IVM interpolation and the red bars indicate the MSD between the KF points and the KF interpolation. The lowest MSD, i.e., averaged scatter, is always found using the KF points, even if they are compared with the IVM interpolation. For some modes, the difference of the MSD is small. However, reliably cleaning outliers and missing identifications is a significant advantage. The effect of smoothing using the KF can be increased significantly using smaller values for the noise covariance matrix Q. However, in this thesis, the basic applicability is proven, and further improvement is being carried out in future research. To visualize the overall effect of the data fusion approach for real-time modal parameter monitoring at ISTAR FVT, the tracking of the first four modes is shown for the basic MIDs together with the fusion results in Figure 5.17. It can be seen that a continuous identification of all modes is possible only using the fusion approaches. However, the identification of some modes, e.g., the damping ratio of the second mode in Figure 5.15b and 5.17h, shows a significant discrepancy between the MIDs and therefore the fusion shows scatter. In such a case, the KF could be extended in future research to estimate the probability of measurement outliers. This can be done, for example, by using a KF with integrated probabilistic data association (IPDA)[61].

(a) SSI-COV eigenfrequency

(b) SSI-COV damping ratio

(c) SSI-DAT eigenfrequency

(d) SSI-DAT damping ratio

(e) LSCF eigenfrequency

(f) LSCF damping ratio

(g) IVM eigenfrequency

(h) IVM damping ratio

(i) KF eigenfrequency

(j) KF damping ratio
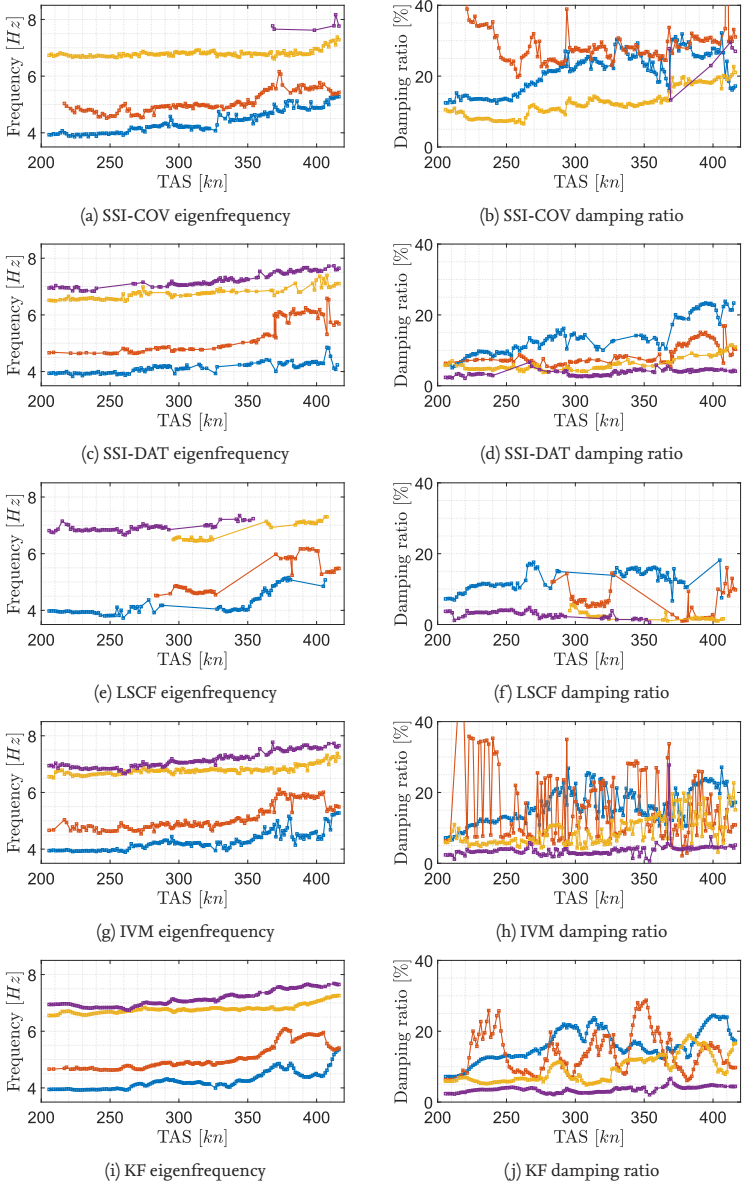
Figure 5.17: Comparison of SSI-COV, SSI-DAT, LSCF, IVM fusion and KF fusion results for first four modes in ISTAR FVT.

In this specific FVT, the most reliable MID is SSI-DAT. LSCF struggles with anti-symmetric modes. Some modes are not identified using SSI-COV, but other modes, e.g., mode number twelve, are identified almost exclusively using SSI-COV, see Figure 5.9e. As discussed in Chapter 3, a good choice of hyperparameters is crucial for the performance of MIDs. Therefore, all three MIDs are optimized using BO individually to identify as many modes from the GVT from the flight data as possible while keeping the number of spurious modes small. It is not a surprise that the optimal time buffer length is different for the different estimators. Different time buffers result in different state estimations because the aeroelastic system might have changed within the non-overlapping part of the buffers. This would result in smearing different state estimations using different MIDs. Therefore, the same time buffer length is prescribed for all MIDs. In this study, the time buffer length from HO of SSI-DAT is chosen for all MIDs, namely 60 s. Therefore, the hyperparameters are optimal for SSI-DAT. The optimal time buffer length of LSCF for this data set was 90 s, and the one of SSI-COV was 53 s. The hyperparameters of SSI-COV and LSCF are optimized again with a set time buffer length of 60 s. The final optimized hyperparameters of the MIDs used in this test are given in Table 5.2. The references DoFs for the generation of CPSDs are shown in Figure 5.18. Notably, many references DoFs are chosen. There might be hyperparameter sets with fewer references DoF and similar accuracies; however, the optimization does not search for a minimal number of reference DoFs as long as the run time is less than two seconds. The final tracking of modal param-
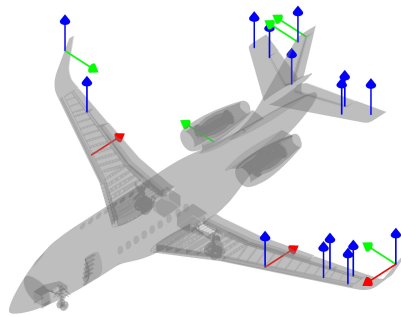
Figure 5.18: CPSDs references for real-time identification in ISTAR level acceleration maneuvers

eters using the KF fusion leads to clean curves for most modes. Because of the reliable tracking, the test results can be used to compare different maneuvers concerning OMA-based modal parameter monitoring of LTV systems. A crucial question is whether the variation of the aeroelastic system is sufficiently slow to be identified incrementally using the LTI approach. In addition to the slow acceleration maneuver, a slow deceleration, a fast acceleration, and a fast deceleration maneuvers were part of the flight test campaign. The slow maneuvers had an average acceleration rate of 0.64 kn/s and a deceleration rate of 0.56 kn/s. The fast maneuvers had an acceleration rate of 2.32 kn/s and a deceleration rate of 1.22 kn/s. The results of these maneuvers are compared in Figure 5.19 for the first

Parameter	MID	Value
Time buffer length	all (optimized for SSI-DAT)	60 s
Time decimation factor	SSI-COV	4
Time decimation factor	SSI-DAT	4
Spectra window length	CPSDs for LSCF	728 samples
Spectra window overlap	CPSDs for LSCF	0.66
Spectra references	CPSDs for LSCF	see Figure 5.18
Model order	LSCF (two identification bands)	36
Model order	SSI-COV (one band)	50
Model order	SSI-DAT (one band)	56
Hankel matrix block size	SSI-COV	12
Hankel matrix block size	SSI-DAT	14
Frequency stability	SSI-COV	30 %
Damping stability	SSI-COV	100 %
Frequency stability	SSI-DAT	37 %
Damping stability	SSI-DAT	41 %
Frequency stability	LSCF	12 %
Damping stability	LSCF	23 %
Clustering dimensions	SSI-COV	MAC-XP
Clustering dimensions	SSI-DAT	MAC-XP, MIF$_\psi$
Clustering dimensions	LSCF	HDM, MPD
Clustering distance	SSI-COV	0.2
Clustering distance	SSI-DAT	0.3
Clustering distance	LSCF	0.65
Min. cluster size	SSI-COV	0.6 of model orders
Min. cluster size	SSI-DAT	0.79 of model orders
Min. cluster size	LSCF	0.62 of model orders

Table 5.2: Optimized hyperparameters for real-time identification in ISTAR level acceleration maneuvers

two modes. The fast maneuvers are performed significantly earlier in the flight than the slow maneuvers. Therefore, the eigenfrequency shift between those curves results from mass change due to fuel burning and can be ignored. However, the mass change between an acceleration and deceleration maneuver is insignificant. Under the assumption that the LTV effect is negligible, the direction of flight speed variation must be negligible, too. Therefore, the yellow lines on the one hand and the blue lines on the other hand should match. Right-pointing and left-pointing triangles indicate the acceleration and deceleration maneuvers, respectively. One can see that the yellow lines show an overall similar trend in most TAS ranges, whereas the blue curves have a significant offset. This means that for the fast maneuvers, the direction of flight speed variation (acceleration or deceleration) biases the identification results using the LTI identification methods. In contrast to this, no bias is present for the slow maneuvers. The consistency of the curves for the slow maneuvers can be interpreted as proof that continuous identification works for slowly time-varying systems. Nevertheless, the yellow curves have discrepancies in some TAS ranges. Those might be a result of excitation that is too weak or non-stationary. Artificial excitation in FVT exceeds the scope of this thesis but is an ongoing research topic. An example discussion about artificial excitation concerning the ISTAR flight test campaign can be found in [106]. However, the topic should be further investigated.

(a) First mode

(b) Second mode
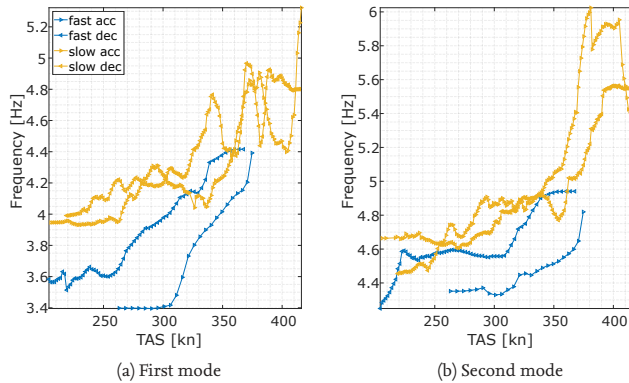
Figure 5.19: Comparison of fast and slow acceleration and deceleration maneuvers using KF-based mode tracking

5.3.2 Fixed-Wing UAV FVT

The fixed-wing UAV has a wing span of seven meters and is shown in Figure 5.20. The aircraft is equipped with microelectromechanical systems (MEMs) acceleration sensors and a Raspberry Pi 4 to record acceleration time data. A sensor plan is shown in Figure 5.21.

Within the European Union Horizon 2020 project called FliPASED (Flight Phase Adap-

(a) On ground

(b) At take-off

(c) In flight

Figure 5.20: UAV at FVT

tive Aero-Servo-Elastic Aircraft Design Methods, grant agreement ID 815058, a flight test campaign took place at the DLR National Test Center for Unmanned Aircraft Systems in Cochstedt, Germany. The project aimed to demonstrate active flutter suppression using actively controlled flaps. Before the active flutter control was applied, the aircraft was flown in open-loop to approach and verify the flutter boundary in a FVT. Figure 5.22 shows the time data of a flight without the active flutter suppression system (flight test number FT32 for reference). The altitude of the flight is almost constant at 365 m. The flight velocity is increased step-wise from 44 m/s to 54 m/s. At 55 m/s, the aircraft encountered flutter of the seventh mode, i.e., the symmetric wing torsion in a later flight after the active controller tests. The aircraft was equipped with beams and additional movable masses, called flutter stoppers, at the wing tips to change the wing torsion eigenfrequency
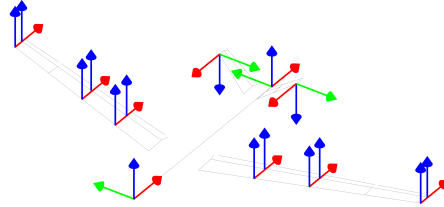
Figure 5.21: UAV acceleration sensor plan

if flutter is detected rapidly. In the final test of the project, the large vibration amplitudes due to the flutter destroyed the flutter stopper beams. This was not intended. However, it changed the mass configuration of the wing, and the eigenfrequency of the wing torsion was changed; therefore, the aircraft was flutter stable again.

In contrast to a business jet, the flight conditions such as, e.g., altitude, velocity, angle of
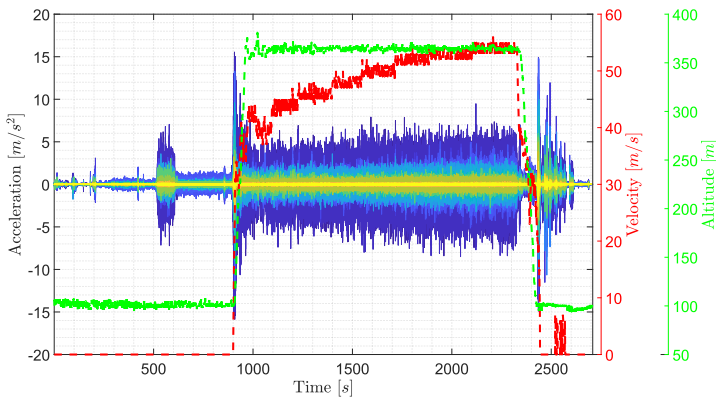
Figure 5.22: Acceleration time data with flight velocity and altitude from UAV FVT

attack, or bank angle vary more in a FVT of such a small and light aircraft. Therefore, there are more potential sources of modal parameter variation. The flight speed was increased step-wise as for a conventional FVT to reduce the sources of modal parameter variation in this FVT. This reduces the system variation over time because it leads to almost stable test points at specific flight speeds. The acceleration time data is shown in Figure 5.22 with the flight velocity in red and the altitude in green. The velocity shows a step-wise increase, indicating the constant measurement points. The transition matrix of the KF is therefore chosen such that the KF assumes constant modal parameters ($A = I_2$). Figure 5.23 shows an overview of eigenfrequency tracking over the flight duration using the KF.
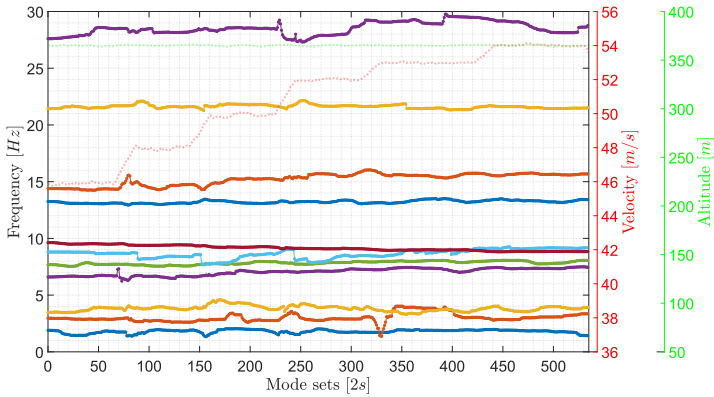
Figure 5.23: Eigenfrequency tracking overview using AMA and a KF for flutter flight test of the UAV

 Figure 5.24 shows a comparison of eigenfrequency tracking using the separate MIDs and the KF version. For the sake of simplicity, only four example modes are plotted, namely the 2n wing bending, symmetric wing torsion, 3n wing bending, and 4n wing bending. The mode shapes of these modes are shown in Figure 5.25. All identification methods track the eigenfrequency of the flutter critical mode symmetric wing torsion from about 9.6 Hz to 8.8 Hz. However, the identification of the other eigenfrequencies differs slightly. One can see many identifications at the discrete flight velocities of the different measurement points. Obviously, the identification is less stable between the measurement points using the individual MIDs. The proposed KF method results in continuous identification. As expected, the uncertainties for the damping estimates are more considerable. Figure 5.26 compares the damping tracking of the same four modes. One can see that during the transition phases, the change in flight velocity is too fast to be identified as unbiased. Therefore, the identifications between the measurement points do not connect the point clouds of the measurement points ideally, as can be seen in Figure 5.26b or 5.26d for the blue mode (2n wing bending). The identifications of those transition phases can be filtered out to create the flutter curve interpolation as part of the flight postprocessing.
 In Figure 5.27, the damping is zoomed towards the flutter mode. One can see continuous and clean trends of the flutter mode up to 54 m/s, which is close to the flutter boundary (55 m/s). The bias of the damping ratio during the transition phase is not present for the flutter mode. Because of lower damping, the vibration amplitude is more prominent, so the identification of this mode is better. The unbiased identification of the flutter mode during the transition phases can be used to improve the flutter prediction.
As mentioned above, the KF in these figures used the identity transition model, i.e., the modal parameters are assumed to be constant from k to $k+1$. This model works best for stationary test points with constant flight speeds. However, the model is not well suited in the transition phase from one flight speed to the next. It takes some time steps until the KF estimates converge to the stationary modal parameters of the next stationary flight

(a) SSI-COV

(b) SSI-DAT

(c) LSCF

(d) KF
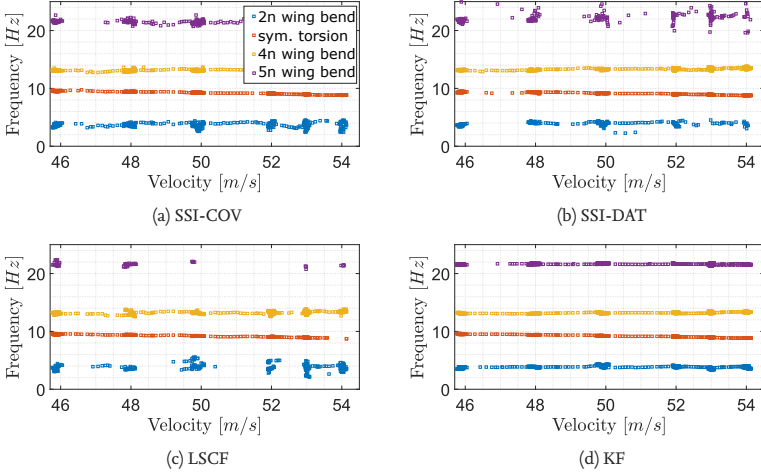
Figure 5.24: UAV eigenfrequency tracking comparison

(a) 2n wing bending

(b) sym. wing torsion

(c) 4n wing bending

(d) 5n wing bending
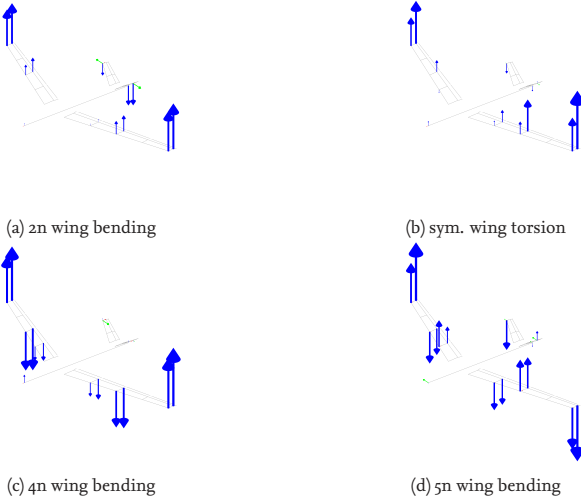
Figure 5.25: UAV example mode shapes identified in FVT

velocity. Therefore, the IMM-KF version is also applied for this test case. In the IMM-KF version, two models are combined: once the constant transition model and once the constant change transition model. The standard deviation of the flight velocity in the
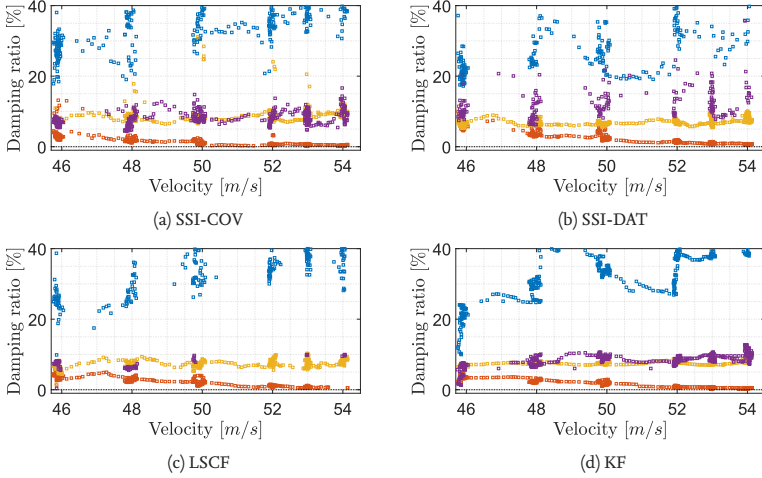
Figure 5.26: UAV damping tracking comparison
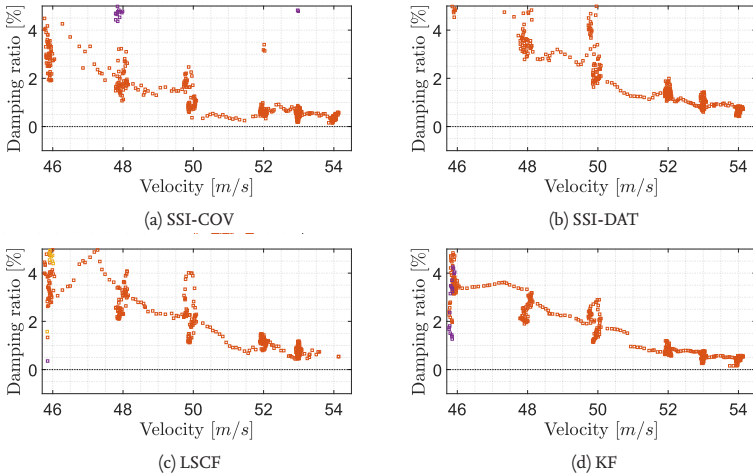
Figure 5.27: UAV damping tracking comparison zoomed to flutter mode

time buffer is used to weight those two transition models in the IMM-KF automatically. The results of the constant transition model, the constant change transition model, and the IMM-KF transition model are compared as eigenfrequencies and damping ratios in Figure 5.28. Since, most of the time, the aircraft is in a stationary test point, the IMM-KF

result is very close to the constant transition model. The constant change transition model shows the largest scatter for this example. This is as expected since the constant change transition model assumes a different testing strategy than the one applied in this FVT. In Figure 5.28a and 5.28c, one can see the eigenfrequency and damping ratio, respectively, of the 2n wing bending mode. Because of the very high aerodynamic and, therefore, high aeroelastic damping, the modal parameters show significant scatter due to low vibration amplitudes. The scatter is in the same magnitude as the changes from one test point to the next. The main advantage of the IMM-KF is within the transition phase between the test points. Those transition phases, however, have a negligible effect on the overall high scatter of the modal parameters. In the conventional FVT, one would analyze the whole time sequence of a test point or average all identification results within a test point to reduce the uncertainty. Therefore, the constant transition model seems to smooth the data better for this mode. However, the identification results of a mode from flight data with damping at about 40% is always superimposed by high scatter due to small vibration amplitudes and, therefore, a low signal-to-noise ratio. In Figure 5.28b and 5.28d, the eigenfrequency and damping tracking of the flutter mode (symmetric wing torsion) is shown. For this mode, the damping ratio is low; therefore, the identification shows only small uncertainties. The eigenfrequency tracking especially results in a clean step-wise identification. In this case, the IMM-KF can improve the identification since the filter reaches the correct identification of the test point faster, e.g., at mode set 80. During the test point, the IMM-KF shows an identification similar to the constant transition model. In this flutter test, detecting when the flutter boundary was reached as quickly as possible to save the aircraft was of great interest. The new method shows an accurate and fast indication of approaching the flutter boundary.

(a) 2n wing bending eigenfrequency

(b) sym. wing torsion eigenfrequency

(c) 2n wing bending damping ratio

(d) sym. wing torsion damping ratio
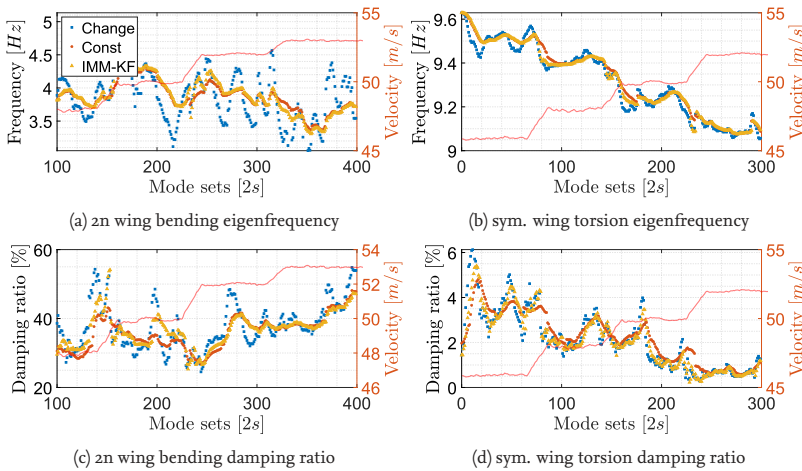
Figure 5.28: Comparison of tracking results based on different KF transition models

5.4 Discussion

The main idea of the continuous aeroelastic system identification is the more extensive exploitation of data recorded in FVTs and the online assessment of the aeroelastic behavior during flight in terms of modal parameters. The core difference with respect to conventional FVT is the continuous and real-time identification and tracking of modal parameters, which allows monitoring the aeroelastic behavior under changing conditions. The continuous system identification using OMA is possible if the system variation can be considered slow. However, due to several challenges and violations of basic assumptions made in system identification, the scatter of real-time modal parameter identification is significant. In addition, different OMA methods can lead to different results, especially when the signal-to-noise ratio is poor, and the MIDs are biased.

In this chapter, the proposed AMA method is applied to real-time identification in flight tests. The HO is applied to optimize the AMA process as well as optimize the applied MIDs for OMA applications, namely SSI-COV, SSI-DAT and LSCF. The intermediate clustering results as part of AMA are used to estimate modal parameter uncertainties in real-time. Since AMA and its cluster-based uncertainty estimation is a unified process across the different MIDs, the identification results of the MIDs can be fused. The uncertainty estimation does not lead to correct uncertainty values but is suitable for the fusion approaches. The fusion is performed between different MIDs as well as between subsequent estimations over time. The data fusion over time is performed using tailored KFs.

The applied data fusion methods IVM and KF have been tested on two FVTs: a business jet with continuous acceleration maneuvers and a fixed-wing UAV with stepwise flight speed changes. It has been shown that the data fusion approaches increase the reliability of continuous modal parameter identification: almost all modes are identified continuously. The few missing modes are not well observable because of missing sensors at specific locations or the excitation of particular modes being too weak. The continuous identification of these several (i.e., 15) modes was impossible using individual MIDs. In addition, the KF significantly reduced the scatter of modal parameter tracking. Reliable tracking can be used to compare different maneuvers and prove the consistency of the results from acceleration maneuvers. Additionally, the KF-based monitoring is capable of reliably identifying the approach of the flutter boundary in the UAV FVT.

However, the linear KF transition model is not ideal for some test cases. The IMM-KF could improve some transition phases for the flutter critical mode in the UAV FVT. Nevertheless, more sophisticated approaches like statistical models incorporating external parameters (e.g., altitude, flight speed) or an aeroelastic simulation model could further improve the KF results. This should be investigated for future flutter testing. Suppose multiple MIDs repeatedly identify parameters with considerable differences. In that case, it is difficult to fuse the identifications consistently as shown for, e.g., the damping estimation of the 4n wing bending of the ISTAR FVT. The KF could also be extended to check the measurements (i.e., AMA estimations) for potential biases or outliers using, e.g., a IPDA method.

A noteworthy drawback of the current approach is the rudimentary estimation of modal analysis uncertainties using the modal analysis cluster variances. The already promising results of the KF using only estimated uncertainties emphasize the need to accurately calculate modal analysis uncertainties and modal analysis biases close to real-time.

Using multiple MIDs has been proven helpful since the individual MIDs do not identify all modes continuously. In addition, the mode assignment is improved by collectively using all MIDs. However, the overall KF framework is not limited to the applied MIDs. In future research, additional MIDs (e.g., OMAX) can be integrated into the fusion framework.

Since in both FVTs, even using three MIDs, some modes could be identified better than others, artificial excitation possibilities should be investigated with continuous modal parameter monitoring approaches. Artificial excitation is used in conventional FVT. However, the most widely used approaches have their own drawbacks. The ideal combination of artificial broadband excitation and real-time monitoring of modal parameters should be investigated in the future. Concerning the continuous modal parameter monitoring, as presented in this thesis, the excitation should fulfill several requirements. The excitation bandwidth should be suitable for exciting the relevant eigenfrequencies of the aircraft. For the shown examples (business jet and 7m wing span UAV), the relevant eigenfrequencies are between three and 30 Hz. In contrast, e.g., a control surface pulse excites only a low-frequency band well. Additionally, the excitation is assumed to be stationary in time. Therefore, a pulse once in a while is not well suited for the continuous identification approach. Additional excitation hardware or continuous broadband control surface excitation for fly-by-wire systems might be more suitable than control surface pulses. Since the AMA and KF based monitoring is capable of identifying almost all observable modes in the frequency range of interest, the excitation should ideally excite all modes equally strong, i.e., symmetric and anti-symmetric modes. Alternatively, it should target those modes that are difficult to identify from turbulence only or those most relevant for the stability boundary.

6 Conclusion and Outlook

6.1 Conclusion

The theoretical background described in Chapter 2 summarizes the state-of-the-art and challenges of automated modal parameter identification. Additionally, it emphasizes the challenges of the data analyses applied in GVT and FVT. For GVT, key issues include high time pressure, which must not compromise the thoroughness of modal parameter identification. Additionally, exact damping identification remains an ongoing research topic because the most widely used methods, e.g., LSCF, can introduce a bias. Furthermore, the outcomes of a GVT can depend on the experience of the engineer, introducing potential inconsistencies.

For FVT, challenges arise from the necessity of continuous online identification processes to save time and costs while utilizing expensive flight data more efficiently. Excitation from turbulence is of high interest to avoid any manipulation of the aircraft configuration. Significant scatter exists in the real-time OMA results, as described in the relevant literature and presented in Chapter 5. Different methods offer uncertainty calculation approaches but are not available in real-time. In addition, the different MIDs can lead to different modal parameters. Especially, the high scatter in identified damping values limits their current practical use, necessitating significant averaging in stationary measurement points (i.e., constant flight speed and altitude).

In state-of-the-art automation of EMA and OMA, there is a predominant focus on the identification of eigenfrequencies and mode shapes, with sporadic attention to damping, which is not explicitly optimized except in very few methods. These methods, however, do not adequately optimize all modes if some modes have significantly higher vibration amplitudes than others due to the excitation of limited frequencies. In most of the methods in the literature, the user-dependency of AMA is reduced by explicitly reducing the number of hyperparameters. Therefore, compromises are often made, resulting in either more spurious modes or less robust physical mode identification. Typically, spurious modes are reduced, which leads to incomplete or imprecise identification of all physical modes. In GVT, it is crucial to identify all physical modes while minimizing the identification of spurious modes as far as possible. In FVT, identifying and tracking modal parameters with reasonable uncertainties is essential.

These challenges lead to the main objectives, which can be summarized as

1. Optimization of hyperparameters for AMA to fine-tune the analysis for safety-critical identification of all relevant modes in terms of eigenfrequency, damping ratio, and mode shape

2. Far-reaching automation of the GVT analysis process: From time data to correlated modal models with high accuracy and reduced user interaction

3. Reliable real-time identification and monitoring of relevant modes in FVT with reduced modal parameter uncertainties in continuous and discrete flight test approaches

6.1.1 AMA

The core method developed in this thesis is a novel AMA method that consists of a so-phisticated multi-tier pole clustering and modal model optimization. Multi-tier cluster-ing is applied to ensure the reliable identification of all physical modes while the number of spurious modes is low. This high accuracy is achieved by using intentionally more hyperparameters for AMA. Since a manual choice of these hyperparameters, of which some are interdependent, can lead to non-optimal results, the method is extended to a self-learning framework. The hyperparameters are optimized in a supervised learning scheme. The learning system can train hyperparameters by iteratively comparing AMA results with the results of an engineer and improving the hyperparameters using BO with GP surrogate models. This learning of complete hyperparameter sets is a novelty in the field of automated modal parameter identification. It enables a working procedure that consists of two phases: supervised training of hyperparameters and autonomous analy-sis. At first, the system is trained for a specific test condition, and afterwards, the system can autonomously analyze similar test conditions with high accuracy. The training phase adds one step, incorporating an engineer before the autonomous analysis. However, the amount of retraining is small compared to the effort of performing manual modal analy-sis several times. In addition to the reliable identification of the relevant physical modes, the modal model is optimized autonomously. For EMA, the eigenfrequency and, more importantly, the damping ratio of each mode are tuned individually by optimizing the synthesized spectra. For OMA, the uncertainties of modal parameters are qualitatively estimated in real-time and results of multiple MIDs are fused. Additionally, results of subsequent identifications are fused for uncertainty reduction.

The novel AMA system has been integrated into two essential and safety-critical test ac-tivities of structural dynamic and aeroelastic aircraft identification: GVT and FVT.

6.1.2 SAGVT

The AMA method was extended by an anomaly detection of faulty sensors and simple automated modal model correlation, leading to a fully automated GVT analysis chain. The learning system was extended to retrain the whole hyperparameter set during a GVT whenever the system recommends it. The overall SAGVT system was tested onsite at GVTs of a business jet as well as of a fixed-wing UAV. The SAGVT was implemented parallel to the conventional GVT analysis chain and demonstrated excellent performance across various excitation points, directions, and types. HO led to an AMA accuracy as high as or sometimes higher than the conventional analysis results. Although there is potential to reduce the number of retraining sessions, the system was effectively retrained 16 times for the business jet and three times for the UAV, which proved manageable for the presented GVTs. Concerning the business jet, the time of manual modal analysis could be reduced by 86 % for the 115 measurement runs. For the UAV, in total 54 measurement runs were performed, i.e., a reduction of 94 % manual analysis time using SAGVT. This time reduc-tion enabled the direct assessment of the just acquired measurement run to react imme-diately if a sensor lost connection or the excitation was non-optimal. The system showed satisfactory performance in automatically detecting faulty sensors, which could help di-rectly at the GVT. However, there was an occasional need for manual improvements in the automated correlation of modes within mode families. These improvements were feasible

as hyperparameters rarely needed retraining, allowing the adjustments and the retraining to be managed by a single person as shown in the business jet GVT. An essential result of SAGVT concerns the accuracy of the resulting modal models and mode families. At the business jet GVT, all modes identified manually were also identified by SAGVT. The agreement is very high in mode shape and eigenvalue for most modes. For some local modes, a comparison using the MAC value shows that contributions of other components can blend mode shapes. Differences in damping ratio identification were as expected since the damping ratio is optimized most using AMA and spectra synthesis optimization. At the same time, the conventional results rely on LSCF identifications. For strongly non-linear modes, the system can detect the nonlinearity. However, when identifying modes with strong nonlinearity, it is essential to re-evaluate the identified parameters manually to ensure their accuracy. This re-evaluation helps maintain the integrity and reliability of the results in complex scenarios involving significant nonlinear behavior. Another considerable advantage of this learning system is its ability to produce consistent and unified results, even when different engineers conduct the analysis as shown in the UAV GVT. Even though some engineers missed the identification of some suspension modes, these modes were identified robustly by SAGVT. The learning does not lead to a mirroring of the results of the engineer, but indeed to a reasonable way of performing EMA. It shows that the system can achieve reproducible GVT outcomes even when trained by different engineers. This feature is precious for aircraft certification processes, ensuring reproducible and standardized results.

6.1.3 FVT Monitoring using AMA and Data Fusion

The scatter of modal parameters identified during FVT is generally high. The scatter becomes even more significant when performing modal parameter monitoring while continuously but slowly varying the system (e.g., air speed). In addition to the scatter, different MIDs lead to different results, making it difficult to decide which best suits a specific test setup. Different MIDs have different advantages and disadvantages. The processing using AMA and HO can unify the use of all MIDs, but the combination of, e.g., SSI and AMA still leads to different results than the combination of, e.g. LSCF and AMA. However, the unified use of SSI and LSCF together with AMA and the HO leads to well-comparable results. Additionally, the pole clusters as an intermediate step of AMA can provide a simple yet qualitatively acceptable estimation of uncertainties of modal parameters. While these uncertainties should not be used for specifying confidence intervals, they can effectively merge estimations from different methods at a single point in time and across subsequent results. Fusing time-domain and frequency-domain methods in OMA is a novel approach that reduces uncertainties and enables complete and robust identification of all modes. This hybrid method leverages the strengths of both domains, ensuring more accurate and comprehensive modal analysis. An example is the FVT of the research aircraft, in which all relevant modes were monitored by fusing three MIDs. High damping ratios are complicated to identify because of the low vibration amplitudes. However, to investigate the overall flutter curves, the scatter of all modes should be reduced. This uncertainty reduction is achieved by applying a KF. By selecting appropriate transition models within the KF for different flight test maneuvers, uncertainties are minimized, as demonstrated for different maneuvers at two distinct FVTs. The reduction in scatter has been quantitatively shown for MIDs fusion using IVM and subsequent estimation fusion using a KF. In the

shown flutter test, this approach improves the generation of the flutter curve, leading to a more confident prediction of the flutter boundary. In the FVT of the business jet, almost all relevant modes could be tracked with acceptable uncertainties in real-time while changing the flight speed continuously.

Correctly assigning new mode estimates to a tracked mode family requires a well-chosen tracking metric and appropriate thresholds. In this work, these values are determined along with the hyperparameters during the training phase. If modes cross or come close in frequency, the tracking can sometimes fail if the mode shapes change significantly. The challenge of matching newly identified modes to mode families in mode tracking is comparable to the correlation of modes during the GVT. In both applications, a simple tracking using MAC or MAC-XP works for some situations but not reliably for all situations of complex aircraft structures.

6.1.4 Research Questions

In conclusion, this research successfully addresses all the research questions outlined in Section 2.6. Implementing a learning-based AMA system demonstrates improved accuracy in modal parameter identification, as evidenced by simulation and real aircraft vibration test data. In GVT analysis, the application of the learning AMA system enhances standardization, reducing user-dependency without compromising the quality of the identification results. Application to real FVT data shows that the unified AMA process enables the fusion of results from multiple MIDs, resulting in complete and reliable modal models. Furthermore, it is shown that the fusion of consecutive estimates effectively reduces the scatter in identified modal parameters.

6.2 Outlook

Based on the findings in this thesis, multiple topics are addressed in this section, which are promising for future investigation. The following list of issues is not exhaustive but highlights some important points for potential future research projects. Those topics are sorted into the three fields of general automation of modal parameter identification, autonomous GVT data analysis, and autonomous monitoring of modal parameters in FVT.

6.2.1 Autonomous Modal Parameter Identification

A key feature of the novel AMA system is the ability to learn hyperparameters semi-autonomously. The results showed that the hyperparameter training scheme could reduce user-dependency significantly while maintaining identification accuracy. However, some user workload remains in the training process. Future work will focus on training the hyperparameters using simulations, such as the FEM and aeroelastic simulation models reduced to the measurement or FTI DoFs, respectively. The simulation-based training could enable fully autonomous learning and become fully user-independent.

The trained hyperparameters are assumed to be optimal for the explicit data set used for training. One assumes it is well suited for similar data sets; however, some hyperparameter differences might be better. Therefore, different hyperparameter sets from similar yet different measurement conditions could be used to estimate the uncertainties in the

identification using multiple hyperparameter sets when applied to new measurement conditions. This approach may not only strengthen the identification robustness but could also provide deeper insights into the impact of hyperparameters on the identification performance.

The techniques and insights gained from hyperparameter training and uncertainty analysis can be extended to various fields, including wind energy, civil engineering (e.g., bridge or tower analysis), or the automotive industry. These sectors can benefit from the advanced identification techniques and uncertainty reduction methods developed in this thesis. Evaluating and potentially increasing the technology readiness level (TRL) is an essential next step towards application in certification tests. A higher TRL is achieved by extensive testing and validation by different users to ensure the identification system is robust and practical for real-world applications. This widespread testing will help identify potential weaknesses and confirm the accuracy of the system.

6.2.2 Autonomous GVT Data Analysis

Similar to the overall AMA system, its application in GVT in the SAGVT framework needs further validation on different tests, such as GVT of very large aircraft, helicopters, and new flight vehicles such as, e.g., for vertical take-off and landing (VTOL). These possible applications require each engineer to exert a high cognitive effort to perform the test successfully. Therefore, the usability, intuitiveness, and efficiency of the SAGVT need to be validated comprehensively by multiple users. Maybe a step-wise integration into the conventional GVT analysis chain can increase the trust in the semi-autonomous analysis. For example, the fast detection of faulty sensors through anomaly detection has proven helpful in addition to the conventional analysis. Advancing the faulty sensor detection by reinforcement after confirmed anomalies could increase the motivation to integrate and use the sub-system in the analysis chain.

Additionally, reducing the number of retraining or achieving fully automated training via FEM is a future goal. Since one purpose of the GVT is to update the FEM model, the usage of this model for hyperparameter training should be done with caution. Nevertheless, it is common practice to define the GVT setup using the aircraft FEM model.

Since the correlation requires user postprocessing, the automated correlation based on mode shapes and eigenvalues should be enhanced. The correlation could be implemented as a classification problem, and artificial neural network (ANN) such as, e.g., an Auto-Encoder could be applied to classify mode shapes and even help find reasonable names for the modes. Incorporating some meta information of the measurement run, i.e., excitation level, position, and direction, could further improve the mode classification by adapting the classification procedure or thresholds since, e.g., the mode shape complexity of well-excited modes is often lower than those of weakly excited modes.

Identifying nonlinear modes could be improved by considering the mode families already during identification. If a mode family shows significant trends with changing force levels, this could be considered for the next identification of the same mode. However, a clear indication signal should be given to the user as feedback to emphasize such an analysis adaption.

An essential part of the HO is the objective function to assess an autonomously identified modal model. This objective function builds on separate assessments of the quality of each mode. This information could be used to quickly determine modes that require

better excitation, potentially saving redundant excitation runs. However, while most modes are identified repeatedly in many measurement runs, some (mainly local) modes require specific excitation. Those excitation runs must not be removed for time savings. Nevertheless, an indicator of which modes are well identified and which need better identification can be helpful for the test execution.

For some structures, very low-frequency and high-frequency ranges are of interest. Performing multiple HOs for different frequency ranges might make sense. Those would lead to optimized spectra calculation settings and individual frequency resolutions for different frequency ranges.

The GVT of the UAV highlighted the importance of correctly identifying suspension modes to distinguish them from structural modes. It also showed that inconsistencies in the suspension identification can occur. In the presented GVT, all those inconsistencies could be fixed as part of the postprocessing. In the future, the autonomous system can guide engineers immediately in identifying which modes are structural and which are influenced by suspension, improving the accuracy of the overall modal model identification.

6.2.3 Autonomous Monitoring of Modal Parameters in FVT

Future research concerning modal parameter monitoring in FVT will focus on accelerating the quantitatively correct calculation of uncertainties of OMA. Exact uncertainties would lead to optimal KF fusion results. Moreover, the uncertainties would enable online indications of confidence intervals.

Comparing the continuous analysis results with stationary points should be explored since this cannot be tested in the current study. In addition, a comprehensive comparison of the experimental flutter curves with aeroelastic simulation models will be conducted.

The mode matching challenge, which also occurred in GVT analysis, could be improved in the monitoring framework using the KF. The prediction capabilities of the KF can be utilized to assign new modes to the mode family, which is predicted to be closest to the new mode, instead of using the modes from the past only. Since the modes are assumed to change, the prediction of the KF could be closer to the next mode than the preceding identification. Additionally, a KF can calculate the probability of incorrect mode assignment (clutter likelihood), similar to the IPDA method. The basic idea of using machine learning methodologies, like an Auto-Encoder, for mode matching in GVT could also be applied in FVT. Moreover, the same Auto-Encoder could learn what a mode shape looks like in a GVT setup and how the same mode would look like during flight with a reduced sensor setup.

The transition model used in the KF should be explored further, moving beyond linear transition matrices to consider nonlinear transitions, potentially based on an aeroelastic simulation model. An aeroelastic simulation model as part of the tracking could significantly enhance the accuracy and reliability of modal parameter predictions.

A prerequisite for reliable identification of modes is the excitation. This thesis relied on aerodynamic turbulence excitation to keep the aircraft configuration clean. The excitation from turbulence is not always stationary, i.e., it changes over time. Therefore, when monitoring modal parameters, some mode estimations at time k are based on more excitation and are more reliable than mode estimations from lower turbulence at time $k + n$. An inverse estimation of the excitation force could be used to weight the mode estimations

more accurately for later fusion by the KF. However, the findings show that some modes in higher frequencies are not excited sufficiently and, therefore, would benefit from artificial excitation. Concerning continuous monitoring, excitation during flight testing is not trivial. For example, a pulse would have to be repeated frequently, and depending on the time duration of the pulse, the highest excited frequency is limited. Further investigations on other excitation maneuvers and additional hardware for broadband excitation could be carried out.

Own Publications

Journal Articles

1. **R. Volkmar**, et al., Experimental and operational modal analysis: Automated system identification for safety-critical applications, Mechanical Systems and Signal Processing, 2023. doi: 10.1016/j.ymssp.2022.109658.

   In this paper, the novel AMA method, including HO using BO and GP is described. RV formulated the idea of the method and developed the algorithm. RV tested the system at the UAV ground vibration test and applied it to UAV flight vibration test data. This paper presents parts of the thesis Chapters 3, 4 and 5.

2. C. Van Zijl, K. Soal, **R. Volkmar**, et al., The use of operational modal analysis and mode tracking for insight into polar vessel operations, Marine Structures, 2021. doi:10.1016/j.marstruc.2021.103043.

   In this paper, OMA and modal tracking are applied to a polar vessel to predict the structural dynamics of the ship under changing environmental loads. RV developed the automated tracking algorithm.

Conference Proceedings

3. **R. Volkmar**, et al., Reliable monitoring of modal parameters during a flight vibration test using autonomous modal analysis and a Kalman filter, in International Forum on Aeroelasticity and Structural Dynamics (IFASD), Jun. 2024.

   In this paper, the KF modal parameter tracking system has been applied online during a FVT with the research aircraft ISTAR. The results of the system using AMA and the KF for different flight maneuvers are compared. RV developed the system, implemented it on an integrated measurement computer, and applied it in flight during the FVT. Additionally, other colleagues applied the developed system in the flight test. This paper presents parts of the thesis Chapter 5.

4. K. I. Soal, J. Schwochow, **R. Volkmar**, et al., Flutter flight testing: Using operational modal analysis to identify, track and predict flutter for safe and efficient flight test campaigns, in International Forum on Aeroelasticity and Structural Dynamics (IFASD), Jun. 2024.

   This paper presents the results from an UAV flutter test. RV developed the automated tracking algorithm. The recorded flutter test data is used in this thesis Chapter 5.

5. **R. Volkmar**, et al., Adaptive Kalman filter tracking for instantaneous aircraft flutter monitoring, in International Conference on Information Fusion (FUSION), Jun. 2023.

    In this paper, the real-time modal analysis method for flight vibration tests is enhanced using an improved tracking method. An adaptive KF is developed to reduce the uncertainties of modal parameter tracking during FVT. RV developed the method and implemented the algorithm. RV tested the system on simulated and real FVT data. This paper presents parts of the thesis Chapter 5. However, the transition models presented in Chapter 5 together with the IMM-KF were found to give more robust results than the adaptive KF in actual flight tests.

6. **R. Volkmar**, Autonomous and reliable aeroelastic system identification using density-based clustering, Gaussian processes, and Kalman filtering, in Advances in Artificial Intelligence for Aerospace Engineering at ONERA DLR Aerospace Symposium, Mai 2023.

    In this presentation, the framework of the AMA method is presented, and how it can be adjusted and integrated into GVT and FVT data analysis chains.

7. K. I. Soal, **R. Volkmar**, et al., Flight vibration testing of the T-FLEX UAV using online modal analysis, in AIAA SciTech Forum, Jan. 2023.

    In this paper, a miniaturized real-time modal analysis system is used in a FVT of a UAV. RV developed the automated tracking algorithm and supported the flight vibration test activities.

8. **R. Volkmar**, et al., Optimization of time and frequency domain methods for real-time modal parameter identification of aircraft, in International Conference on Noise and Vibration Engineering (ISMA), Sep. 2022.

    In this paper, the AMA method is optimized for real-time monitoring. The HO using BO is adjusted concerning real-time capability. In addition, multiple modal identification methods are applied in parallel, their uncertainties are estimated, and the inverse-variance mean is used for MIDs fusion. RV developed the algorithm and tested it on a laboratory structure. This paper presents parts of the thesis Chapter 5.

9. K. I. Soal, M. Nagy, D. Teubl, **R. Volkmar**, et al., Hardware-in-the-loop testing of a miniaturized real-time flutter monitoring system for UAVs, in International Conference on Noise and Vibration Engineering (ISMA), Sep. 2022.

    This paper presents a miniaturized real-time modal analysis system that runs on a Raspberry Pi. RV developed the automated tracking algorithm.

10. K. I. Soal, C. Thiem, T. Meier, **R. Volkmar**, et al., Embedded flight vibration testing system for online flutter monitoring of UAVs, in International Forum on Aeroelas-

ticity and Structural Dynamics (IFASD), Jun. 2022.

This paper presents a miniaturized real-time modal analysis system that runs on a Raspberry Pi and can be integrated into a small UAV. RV developed the automated tracking algorithm and supported the FVT activities.

11. **R. Volkmar**, et al., Semi-autonomous analysis of large aircraft ground vibration tests, in International Forum on Aeroelasticity and Structural Dynamics (IFASD), Jun. 2022.

This paper extends the AMA method by faulty sensor detection and automated correlation for GVT analysis. A novel software framework is developed to enable the application of SAGVT at a real GVT. RV developed the method and implemented the algorithm. RV tested the system on-site at the GVT of a business jet research aircraft. This paper presents parts of the thesis Chapter 4.

12. K. I. Soal, **R. Volkmar**, et al., Evolutionary based approach to modal parameter identification, in International Operational Modal Analysis Conference (IOMAC), Mai 2019.

This paper presents a genetic algorithm to optimize a modal model. RV developed the synthesized spectra error function to be used by KS for the genetic algorithm.

13. **R. Volkmar**, et al., Automated optimization of output only modal parameter identification, in International Operational Modal Analysis Conference (IOMAC), Mai 2019.

This paper describes the error function that uses the synthesized spectra and spectra based on measured data to optimize a modal model. In further studies, PSO provided better results for modal model optimization. However, the synthesis error for individual mode clusters is introduced in this paper. RV formulated the idea of the method, developed the algorithm and tested it on a laboratory structure. This paper presents parts of the thesis Chapter 3.

Bibliography

[1] Randall J Allemang. "The modal assurance criterion–twenty years of use and abuse". In: Sound and Vibration 37.8 (2003), pp. 14–23.

[2] Yaakov Bar–Shalom, X Rong Li, and Thiagalingam Kirubarajan. "Estimation with applications to tracking and navigation: theory algorithms and software". In: John Wiley & Sons (2004).

[3] Yaakov Bar-Shalom, K.C. Chang, and H.A.P. Blom. "Tracking a maneuvering target using input estimation versus the interacting multiple model algorithm". In: IEEE Transactions on Aerospace and Electronic Systems 25.2 (1989), pp. 296–300. DOI: 10.1109/7.18693.

[4] Michele Basseville et al. "In-flight vibration monitoring of aeronautical structures". In: IEEE Control Systems Magazine 27.5 (2007), pp. 27–42.

[5] Ruben Boroschek and Joaquin Bilbao. "Evaluation of an automatic selection methodology of model parameters from stability diagrams on a damaged building". In: International Operational Modal Analysis Conference (IOMAC). 2015, pp. 12–14.

[6] Marc Böswald. "Analysis of the bias in modal parameters obtained with frequency-domain rational fraction polynomial estimators". In: International Conference on Noise and Vibration Engineering (ISMA). Sept. 2016, pp. 2907–2921.

[7] Marc Böswald, Michael Link, and Carsten Schedlinski. "Computational model updating and validation of aero-engine finite element models based on vibration test data". In: International Forum on Aeroelasticity and Structural Dynamics (IFASD). 2005.

[8] Marc Böswald et al. "A Review of Experimental Modal Analysis Methods with Respect to their Applicability to Test Data of Large Aircraft Structures". In: International Conference on Noise and Vibration Engineering (ISMA). 2006, pp. 2461–2481. ISBN: 90-73802-83-0.

[9] Marc Böswald et al. "Online monitoring of flutter stability during wind tunnel testing of an elastic wing with pylon and engine nacelle within the HMAE1 project". In: International Forum on Aeroelasticity and Structural Dynamics (IFASD). 2019.

[10] Anders Brandt. Noise and Vibration Analysis. John Wiley & Sons, Ltd, 2011. ISBN: 9780470978160. DOI: 10.1002/9780470978160.

[11] Elmar J. Breitbach. "Recent Developments in Multiple Input Modal Analysis". In: Journal of Vibration, Acoustics, Stress, and Reliability in Design 110.4 (1988), pp. 478–484. ISSN: 0739-3717. DOI: 10.1115/1.3269554.

[12] Martin Brenner et al. "Overview of recent flight flutter testing research at NASA Dryden". In: 38th Structures, Structural Dynamics, and Materials Conference. 1997, p. 1023.

[13]   Markus M. Breunig et al. "LOF: Identifying Density-Based Local Outliers". In: SIG-
       MOD Rec. 29.2 (May 2000), pp. 93–104. ISSN: 0163-5808. DOI: 10.1145/335191.
       335388.

[14]   Rune Brincker and Palle Andersen. "Understanding stochastic subspace identifica-
       tion". In: International Modal Analysis Conference (IMAC). Society for Experimen-
       tal Mechanics. 2006.

[15]   Ralf Buchbach et al. "Datenbankgestützte Korrelation von Modaldaten - Das DLR
       Correlation Tool". In: VDI Fachtagung Schwingungen. VDI-Berichte. VDI Verlag
       GmbH, Nov. 2023, pp. 267–283.

[16]   Alessandro Cabboi. "Automatic operational modal analysis: challenges and appli-
       cations to historic structures and infrastructures". Thesis. University of Cagliari,
       Italy, 2014.

[17]   Alessandro Cabboi et al. "Automated modal identification and tracking: Applica-
       tion to an iron arch bridge". In: Structural Control and Health Monitoring 24.1
       (2017), e1854.

[18]   E. Peter Carden and James M.W. Brownjohn. "Fuzzy clustering of stability diagrams
       for vibration–based structural health monitoring". In: Computer–Aided Civil and
       Infrastructure Engineering 23.5 (2008), pp. 360–372. DOI: 10.1111/j.1467-8667.
       2008.00543.x.

[19]   Bart Cauberghe. "Applied frequency-domain system identification in the field of
       experimental and operational modal analysis". PhD Thesis. Vrije University Bel-
       gium, Belgium, 2004.

[20]   Katrien De Cock, Guillaume Mercere, and Bart De Moor. "Recursive subspace iden-
       tification for in flight modal analysis of airplanes". In: International Conference on
       Noise and Vibration Engineering (ISMA). 2006.

[21]   Katrien De Cock et al. "Subspace system identification for mechanical engineer-
       ing". In: International Conference on Noise and Vibration Engineering (ISMA).
       2002.

[22]   Matthew J. Desforges, Jonathan E. Cooper, and Janet R. Wright. "Mode tracking dur-
       ing flutter testing using the modal assurance criterion". In: Proceedings of the In-
       stitution of Mechanical Engineers, Part G: Journal of Aerospace Engineering 210.1
       (1996), pp. 27–37.

[23]   Christof Devriendt et al. "Continuous dynamic monitoring of an offshore wind
       turbine on a monopile foundation". In: International Conference on Noise and
       Vibration Engineering (ISMA). 2012.

[24]   Grigorios Dimitriadis and Jonathan E. Cooper. "A time-frequency stability analysis
       of non-linear aeroelastic systems". In: International Forum on Aeroelasticity and
       Structural Dynamics (IFASD). 2001, pp. 237–248.

[25]   Michael Döhler and Laurent Mevel. "Efficient multi-order uncertainty computa-
       tion for stochastic subspace identification". In: Mechanical Systems and Signal Pro-
       cessing 38.2 (2013), pp. 346–366.

[26]   EASA. Certification Specifications for Large Aeroplanes CS-25. Tech. rep. 2019.

[27] Martin Ester et al. "A density-based algorithm for discovering clusters in large spatial databases with noise". In: International Conference on Knowledge Discovery and Data Mining (KDD). Vol. 96. 34. 1996, pp. 226–231.

[28] Michael Friswell and John E. Mottershead. Finite element model updating in structural dynamics. Vol. 38. Springer Science & Business Media, 1995.

[29] Ulrich Füllekrug et al. "Measurement of FRFs and Modal Identification In Case of Correlated Multi-Point Excitation". In: Proceedings of the International Conference on Engineering Dynamics (ICED). 2007.

[30] Carmelo Gentile and Antonella Saisi. "Continuous dynamic monitoring of a centenary iron bridge for structural modification assessment". In: Frontiers of Structural and Civil Engineering 9 (2015), pp. 26–41.

[31] Ivan Goethals, Bart Vanluyten, and Bart De Moor. "Reliable spurious mode rejection using self learning algorithms". In: International Conference on Noise and Vibration Engineering (ISMA). Citeseer, 2004, pp. 991–1003.

[32] Dennis Göge. "Automatic updating of large aircraft models using experimental data from ground vibration testing". In: Aerospace Science and Technology 7.1 (2003), pp. 33–45. ISSN: 1270-9638. DOI: https://doi.org/10.1016/S1270-9638(02)01184-7.

[33] Dennis Göge et al. "Ground vibration testing of large aircraft–state-of-the-art and future perspectives". In: International Modal Analysis Conference (IMAC). 2007.

[34] Yves Govers. "Parameter identification of structural dynamic models by inverse statistical analysis". Thesis. University of Kassel, Germany, 2012.

[35] Yves Govers and Michael Link. "Stochastic model updating—Covariance matrix adjustment from uncertain experimental modal data". In: Mechanical Systems and Signal Processing 24.3 (2010), pp. 696–706. ISSN: 0888-3270. DOI: https://doi.org/10.1016/j.ymssp.2009.10.006.

[36] Yves Govers et al. "AIRBUS A350XWB Ground Vibration Testing: Efficient techniques for customer oriented on-site modal identification". In: International Conference on Noise and Vibration Engineering (ISMA). 2014, pp. 2503–2516. ISBN: 9789073802919.

[37] Yves Govers et al. "Wind tunnel flutter testing on a highly flexible wing for aeroelastic validation in the transonic regime within the HMAE1 project". In: International Forum on Aeroelasticity and Structural Dynamics (IFASD). 2019.

[38] Patrick Guillaume et al. "A poly-reference implementation of the least-squares complex frequency-domain estimator". In: International Modal Analysis Conference (IMAC). Vol. 21. 183-192. 2003, p. 214.

[39] Patrick Guillaume et al. "OMAX–a combined experimental-operational modal analysis approach". In: International Conference on Noise and Vibration Engineering (ISMA). 2006, pp. 2985–2996.

[40] Frank E. Harrell et al. Regression modeling strategies: with applications to linear models, logistic regression, and survival analysis. Vol. 608. Springer, 2001, pp. 20–21.

[41] Joachim Hartung, Guido Knapp, and Bimal K. Sinha. Statistical meta-analysis with applications. John Wiley & Sons, 2011.

[42] M. Danial A. Hasan et al. "Cluster analysis for automated operational modal analysis: A review". In: MATEC Web of Conferences. Vol. 255. EDP Sciences. 2019, p. 02012.

[43] Luc Hermans, Herman Van der Auweraer, and Maher Abdelghani. "Identification of Structural Models during System Operation with Application to Flutter Data Analysis". In: AIAA/CEAS Forum on Aeroelasticity and Structure Dynamics. 1997, pp. 323–330.

[44] D Hunt et al. "Optimal selection of excitation methods for enhanced modal testing". In: 25th Structures, Structural Dynamics and Materials Conference. 1984, p. 1068.

[45] Frank Hutter, Lars Kotthoff, and Joaquin Vanschoren. Automated machine learning: methods, systems, challenges. Springer Nature, 2019.

[46] IMC Test & Measurement GmbH. `https://www.imc-tm.de/`. Accessed: 2024-07-18. 2024.

[47] Michael Iovnovich et al. "Assessment of advanced flutter flight-test techniques and flutter boundary prediction methods". In: Journal of Aircraft 55.5 (2018), pp. 1877–1889.

[48] Goran Jelicic. "System identification of parameter-varying aeroelastic systems using real-time operational modal analysis". PhD Thesis. Syddansk Universitet (SDU), 2022.

[49] Goran Jelicic et al. "Online Monitoring of Aircraft Modal Parameters during Flight Test based on permanent Output-Only Modal Analysis". In: AIAA SciTech Forum. 2017. DOI: 10.2514/6.2017-1825.

[50] Mahmoud El-kafafy et al. "Fast maximum-likelihood identification of modal parameters with uncertainty intervals: a modal model-based formulation". In: Mechanical Systems and Signal Processing 37.1-2 (2013), pp. 422–439. ISSN: 0888-3270.

[51] Altan Kayran. "Flight flutter testing and aeroelastic stability of aircraft". In: Aircraft engineering and aerospace technology 79.2 (2007), pp. 150–162.

[52] Michael W. Kehoe. "A historical overview of flight flutter testing". In: AGARD Structures and Materials Panel Meeting. NASA-TM-4720. 1995.

[53] James Kennedy and Russell Eberhart. "Particle swarm optimization". In: International Conference on Neural Networks (ICNN). Vol. 4. IEEE, 1995, pp. 1942–1948. ISBN: 0780327683.

[54] Rick Lind and Marty Brenner. "Flutterometer: an on-line tool to predict robust flutter margins". In: Journal of Aircraft 37.6 (2000), pp. 1105–1112.

[55] Tamás Luspay et al. "Model reduction for LPV systems based on approximate modal decomposition". In: International Journal for Numerical Methods in Engineering 113.6 (2018), pp. 891–909.

[56] Filipe Magalhaes, Alvaro Cunha, and Elsa Caetano. "Online automatic identification of the modal parameters of a long span arch bridge". In: Mechanical Systems and Signal Processing 23.2 (2009), pp. 316–329. ISSN: 0888-3270.

[57] Laurent Mevel et al. "Input/output versus output-only data processing for structural identification—Application to in-flight data analysis". In: Journal of Sound and Vibration 295.3 (2006), pp. 531–552. ISSN: 0022-460X. DOI: https://doi.org/10.1016/j.jsv.2006.01.039.

[58] Jonas Mockus. "Application of Bayesian approach to numerical methods of global and stochastic optimization". In: Journal of Global Optimization 4 (1994), pp. 347–365.

[59] Pratyasish Mohanty, Paul Reynolds, and Aleksandar Pavic. "Automated Interpretation of Stability Plots for Analysis of a Non-Stationary Structure". In: International Modal Analysis Conference (IMAC). Vol. 25. 2007.

[60] John E. Mottershead and Michael I. Friswell. "Model Updating In Structural Dynamics: A Survey". In: Journal of Sound and Vibration 167.2 (1993), pp. 347–375. ISSN: 0022-460X. DOI: https://doi.org/10.1006/jsvi.1993.1340.

[61] Darko Musicki, Robin Evans, and Srdjan S. Stankovic. "Integrated probabilistic data association". In: IEEE Transactions on Automatic Control 39.6 (1994), pp. 1237–1241. DOI: 10.1109/9.293185.

[62] Hans Günther Natke. Einführung in Theorie und Praxis der Zeitreihen-und Modalanalyse: Identifikation schwingungsfähiger elastomechanischer Systeme. Springer-Verlag, 2013.

[63] Michael Osborne. "Bayesian Gaussian processes for sequential prediction, optimisation and quadrature". Thesis. Oxford University, UK, 2010.

[64] Richard S. Pappa, Kenny B. Elliott, and Axel Schenk. "Consistent-mode indicator for the eigensystem realization algorithm". In: Journal of Guidance, Control, and Dynamics 16.5 (1993), pp. 852–858.

[65] Bart Peeters. "System identification and damage detection in civil engeneering". Thesis. Katholieke Universiteit Leuven, Belgium, 2000.

[66] Bart Peeters and Guido De Roeck. "Reference-based stochastic subspace identification for output-only modal analysis". In: Mechanical Systems and Signal Processing 13.6 (1999), pp. 855–878. ISSN: 0888-3270.

[67] Bart Peeters, Herman Van der Auweraer, et al. "PolyMAX: a revolution in operational modal analysis". In: International Operational Modal Analysis Conference (IOMAC). Vol. 820. 2005, pp. 1–12.

[68] Bart Peeters et al. "In-flight modal analysis-a comparison between sweep and turbulence excitation". In: International Conference on Noise and Vibration Engineering (ISMA). Vol. 8. 2006.

[69] Bart Peeters et al. "The PolyMAX frequency-domain method: a new standard for modal parameter estimation?" In: Shock and Vibration 11.3, 4 (2004), pp. 395–409. ISSN: 1070-9622.

[70] Sérgio Pereira et al. "The role of modal parameters uncertainty estimation in automated modal identification, modal tracking and data normalization". In: Engineering Structures 224 (2020), p. 111208.

[71] Charles R. Pickrel and Philip J. White. "Flight flutter testing of transport aircraft: in-flight modal analysis". In: International Modal Analysis Conference (IMAC). 2003.

[72] Mircea Radeş. "A comparison of some mode indicator functions". In: Mechanical Systems and Signal Processing 8.4 (1994), pp. 459–474. ISSN: 0888-3270.

[73] Carlo Rainieri, Giovanni Fabbrocino, and E Cosenza. "Near real-time tracking of dynamic properties for standalone structural health monitoring systems". In: Mechanical Systems and Signal Processing 25.8 (2011), pp. 3010–3026.

[74] Carl Edward Rasmussen. "Gaussian Processes in Machine Learning". In: Advanced Lectures on Machine Learning: ML Summer Schools 2003, Canberra, Australia, February 2 - 14, 2003, Tübingen, Germany, August 4 - 16, 2003, Revised Lectures. Springer Berlin Heidelberg, 2004, pp. 63–71. ISBN: 978-3-540-28650-9. DOI: 10.1007/978-3-540-28650-9_4.

[75] Edwin Reynders, Jeroen Houbrechts, and Guido De Roeck. "Fully automated (operational) modal analysis". In: Mechanical Systems and Signal Processing 29 (2012), pp. 228–250. ISSN: 0888-3270.

[76] Edwin Reynders, Rik Pintelon, and Guido De Roeck. "Uncertainty bounds on modal parameters obtained from stochastic subspace identification". In: Mechanical Systems and Signal Processing 22.4 (2008). Special Issue: Crack Effects in Rotordynamics, pp. 948–969. ISSN: 0888-3270. DOI: https://doi.org/10.1016/j.ymssp.2007.10.009.

[77] S. Schulze. Numerische Simulation des Flatterverhaltens eines nichtlinearen 2D-Flügel-Ruder-Systems in subsonischer Strömung. Tech. rep. DLR Forschungsbericht 1999-23, 1999.

[78] Jan Schwochow and Goran Jelicic. "Automatic operational modal analysis for aeroelastic applications". In: International Operational Modal Analysis Conference (IOMAC). 2015. ISBN: 8461738802.

[79] Jan Schwochow and Martin Zöger. "Flight vibration testing - we always did it this way". In: 24rth SFTE-EC Symposium. June 2013.

[80] Marco Scionti and Jeroen Lanslots. "Stabilisation diagrams: Pole identification using fuzzy clustering techniques". In: Advances in Engineering Software 36.11 (2005). Selected papers from Civil-Comp 2003 and AICivil-Comp 2003, pp. 768–779. ISSN: 0965-9978. DOI: 10.1016/j.advengsoft.2005.03.029.

[81] Marco Scionti et al. "Tools to improve detection of structural changes from in-flight flutter data". In: International Conference on Recent Advances in Structural Dynamics. 2003.

[82] C.Y. Shih et al. "Complex mode indication function and its applications to spatial domain parameter estimation". In: Mechanical Systems and Signal Processing 2.4 (1988), pp. 367–377. ISSN: 0888-3270.

[83] Julian Sinske et al. "Flight testing using fast online aeroelastic identification techniques with DLR research aircraft HALO". In: International Forum on Aeroelasticity and Structural Dynamics (IFASD). June 2017.

[84] Julian Sinske et al. "HALO flight test with instrumented under-wing stores for aeroelastic and load measurements in the DLR project iLOADS". In: CEAS Aeronautical Journal 9.1 (Feb. 2018), pp. 207–218. DOI: 10.1007/s13272-018-0294-3.

[85] Jasper Snoek, Hugo Larochelle, and Ryan Adams. Practical bayesian optimization of machine learning algorithms. Online Database. 2012. DOI: https://doi.org/10.48550/arXiv.1206.2944.

[86] Keith Soal. "System identification and modal tracking of ship structures". PhD Thesis. Stellenbosch University, 2018.

[87] Keith Soal et al. "System identification and tracking using a statistical model and a Kalman filter". In: Mechanical Systems and Signal Processing 133 (2019), p. 106127. ISSN: 0888-3270.

[88] Jurij Sodja et al. "Ground testing of the flexop demonstrator aircraft". In: AIAA SciTech Forum. 2020, p. 1968.

[89] Cyrille Stephan et al. "Airbus Beluga XL state-of-the-art techniques to perform a Ground Vibration Test campaign of a large aircraft". In: International Forum on Aeroelasticity and Structural Dynamics (IFASD). 2019.

[90] Martin Tang, Marc Böswald, and Yves Govers. "Phase resonance method for linearized identification of nonlinear mechanical structures". In: International Forum on Aeroelasticity and Structural Dynamics (IFASD). 2022.

[91] Jun Teng et al. "Automated modal analysis for tracking structural change during construction and operation phases". In: Sensors 19.4 (2019), p. 927.

[92] Theodore Theodorsen. General theory of aerodynamic instability and the mechanism of flutter. Tech. rep. NACA. 1979.

[93] Filippo Ubertini, Carmelo Gentile, and Annibale Luigi Materazzi. "Automated modal identification in operational conditions and its application to bridges". In: Engineering Structures 46 (2013), pp. 264–278. ISSN: 0141-0296.

[94] Pierre Vacher, Beatrice Jacquier, and Alain Bucharles. "Extensions of the MAC criterion to complex modes". In: International conference on noise and vibration engineering (ISMA). 2010, pp. 2713–2726.

[95] Herman Van der Auweraer and Bart Peeters. "Discriminating physical poles from mathematical poles in high order systems: use and automation of the stabilization diagram". In: IEEE Instrumentation and Measurement Technology Conference (IEEE Cat. No. 04CH37510). 2004.

[96] Herman Van der Auweraer et al. "Modal parameter estimation from inconsistent data sets". In: Proceedings of SPIE-The International Society for Optical Engineering. Vol. 4062. 2000.

[97] Peter Van Overschee and Bart De Moor. Subspace identification for linear systems: Theory—Implementation—Applications. Springer Science & Business Media, 2012.

[98] Steve Vanlanduit et al. "An automatic frequency domain modal parameter estimation algorithm". In: Journal of Sound Vibration 265.3 (2003), pp. 647–661. ISSN: 0022-460X.

[99]   Peter Verboven. "Frequency Domain System Identification for Modal Analysis". English. PhD Thesis. Vrije Universiteit Brussel, 2002.

[100]   Peter Verboven et al. "Autonomous structural health monitoring—part I: modal parameter estimation and tracking". In: Mechanical Systems and Signal Processing 16.4 (2002), pp. 637–657. ISSN: 0888-3270.

[101]   Peter Verboven et al. "Modal parameter estimation and monitoring for on-line flight flutter analysis". In: Mechanical Systems and Signal Processing 18.3 (2004), pp. 587–610. ISSN: 0888-3270. DOI: https://doi.org/10.1016/S0888-3270(03)00074-8.

[102]   Peter Verboven et al. "Stabilization charts and uncertainty bounds for frequency-domain linear least squares estimators". In: International Modal Analysis Conference (IMAC). 2003.

[103]   Robin Volkmar et al. "Adaptive Kalman Filter Tracking for Instantaneous Aircraft Flutter Monitoring". In: International Conference on Information Fusion (FUSION). IEEE, 2023.

[104]   Robin Volkmar et al. "Experimental and operational modal analysis: Automated system identification for safety-critical applications". In: Mechanical Systems and Signal Processing 183 (2023), p. 109658. ISSN: 0888-3270. DOI: https://doi.org/10.1016/j.ymssp.2022.109658.

[105]   Robin Volkmar et al. "Optimization of time and frequency domain methods for real-time modal parameter identification of aircraft". In: International Conference on Noise and Vibration Engineering (ISMA). 2022.

[106]   Robin Volkmar et al. "Reliable monitoring of modal parameters during a flight vibration test using autonomous modal analysis and a Kalman filter". In: International Forum on Aeroelasticity and Structural Dynamics (IFASD). 2024.

[107]   Roger Williams, John Crowley, and Havard Vold. "The multivariate mode indicator function in modal analysis". In: International Modal Analysis Conference (IMAC). Citeseer, 1985, pp. 66–70.

[108]   Li Yang and Abdallah Shami. "On hyperparameter optimization of machine learning algorithms: Theory and practice". In: Neurocomputing 415 (2020), pp. 295–316. ISSN: 0925-2312. DOI: https://doi.org/10.1016/j.neucom.2020.07.061.